MORPHOLOGICAL, IMMUNOCYTOCHEMICAL AND FUNCTIONAL CHARACTERIZATION OF THE MICROGLIAL PHENOTYPE IN CULTURE

Melinda Szabó

Department of Cell Biology and Molecular Medicine
Faculty of Medicine and Faculty of Science and Informatics
University of Szeged

Ph.D. Thesis

Szeged, 2015

PUBLICATIONS RELATED TO THE THESIS

I. **Szabo M**, Gulya K (2013) Development of the microglial phenotype in culture. *Neuroscience* 241:280-295. (IF: 3.327)

II. **Szabo M**, Dulka K, Gulya K (2016) Calmodulin inhibition regulates morphological and functional changes related to the actin cytoskeleton in microglial cell cultures. *Brain Research Bulletin* 120:41-57. (IF: 2.718 – legfrissebb adat 2014-re)

ABSTRACTS RELATED TO THE THESIS

I. **Szabo M**, Gulya K (2009) Glial cell population dynamics in vitro. *Euroglia 2009. 9th European Meeting on Glial Cells in Health and Disease Paris, France, 2009. Glia 57:S29-30.*

II. Gulya K, **Szabo M** (2011) Development of the microglial phenotype *in vitro. 8th IBRO World Congress of Neuroscience, Florence, Italy, 2011. D085.*

III. Gulya K, **Szabo M** (2012) Calmodulin in cultured microglial cells. *8th FENS Forum of Neuroscience, Barcelona, Spain, 2012. A46-430 vol 7, p025.17.*

IV. **Szabó M**, Gulya K (2012) Development of the microglial phenotype in embryonic rat forebrain cultures. *IBRO International Workshop, Szeged, Hungary 2012. Ideggyógy Sz 2012 65(S1):63.*

V. Dulka K, **Szabo M**, Gulya K (2015) Calmodulin inhibition affects proliferation and cell viability in unchallenged and LPS-challenged pure microglial cultures. *XII European Meeting on Glial Cells in Health and Disease, Bilbao, Spain, 2015. Glia 63:E95.*

TABLE OF CONTENTS

Abbreviations

Ca^{2+}: calcium ion; CALMID: calmidazolium; 1-[bis(4-chlorophenyl)methyl]-3-[2-(2,4-dichlorophenyl)-2-(2,4-dichlorobenzyloxy)ethyl]-1H-imidazolium chloride; CaM: calmodulin; CD11b/c: cluster of differentiation 11b/c, the rat CR3 complement receptor; CNPase: 2', 3'-cyclic nucleotide 3'-phosphodiesterase; CNS: central nervous system; DIV: days in vitro; DMEM: Dulbecco's Modified Eagle's Medium; FBS: fetal bovine serum; GAPDH: glyceraldehyde 3-phosphate dehydrogenase (EC 1.2.1.12); GFAP: glial fibrillar acidic protein; HLA: human leukocyte antigens; Iba1: ionized calcium binding adaptor molecule 1; Ki67: proliferation marker antigen identified by the monoclonal antibody Ki67; LPS: bacterial lipopolysaccharide; MHC: major histocompatibility complex; mRNA: messenger ribonucleic acid; PBS: phosphate-buffered saline; RT: room temperature; S.D.: standard deviation; S.E.M.: standard error of mean; subDIV: subcloned days in vitro; TBS: Tris-buffered saline; TFP: trifluoperazine (10-[3-(4-methylpiperazin-1-yl)propyl]-2-trifluoromethyl-10H-phenothiazine dihydrochloride); TI: transformation index

SUMMARY

Selected morphological, immunocytochemical and functional aspects of various microglial cell populations were characterized in mixed neuronal/glial and pure microglial cultures. The mixed primary cortical cultures were prepared from the forebrains of embryonic (E18) rats and maintained for up to 28 days (DIV1–DIV28) using routine culturing techniques. The pure microglial cells were subcloned (subDIV4) from the mixed primary cultures and maintained for up to 7 days (DIV7). During culturing, expansion of the microglial cells was observed, as evidenced by quantitative assessment of selected monocyte/macrophage/microglial cell-specific markers (HLA DP, DQ, DR, CD11b/c and Iba1) via immunocyto- and histochemistry and Western blot analysis. The Iba1 immunoreactivity in Western blots steadily increased about 750-fold, and the number of Iba1-immunoreactive cells rose at least 67-fold between DIV1 and DIV28. Morphometric analysis on binary (digital) silhouettes of the microglia revealed their evolving morphology during culturing. Microglial cells were mainly ameboid in the early stages of in vitro differentiation, while mixed populations of ameboid and ramified cell morphologies were characteristic of older cultures as the average transformation index (TI) increased from 1.96 (DIV1) to 15.17 (DIV28). Multiple immunofluorescence labeling of selected biomarkers revealed different microglial phenotypes during culturing. For example, while HLA DP, DQ, DR immunoreactivity was present exclusively in ameboid microglia (TI < 3) between DIV1 and DIV10, CD11b/c- and Iba1-positive microglial cells were moderately (TI < 13) and progressively (TI < 81) more ramified, respectively, and always present throughout culturing. Regardless of the age of the cultures, proliferating microglia were Ki67-positive and characterized by low TI values (TI < 3). The microglial function was assessed by an in vitro phagocytosis assay. Unstimulated microglia with low TI values were significantly more active in phagocytosing fluorescent microspheres than the ramified forms.

The roles of calmodulin (CaM), a multifunctional intracellular calcium receptor protein, as concerns selected morphological and functional characteristics of pure microglial cells were investigated through use of the CaM antagonists calmidazolium (CALMID) and trifluoperazine (TFP). The intracellular localization of the CaM protein relative to phalloidin, a bicyclic heptapeptide that binds only to filamentous actin, and the ionized calcium-binding adaptor molecule 1 (Iba1), a microglia-specific actin-binding protein, was determined by immunocytochemistry, with quantitative analysis by immunoblotting. In unchallenged and untreated (control) microglia, high concentrations of CaM protein were found mainly perinuclearly in ameboid microglia, while the cell cortex had a smaller CaM content that diminished progressively deeper into the branches in the ramified microglia. The amounts and

intracellular distributions of both Iba1 and CaM proteins were altered after lipopolysaccharide (LPS) challenge in activated microglia. CALMID and TFP exerted different, sometimes opposing, effects on many morphological, cytoskeletal and functional characteristics of the microglial cells. They affected the CaM and Iba1 protein expressions and their intracellular localizations differently, inhibited cell proliferation, viability and fluid-phase phagocytosis to different degrees both in unchallenged and in LPS-treated (immunologically challenged) cells, and differentially affected the reorganization of the actin cytoskeleton in the microglial cell cortex, influencing lamellipodia, filipodia and podosome formation.

We concluded that in vitro studies on microglial population dynamics combined with phenotypic characterization can be of importance when different in vivo pathophysiological situations are modeled in vitro. Moreover, the CaM antagonists altered different aspects of filamentous actin-based cell morphology and related functions with variable efficacy, which could be important in deciphering the roles of CaM in regulating microglial functions in health and disease.

1. INTRODUCTION

Microglial cells, the resident immune cells of the central nervous system (CNS), share a number of phenotypic characteristics and lineage properties with other bone marrow-derived myeloid cell populations, and are regarded as members of the monocyte/macrophage lineage (Gehrmann et al., 1995; Geissmann et al., 2003, 2010; Ginhoux et al., 2010; Kreutzberg, 1996; Prinz and Mildner, 2011; Prinz et al., 2011). Recent in vivo lineage tracing studies demonstrated that adult microglial cells originate from primitive myeloid progenitors that arise early in embryonic development, and constitute an ontogenetically distinct population in the mononuclear phagocyte system (Ginhoux et al., 2010; Saijo and Glass, 2011). Microglia are highly plastic and, by virtue of their location and current role in the nervous tissue, are able to undergo a variety of morphological and functional changes in response to various stimuli. In their non-activated or resting state, they display a ramified morphology characterized by numerous, fine-branched processes with relatively small somata and subdued macrophage-like functional properties. In response to neural injury, infection and inflammatory or other signals, however, microglial cells become activated and undergo a series of morphological, molecular and functional changes in proportion to the severity of the damage to the neuronal tissue (Kreutzberg, 1996; Ling and Wong, 1993). Shortly after their initial activation, microglial cells become progressively less ramified and quickly develop an enlarged cell body with several short, thickened processes (activated microglia) that may eventually completely retract (phagocytic microglia). This morphological transformation parallels microglial proliferation, homing and adhesion to damaged cells (Raivich et al., 1999; Streit et al., 1999). The development of the ameboid appearance and phagocytic nature of the microglial cells coincides with their antigen presentation ability and cytotoxic and inflammation-mediating signalization (Drew and Chavis, 2000; Kreutzberg, 1996; Ling and Wong, 1993; Prinz and Miller, 2014; Saijo and Glass, 2011; Streit at al., 1999; Town et al., 2005; Werry et al., 2011).

As regards origin, there are two populations of microglial cells in the CNS at any given time. The resident microglia comprise a distinct pool of cells that respond to stimuli and proliferate accordingly, and regulate their population dynamics in a manner dependent on the severity of the tissue damage. They are distributed more or less evenly throughout the nervous tissue (Milligan et al., 1991a) and exhibit an extremely slow turnover with the bone marrow or the peripheral blood under normal conditions. The resting microglia with ramified morphology lack the major histocompatibility complex (MHC) class I/MHC class II proteins,

interferon-γ, cytokines, CD45 antigens and many other surface receptors required to serve in the antigen-presenting, phagocytic and cytotoxic roles characteristic of the normal macrophage functions. Another population of cells, however, among which the perivascular microglial cells are prominent in number, is located in the close vicinity of blood vessels, and can be replaced regularly by bone marrow-derived precursor cells (Eglitis and Mezey, 1997; Hickey and Kimura, 1988) that express MHC class II antigens, indicating their monocyte/macrophage origin (Gehrmann et al., 1995; Streit et al., 1989). In cases of extreme damage to the CNS, as in infection or stroke, the blood-brain barrier may weaken considerably, and hematogenous, bone marrow-derived cells, such as myeloid progenitor cells and macrophages, may enter the brain (Priller et al., 2001). Once the damage has abated, the peripheral and central systems are disconnected for the recovery and regrowth period (Gehrmann, 1996). Although macrophages and microglia may have similar roles, the populations of resident microglia and recently migrated hematogenous myeloid progenitors/macrophages differ in many important aspects (Geissmann et al., 2003; Ladeby et al., 2005; Wirenfeldt et al., 2007).

Similarly to the extensive studies on the origin and the morphological and functional development of the microglial phenotype in vivo (Dalmau et al., 1997, 1998, 2003; Geissmann et al., 2010; Ling and Wong, 1993; Ling et al., 1990; Milligan et al., 1991a, b; Orłowski et al., 2003; Streit et al., 1999), a large body of information is available on the characteristics of the different microglial populations maintained in cell cultures. However, as a variety of proinflammatory factors are produced by activated microglial cells on the one hand (Kreutzberg, 1996), and activation of microglial cells by a number of agents has been demonstrated on the other (Berger et al., 2012; Liu et al., 2000; Werry et al., 2011), characterization of the activated microglial cells in response to an in vitro stimulation/challenge predominates in the literature. Recent studies have demonstrated, for example, that under specific polarization conditions microglial cells, similarly to peripheral macrophages, develop into different inflammation-related phenotypes, termed M1 and M2 (Gordon, 2003; Mosser and Edwards, 2008).

Microglial functions such as motility and phagocytosis are closely associated with dynamic changes in the cytoskeleton and related to intracellular calcium (Ca^{2+}) signaling (Greenberg, 1995; Kalla et al., 2003; Mitchison and Cramer, 1996). The ubiquitous Ca^{2+}-binding proteins participate in Ca^{2+}-elicited intracellular events, either as Ca^{2+}-sensing/receptor/trigger or as Ca^{2+}-buffering/transport proteins, by binding intracellularly stored Ca^{2+} (Ikura, 1996). They contribute to nearly all aspects of the functioning of the cell,

and are important in numerous intracellular signaling processes, from the regulation of cellular homeostasis to learning and memory (Berridge et al., 2010; Clapham, 2007). Calmodulin (CaM), one of the most important intracellular Ca^{2+} receptors, exerts its biological action through its heterogenous population of target proteins, which are involved in a number of cellular regulatory processes (Kennedy, 1989; Palfi et al., 2002).

The nervous tissue is especially abundant in CaM. While its distribution has been characterized in detail for a number of neuronal cell types (Kovacs and Gulya, 2002, 2003; Palfi et al., 1999, 2001, 2005), its localization and functions in glial cells are much less known. Astrocytes express CaM protein in low quantities (Kortvely et al., 2003), but mRNA populations from all three CaM genes could still be localized both perinuclearly and in the astrocytic endfeet (Palfi et al., 2005). The expression of CaM in oligodendroglia is similarly low and has not been characterized extensively, albeit the regulatory effects of this protein on a number of membrane-bound target proteins such as the myelin basic protein (Libich and Harauz, 2008) or the 2',3'-cyclic nucleotide 3'-phosphodiesterase (Myllykoski et al., 2012) have been established. Of all the glial components, only the microglia seem to have a considerable amount of CaM. They express a relatively large amount of CaM when activated (Casal ez al., 2001; Solá et al., 1997), and many aspects of their Ca^{2+} signaling are well documented (Färber and Kettelmann, 2006; Wong and Schlichter, 2014).

CaM immunoreactivity or CaM gene-specific transcripts are often colocalized with those of the target enzymes of CaM within the same cytoplasmic compartments (Erondu and Kennedy, 1985; Sanabria et al., 2008; Seto-Ohshima et al., 1983; Strack et al., 1996). For example, actin is accompanied by CaM in the cell cortex, helping to remodel the actin-based cytoskeleton in accordance with the actual (patho)physiological signals (Mitchison and Cramer, 1996; Psatha et al., 2004). Ionized calcium-binding adaptor molecule 1 (Iba1) is another intracellular Ca^{2+}-binding protein with actin-binding capability that is expressed in macrophages and microglia, and is widely used to detect both resting and activated microglial phenotypes (Imai et al., 1996). CaM and Iba1 proteins share a number of molecular structural variants that are related to either their Ca^{2+} binding or their target protein recognition (Yamada et al., 2006). In contrast with the wide-ranging regulatory roles of CaM, Iba1 plays a much more restricted role in microglial functions, e.g. remodeling the actin cytoskeleton during migration (Siddiqui et al., 2012; Vincent et al., 2012).

The modulatory action of Ca^{2+}-bound CaM on multiple target proteins can be regulated by a number of compounds. Calmidazolium (CALMID; 1-[bis(4-chlorophenyl)methyl]-3-[2-(2,4-dichlorophenyl)-2-(2,4-dichlorobenzyloxy)ethyl]-1H-imidazolium chloride) and

trifluoperazine (TFP; 10-[3-(4-methylpiperazin-1-yl)propyl]-2-trifluoromethyl-10H-phenothiazine dihydrochloride) are potent inhibitors of CaM-related cellular activities (Borsa et al., 1986; Sunagawa et al., 2000). It is presumed that, apart from binding to the CaM protein (Mashushima et al., 2000; Vandonselaar et al., 1994; Vertessy et al., 1998), they can also exert their effects on some of the CaM-regulated targets directly (Sunagawa et al., 2000).

2. SPECIFIC AIMS

Under physiological conditions, the vast majority of the resident microglial cells in the CNS are certainly unstimulated and characterized by ramified morphology. Despite the recent in vivo experimental approaches that unveiled new aspects of the functional, developmental and lineage characteristics of the microglial cell populations (Auffray et al., 2009; Durafourt et al., 2012; Geissmann et al., 2003, 2010; Ginhoux et al., 2010; Xu et al., 2012), only limited data are available on the development of the microglial phenotype in vitro under unstimulated/immunologically unchallenged conditions.

In an attempt to shed more light on the nature of the unstimulated microglia in vitro, we set out to characterize selected morphological, immunocytochemical and functional aspects of such cells, partially by quantitative techniques, in rat primary cortical cell cultures maintained routinely up to DIV28, in order to monitor the “normal” development of their phenotype. We analyzed the population dynamics of the microglial cells in terms of their percentage of the total number of cells during culturing, quantitatively characterized the different microglial populations according to their transformation indices, and differentially localized some of the canonical microglial markers to these distinct morphologies. As far as we are aware, a similarly detailed study for a period of up to 28 days on the characteristics of the in vitro development of unstimulated and unchallenged microglial cells of embryonic origin has not been reported previously.

The actin cytoskeleton is of paramount importance in many microglial functions. Its reorganization during cell migration, phagocytosis, or under several pathophysiological conditions, is in the forefront of research. One of the main regulators of the actin cytoskeleton reorganization is CaM. Relatively little is known, however, as concerns the possible involvement of CaM mediation in such important microglial functions as phagocytosis and the cellular functions associated with it, e.g. dynamic cytoskeletal reorganization. Thus, in view of the importance of CaM-mediated cell functions and the paucity of data on specific microglial functions related to and possibly regulated by CaM, we set out to investigate the localization and intracellular distribution of CaM in pure microglial cell populations derived

from rat primary mixed forebrain cultures by using immunocytochemical and Western blot techniques. Selected CaM inhibitors such as CALMID and TFP, previously reported to have different modes of action (Matsushima et al., 2000; Sunagawa et al., 2000), were quantitatively tested for their ability to modify the microglial morphology (cell area, perimeter, transformation index), as well as lamellipodia, filipodia and podosome formation. Stimulation with LPS was used to evaluate the ability of microglial cells to respond to activation (Fricker et al., 2012; Song et al., 2014; Tokes et al., 2011).

Our specific aims were:

1) To determine the cellular composition and the rate of microglial proliferation in primary mixed cultures (DIV1–DIV28) prepared from rat embryonic forebrain tissues;

2) To quantitatively characterize the different microglial populations according to morphological parameters during culturing (DIV1–DIV28);

3) To localize some of the canonical microglial markers to these distinct morphologies during culturing (DIV1–DIV28);

4) To quantitatively characterize and localize microglial CaM immunoreactivities in relation to their morphologies in pure, secondary microglial cultures (subDIV4);

5) To characterize the effects of two CaM inhibitors (CALMID and TFP) on the morphological, including cytoskeletal, and immunocytochemical characteristics of pure microglial cultures (subDIV4).

3. EXPERIMENTAL PROCEDURES

3.1. Animals

All animal experiments were carried out in strict compliance with the European Council Directive (86/609/EEC) and EC regulations (O.J. of EC No. L 358/1, 18/12/1986) regarding the care and use of laboratory animals for experimental procedures, and followed the relevant Hungarian and local legislation requirements. The experimental protocols were approved by the Institutional Animal Welfare Committee of the University of Szeged (I-74-II/2009/MÁB). The pregnant Sprague-Dawley rats (170-200 g; one animal per cage) were kept under standard housing conditions and fed ad libitum.

3.2. Antibodies

The antibodies used in our immunohistochemical, immunocytochemical and Western blot studies are listed in Table 1. For a thorough characterization of different microglial phenotypes developed in vitro, antibodies against the ionized calcium binding adaptor

molecule 1 (Iba1), the human leukocyte antigen (HLA) class II genes HLA DP, DQ, DR and the rat CR3 complement receptor (CD11b/c) were used in our immunohistochemical and Western blot analyses.

Table 1. Antibodies used in immunocytochemistry and immunohistochemistry

Primary antibody, abbrev. name	Primary antibody, full name	Final dilution	Company	Secondary antibody with fluorochrome, full name	Company	Final dilution
Iba1	Rabbit anti-Iba1 polycl. ab.	1/300	Wako, Osaka, Japan	Alexa Fluor 568 goat anti-rabbit	Invitrogen, Carlsbad, CA, USA	1/1,000
CD11b/c (OX42)	Mouse anti-CD11b/c equivalent monocl. ab., clone OX42	1/200	Abcam, Cambridge, England	Alexa Fluor 488 goat anti-mouse or Alexa Fluor 568 goat anti-mouse	Invitrogen, Carlsbad, CA, USA	1/1,000
HLA DP, DQ, DR	Mouse anti-HLA-DP, DQ, DR, monocl. ab., clone CR3/43	1/100	Dako, Glostrup, Denmark	Alexa Fluor 488 goat anti-mouse	Invitrogen, Carlsbad, CA, USA	1/1,000
HLA DRα	Rabbit anti-HLA-DRα, FL-254, polycl. ab., SC-25614	1/50	Santa Cruz Biotechnol., Inc., Santa Cruz, CA, USA	Alexa Fluor 488 goat anti-rabbit	Invitrogen, Carlsbad, CA, USA	1/1,000
β tubulin III	Mouse anti-tubulin, β-III, monocl. ab., clone TU-20	1/400	Abcam, Cambridge, England	Alexa Fluor 488 goat anti-mouse	Invitrogen, Carlsbad, CA, USA	1/1,000
Ki67	Rabbit anti-Ki67, monocl. ab., clone SP6	1/200	Thermo Scientific, Fremonz, CA, USA	Alexa Fluor 488 goat anti-rabbit	Invitrogen, Carlsbad, CA, USA	1/1,000
CaM	Mouse anti-CaM, monocl. ab.	1/100	Millipore	Alexa Fluor 488 goat anti-mouse	Invitrogen, Carlsbad, CA, USA	1/1,000
CaM	Rabbit anti-CaM, monocl. ab., clone EP799Y	1/100	Abcam, Cambridge, UK	Alexa Fluor 568 goat anti-rabbit	Invitrogen, Carlsbad, CA, USA	1/1,000

The anti-Iba1 antibody recognizes the Iba1 protein, an intracellular Ca^{2+}-binding protein expressed in the CNS specifically in macrophages and microglia (Imai et al., 1996), and has been used to detect both resting and activated microglial phenotypes (Ito et al., 1998). The HLA class II genes are composed of three closely linked subregions encoding the

polymorphic HLA class II molecules HLA DP, DQ, DR. The anti-HLA DP, DQ, DR antibody reacts with the α and β-chains of all products of these subregions and recognizes numerous antigen-presenting cells that express these molecules, including the reactive and the resting microglia, the perivascular microglial cells, many macrophages and most monocytes in the CNS (Horejsí et al., 1986; Ulvestad et al., 1994b). The anti-HLA DRα antibody recognizes the α subunit of the class II MHC complex antigen HLA DR, a transmembrane glycoprotein constitutively expressed by microglia (Ulvestad et al., 1994a). The anti-CD11b/c antibody recognizes a common epitope shared between CD11b and CD11c (integrin α_M and α_X chains), reacts with all monocytes and macrophages (Robinson et al., 1986; Wang et al., 1996), and is commonly used as a resident microglial marker in the CNS (Imai et al., 1996). The anti-β tubulin III (Banerjee et al., 1990) antibody has been used to detect neurons, the anti-glial fibrillar acidic protein (GFAP) antibody (Guillemin et al., 1997) to label astrocytes, and the anti-2', 3'-cyclic nucleotide 3'-phosphodiesterase (CNPase) antibody (Zhang et al., 2010) to detect oligodendrocytes. The anti-CaM monoclonal antibody has been used to detect both Ca^{2+}-bound and Ca^{2+}-free forms of the antigen (Sacks et al., 1991), the anti-Ki67 antibody to detect proliferating cells. Ki67 is a nuclear protein expressed in all active phases of the cell cycle from the late G1 phase through the end of the M phase but is absent in non-proliferating and early G1 phase cells (Scott et al., 2004; Starborg et al., 1996). The anti-glyceraldehyde 3-phosphate dehydrogenase (GAPDH) antibody has been used as an internal control in Western blot experiments (Wu et al., 2012).

Various dilutions of primary and secondary antibodies, incubation times and blocking conditions for each antibody used were carefully tested for both immunocytochemistry/-histochemistry and Western blot analysis. To detect the specificities of the secondary antisera, omission control experiments (staining without the primary antibody) were also performed. In such cases, no fluorescent or Western blot signals were detected.

3.3. Paraffin embedding and sectioning

Forebrain samples of embryonic day 18 (E18) rats were carefully removed, fixed by immersion overnight at 4 °C in 0.05 M phosphate-buffered saline (PBS) containing 4% formaldehyde, and then embedded in low-melting point paraffin. Coronal sections (8 μm thick) were cut in a microtome and mounted on slides coated with (3-aminopropyl) triethoxysilane (Menzel, Darmstadt, Germany) to prevent detachment. After deparaffinization and rehydration, the slides were placed in a jar filled with 0.01 M citrate buffer (pH 6.0) and

heated 3 times for 3 min at 800 W in a microwave oven. The sections were then processed for immunohistochemistry.

3.4. Cortical cell cultures

Mixed primary cortical cell cultures were established from E18 wild-type rat embryos by the use of general methods described previously (Kortvely et al., 2003). Briefly, 6-8 fetal rats under ether anesthesia were surgically decapitated and the frontal lobe of the cerebral cortex was removed, minced with scissors, incubated for 10 min at 37 °C in 9 ml of Dulbecco's Modified Eagle's Medium (DMEM; Invitrogen, Carlsbad, CA, USA; containing 1 g/l D-glucose, 110 mg/l Na-pyruvate, 4 mM L-glutamine, 3.7 g/l $NaHCO_3$, 10,000 U/ml penicillin G, 10 mg/ml streptomycin sulfate and 25 μg/ml amphotericin B) supplemented with 0.25% trypsin (Invitrogen) and then centrifuged at 1,000g for 10 min at room temperature (RT). The pellet was resuspended, washed twice in 5 ml of DMEM containing 10% heat-inactivated fetal bovine serum (Invitrogen), and centrifuged for 10 min at 1,000g at RT. The final pellet was resuspended in 2 ml of the same solution as above, after which the cells were seeded in the same medium and cultured at 37 °C in a humidified air atmosphere supplemented with 5% CO_2 in one or other of the following ways: 1) in poly-L-lysine-coated coverslips (18 x 18 mm; 2 x 10^5 cells/coverslip) for immunocytochemistry; 2) in poly-L-lysine-coated Petri dishes (60 mm x 15 mm; 10^6 cells/dish) for Western blot analyses; or 3) in a poly-L-lysine-coated culture flask (75 cm^2 , 12 x 10^6 cells/flask) for the subsequent generation of pure microglial cell cultures. The mixed primary cultures were maintained up to 28 days (DIV1-DIV28; or occasionally with cultures aged up to 2 months. data not shown) for immunocytochemistry and Western blot analyses, and for 7 days (DIV7) for the generation of pure microglial cells. For culturing periods longer than 3 days, the DMEM was changed every 3 days. Apart from the microglial markers, several cell surface and cytoplasmic neuronal, astrocytic and oligodendrocytic markers were used to characterize the primary cultures. Cell proliferation was assessed by the use of the antibody raised against Ki67.

3.5. Preparation of pure microglial cell cultures

Pure microglial cell cultures were subcloned from mixed primary cultures (DIV7) maintained in a poly-L-lysine-coated culture flask (75 cm^2 , 12 x 10^6 cells/flask) by shaking the cultures at 150 rpm in a platform shaker for 20 min at 37 °C. Microglia from the supernatant were collected by centrifugation at 3,000*g* for 10 min at RT and resuspended in 2 ml of DMEM/10% FBS. The cells were seeded at a density of 2 x 10^5 cells/Petri dish for Western

blots and cell viability assays or 10^5 cells/coverslip/Petri dish for immunocytochemistry, proliferation or phagocytosis assays, and cultured in DMEM in a humidified atmosphere supplemented with 5% CO_2 for 4 days at 37 °C. The medium was changed on the first day after seeding (subDIV1). Immunocytochemistry routinely performed on the pure microglial cultures 4 days after seeding (subDIV4) consistently detected a >99% incidence of Iba1-immunopositive microglial cells for the Hoechst 33258 dye-labeled cell nuclei (Fig. 11).

3.6. Treatment of pure microglial cells with LPS and CaM inhibitors

On the fourth day of subcloning (subDIV4), the DMEM was replaced and the expanded pure microglial cells were treated for 24 h with either LPS (100 ng/ml in final concentration, dissolved in DMEM; Sigma, St. Louis, MO, USA), CALMID (5 nM or 50 nM in final concentration, dissolved in dimethylsulfoxide (DMSO); Sigma) or TFP (10 μM or 20 μM final concentration, dissolved in DMSO; Sigma) alone, or with a combination of LPS and one of these CaM inhibitors, and the effects were compared in a variety of morphological and functional tests. LPS treatment served as an immunochallenge. Unchallenged and untreated (control) cultures were maintained under identical conditions, but without these inhibitors, and received 2 μl DMSO solution instead.

3.7. In vitro phagocytosis assay

The fluid-phase phagocytic capacity of the unstimulated microglial cells was determined via the uptake of fluorescent microspheres (2 μm diameter; Sigma, St. Louis, MO, USA) using the general methods described by Szabo and Gulya (2013). Cortical cells from E18 rats were plated on coverslips in 35-mm Petri dishes at a density of 200,000 cells/coverslip in 2 ml of DMEM containing 10% heat-inactivated fetal bovine serum as above, and cultured for 14 days. At the end of the culturing period, 1 μl of a 2.5% aqueous suspension of fluorescent microspheres per ml was added to the primary culture, which was then incubated for 60 min at 37 °C. The cells were next washed 5 times with 2 ml of PBS to remove dish- or cell surface-bound residual fluorescent microspheres, and fixed with 4% formalin in PBS. Negative controls were treated as above with the exception that cultures with beads were incubated for 60 min at 4 °C. For measurement of the phagocytotic activity, cells labeled with phagocytosed microbead(s) were counted. Twenty random fields with a total of 120 bead-labeled cells were counted under a fluorescent microscope with a 10x or 20x objective. For the mixed cultures, the number

of phagocytosed microbeads (mean ± S.D.) was analyzed as a function of the transformation index (TI). Statistically significant differences were determined by the Mann-Whitney Rank Sum test.

3.8. Immunohistochemistry and -cytochemistry

Immunohistochemistry on paraffin-embedded tissue sections was done essentially the same way as immunocytochemistry on cultured cells. For immunocytochemistry, primary cortical cells (DIV1-DIV28) or pure microglial cells (subDIV4) cultured in vitro on poly-L-lysine-coated coverslips were used. At different time intervals (DIV1, DIV4, DIV7, DIV10, DIV14, DIV21, DIV28), or after different treatments (subDIV4), the cultured cells on the coverslips were fixed in 4% formaldehyde in 0.05 M PBS (pH 7.4 at RT) for 5 min, and rinsed in 0.05 M PBS for 3 x 5 min. After permeabilization and blocking of the nonspecific sites in 0.05 M PBS solution containing 5% normal goat serum (Sigma), 1% heat-inactivated bovine serum albumin (Sigma) and 0.05% Triton X-100 for 30 min at 37 °C, the cells on the coverslips were incubated overnight at 4 °C with the appropriate primary antibody (Table 1) in the above solution. The cultured cells were washed for 4 x 10 min at RT in 0.05 M PBS, and then incubated with the appropriate Alexa Fluor fluorochrome-conjugated secondary antibody (Table 1) in the above solution, but without Triton X-100, in the dark for 3 h at RT. The cells on the coverslip were washed for 4 x 10 min in 0.05 M PBS at RT. At this stage, the cells were occasionally stained with rhodamine-phalloidin (5 μl in 200 μl PBS; Molecular Probes, Eugene, OR, USA) for 30 min at RT, then washed for 2 x 10 min at RT. Finally, the nuclei were stained in 0.05 M PBS solution containing 1 mg/ml polyvinylpyrrolidone and 0.5 μl/ml Hoechst 33258 dye (Sigma). The coverslips were rinsed in distilled water for 5 min, air-dried and mounted on microscope slides in Vectashield mounting medium (Vector Laboratories, Burlingame, CA, USA). Cells were viewed on a Nikon Microphot-FXA epifluorescent microscope (Nikon Corp., Tokyo, Japan) and photographed with a Spot RT Color CCD camera (SPOT RT/ke, Diagnostic Instruments, Inc., Sterling Heights, MI, USA).

3.9. Western blot analysis

For Western blotting, the protocols were optimized for each antibody as regards epitope accessibility, polyacrylamide gel separation, antibody dilution and chemiluminescence signal intensity. Cultured primary cells (DIV1-DIV28) or pure microglial cells (subDIV4) with different treatment regimens were collected through use of a rubber policeman, homogenized

in 50 mM Tris-HCl (pH 7.5) containing 150 mM NaCl, 0.1% Nonidet P40, 0.1% cholic acid, 2 μg/ml leupeptin, 1 μg/ml pepstatin, 2 mM phenylmethylsulfonyl fluoride and 2 mM EDTA, and centrifuged at 10,000 g for 10 min. The pellet was discarded and the protein concentration of the supernatant was determined (Lowry et al., 1951).

Table 2. Antibodies used in Western blot analysis

Primary antibody, abbrev. name	Primary antibody, full name	Final dilution	Company	Secondary antibody with fluorochrome, full name	Company	Final dilution
Iba1	Rabbit anti-Iba1 polycl. ab.	1/1,000	Wako, Osaka, Japan	Anti-rabbit IgG, peroxidase conjug.	Sigma, St. Louis, MO, USA	1/1,000 or 1/2,000
β tubulin III	Mouse anti-tubulin, β-III, monocl. ab., clone TU-20	1/1,000	Abcam, Cambridge, England	Anti-mouse IgG, peroxidase conjug.	Sigma, St. Louis, MO, USA	1/3,000
GFAP	Rabbit anti-GFAP polycl. ab.	1/5,000	Abcam, Cambridge, England	Anti-rabbit IgG, peroxidase conjug.	Sigma, St. Louis, MO, USA	1/2,000
CNPase	Mouse anti-CNPase, monocl. ab., clone 11-5B	1/500	Abcam, Cambridge, England	Anti-mouse IgG, peroxidase conjug.	Sigma, St. Louis, MO, USA	1/3,000
CaM	Rabbit anti-CaM, monocl. ab., clone EP799Y	1/2,000	Abcam, Cambridge, UK	Anti-rabbit IGG, peroxidase conjug.	Sigma, St. Louis, MO, USA	1/2,000
GAPDH	Mouse anti-GAPDH, monocl. ab., clone GAPDH-71.1	1/20,000	Sigma, St. Louis, MO, USA	Anti-mouse IGG, peroxidase conjug.	Sigma, St. Louis, MO, USA	1/3,000

For the Western blot analyses of microglial, neuronal, astrocyte or oligodendrocyte immunoreactivities, 5-10 μg of protein was separated on an SDS polyacrylamide gel (4-10% stacking gel/resolving gel), transferred onto Hybond-ECL nitrocellulose membrane (Amersham Biosciences, Little Chalfont, Buckinghamshire, England). Strips of membranes with the transferred bands for CaM and Iba1 (both around 17 kDa) and GAPDH (37 kDa) were cut and processed separately for CaM, Iba1 or GAPDH immunodetection. The membranes were blocked for 1 h in 5% nonfat dry milk (for GFAP, Iba1 and GAPDH Westerns) or 5% bovine serum albumin (for CaM, CNPase and anti-β tubulin III Westerns) in Tris-buffered saline (TBS) containing 0.1% Tween 20, and incubated for 1 h with the

appropriate primary antibodies. After 5 washes in 0.1% TBS–Tween 20, the membranes were incubated for 1 h with the appropriate peroxidase-conjugated secondary antibodies (Table 1), and washed 5 times as before. The enhanced chemiluminescence method (ECL Plus Western blotting detection reagents; Amersham Biosciences) was used to reveal immunoreactive bands according to the manufacturer's protocol. For the determination of CaM immunoreactivities in Western studies, the immunoreactive densities of equally loaded lanes were quantified, and all samples were normalized to internal GAPDH load controls run on the same gels.

3.10. Digital image processing and image analysis

Gray-scale digital images of the immunoblots were acquired by scanning the autoradiographic films with a desktop scanner (Umax PowerLook III; Umax Data Systems, Inc., Taipei, Taiwan, or Epson Perfection V750 PRO; Seiko Epson Corp., Japan). The images were scanned and processed at identical settings in order to allow comparison between the Western blots from different samples. Digital images were acquired with a Nikon Microphot-FXA epifluorescent microscope (Nikon Corp., Tokyo, Japan), using a Spot RT Color CCD camera and Spot RT software (Spot RT/ke Diagnostic Instruments, Sterling Heights, MI, USA). Color correction and cropping of the digital images were occasionally performed when photomicrographs were made for publication (Adobe Photoshop; Adobe Systems, Inc., San Jose, CA, USA).

Microglial cells and cell nuclei in the cultures were counted with the use of the plugins developed for the computer program ImageJ (version 1.38 and 1.47; developed by W. Rasband at the U.S. National Institutes of Health, and available from the Internet at http://rsb.info.nih.gov/ij). Cell nuclei were counted with the use of the "Nucleus Counter" plugin (Image Processing and Analysis in Java, a collection of plugins and macros) installed under ImageJ (www.macbiophotonics.ca). Briefly, digital images in tagged image file formats (.tif) were opened in ImageJ, and Plugins→Particle Analysis→Nucleus Counter menus were then selected and customized as follows: the smallest and largest particle sizes were set to 50 and 10,000, respectively. "Otsu" was selected for automatic thresholding, and "mean 3x3" was chosen for the performance of smooth filtering (Sezgin and Sankur, 2004). After background subtraction, overlapping objects in the resulting binary images were separated, via the menu command "Process/Binary/Watershed" (see Abràmoff et al., 2004, for details, and the documentation web pages for ImageJ at http://rsb.info.nih.gov/ij/docs/index.html). For the counting of microglial cells expressing immunopositivity for the Iba1 antigen, the "Cell

Counter" plugin was used (ImageJ for Microscopy). After the appropriate images (.tif) had been opened, Plugins→Particle Analysis→Cell Counter menus were selected, and the output was copied to a Microsoft Excel spreadsheet (Microsoft Corp., Redmond, WA, USA) for statistical analysis.

Microglial cell silhouettes were acquired by transforming the raw digital files of Iba1-immunoreactive cells recorded under fluorescent microscope light to binary files by means of the ImageJ software. The color cell images were transformed into their binary replicas (silhouettes) by using automatic thresholding procedures. After the values of cell perimeter (μm) and cell area (μm^2) had been determined in at least 3 separate experiments (at least 2 coverslips in each experiment for each culturing time investigated; around 20 randomly selected cells/coverslip), the TI reflecting the degree of process extension was calculated through the expression [perimeter of cell (μm)]^2/4π[cell area (μm^2)] as previously described (Fujita et al., 1996). From the mixed cultures, a total of 398 cell silhouettes were analyzed in this study. For the analysis of TI values from the pure cultures, a total of 261 cells were quantitatively measured (mean ± S.E.M.). Digital image production was performed with Adobe Photoshop CS5.1 software (Adobe Systems, Inc., San Jose, CA, USA). Color correction (brightness, contrast) and cropping of the fluorescent images were occasionally performed when individual photomicrographs were assembled to figure panels for publication. No specific feature within an image was enhanced, obscured, introduced, moved or removed.

3.11. Statistical analysis

For Western blots, values are presented as means ± S.D. from at least 3 blots for each of the 3 independent experiments for each time period examined. For the counting of microglial cells and cell nuclei, at least 10 randomly sampled microscope fields from 2-3 coverslips for each culturing time period from each of the 3 separate cell-culturing experiments were counted. In the computation of semiquantitative cell silhouette characteristics (digital binary pictures), data on 20 cells per coverslip from at least 3 separate experiments for each culturing time were used. Values are presented as means ± S.D. Statistical analyses were carried out with the Mann-Whitney Rank Sum test (SigmaStat 3.11; Systat Software Inc., Chicago, IL, USA, or SigmaPlot v. 12.3, Systat Software Inc., Chicago, IL, USA). For the CaM inhibition studies, results for the phagocytosis and viability assays and the cell silhouette characteristics (TI values) were analyzed with Kruskal-Wallis one-way analysis of variance, followed by Dunn's method for pairwise multiple comparison procedures for statistically significant differences

between the groups. For these studies, values were presented as mean ± S.E.M. from at least three independent experiments and $p<0.05$ was considered significant. For Western blots, values were presented as mean ± S.E.M. from at least three blots, each representing independent experiments for each time period examined. For the determination of the homogeneity of the subcloned microglial cells, Iba1-positive cells and Hoechst 33258 dye-positive cell nuclei from at least 50 randomly sampled microscope fields from 2-3 coverslips for each subcloned culture were counted and the results are presented as mean ± S.E.M.

4. RESULTS

4.1. Microglial cells collected from the forebrains of E18 rats are mainly ameboid

The microglial cells were collected from E18 rat forebrains and maintained in mixed primary neuronal-glial co-cultures. Light microscopic fluorescent immunohistochemistry revealed (Fig. 1) that on E18 the Iba1-labeled microglial cells in the forebrain cortical tissue appeared to be mainly ameboid (arrowheads), though more differentiated forms were also present in smaller numbers. Most of the microglial cells were rounded or slightly ovoid and lacked branching processes; however, rod-like (double-arrowhead) or slightly ramified microglial cells (arrrow) were occasionally also seen in the embryonic rat forebrain.

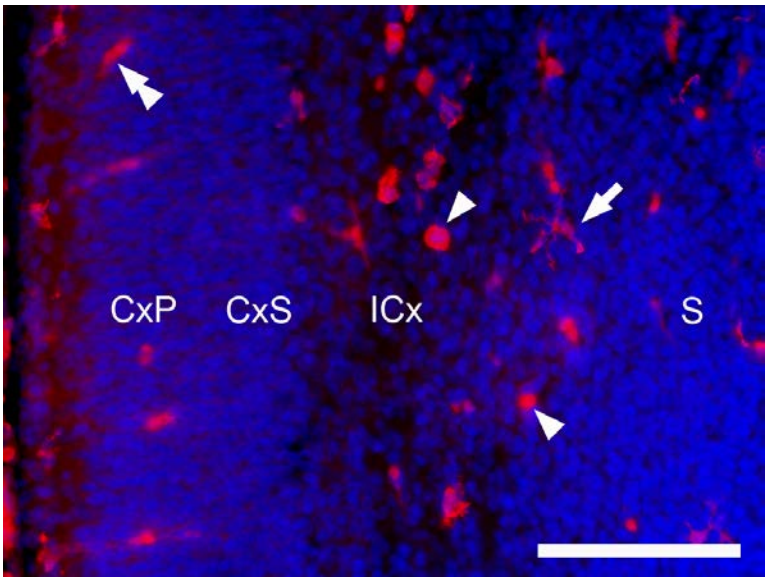

Fig. 1. Microglia in the E18 embryonic rat forebrain.
The immunofluorescent detection of microglial cells (red) in 8-μm-thick paraffin-embedded coronal sections of E18 rat forebrains was achieved through the use of anti-Iba1 antibody. Most Iba1-labeled cells displayed ameboid morphology with ovoid (arrowhead) or slightly rod-shaped forms (double-arrowhead), but occasionally more ramified microglia could also be seen (arrow). Cell nuclei were labeled blue with Hoechst 33258. CxP: cortical plate; CxS: cortical subplate; ICx: intermediate cortical layer; S: subiculum. Scale bar: 100 μm.

4.2. Microglial cells proliferate during in vitro culturing of primary forebrain cells

As concerns the cell number and the presence of numerous microglia-specific antigens, fluorescent immunocytochemistry (Fig. 2) and Western analysis (Fig. 3) demonstrated a massive in vitro expansion of the microglial cells between DIV1 and DIV28. The total numbers of cells at the beginning and at the end of the culturing period did not differ significantly. While the total number of cells exhibited a minimum on DIV10, the number of microglia constantly increased from immediately after seeding throughout the entire culturing period.

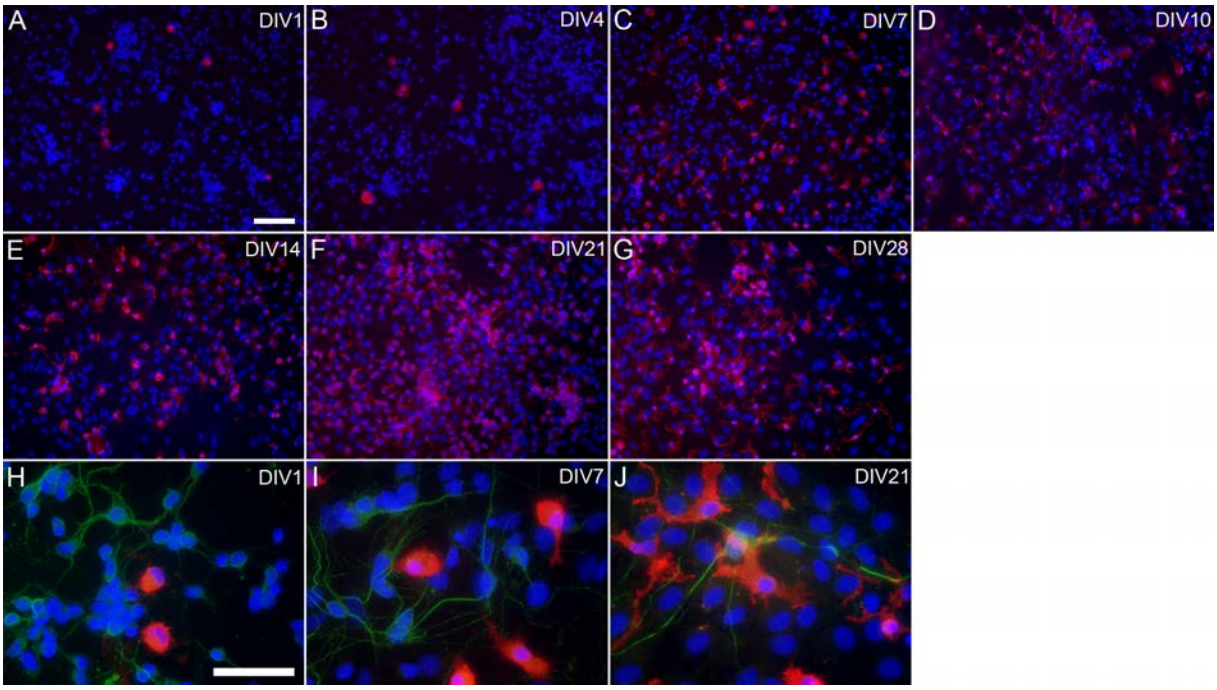

Fig. 2. Development of Iba1 immunoreactivity in primary cortical cultures (DIV1-DIV28). **(A-G)** The number and composition of the cultured cells are tightly controlled. While the total number of cells remains constant, the microglia proliferate during culturing. The microglial cells (red) were first labeled with the rabbit anti-Iba1 primary (polyclonal) antibody, and then with an appropriate Alexa Fluor fluorochrome-conjugated secondary (Alexa Fluor 568 goat anti-rabbit) antibody, while the cell nuclei (blue) were labeled with Hoechst 33258. Culturing times are indicated at the upper right corners of the pictures. Scale bar in **A** for **A-G**: 50 µm. **(H-J)** Microglial cells in characteristic cellular environments. For the detection of microglial cells and neurons, anti-Iba1 (red) and anti-β tubulin III (green) antibodies, respectively, were used. The cell nuclei (blue) were labeled with Hoechst 33258. **(H)** On day 1, the Iba1-positive microglial cells (red) were mostly ameboid around the developing β tubulin III-positive neurons (green). **(I)** On day 7, the majority of the microglial cells (red) had become ramified around a group of β tubulin III-immunopositive developing neurons (green). **(J)** On day 21, the culture was characterized by a heterogeneous, albeit mostly ramified population of microglia (red), located around the occasional β tubulin III-positive neurons (green) and many non-neuronal/non-microglial cells indicated by the blue nuclei. Scale bar in **H** for **H-J**: 50 µm.

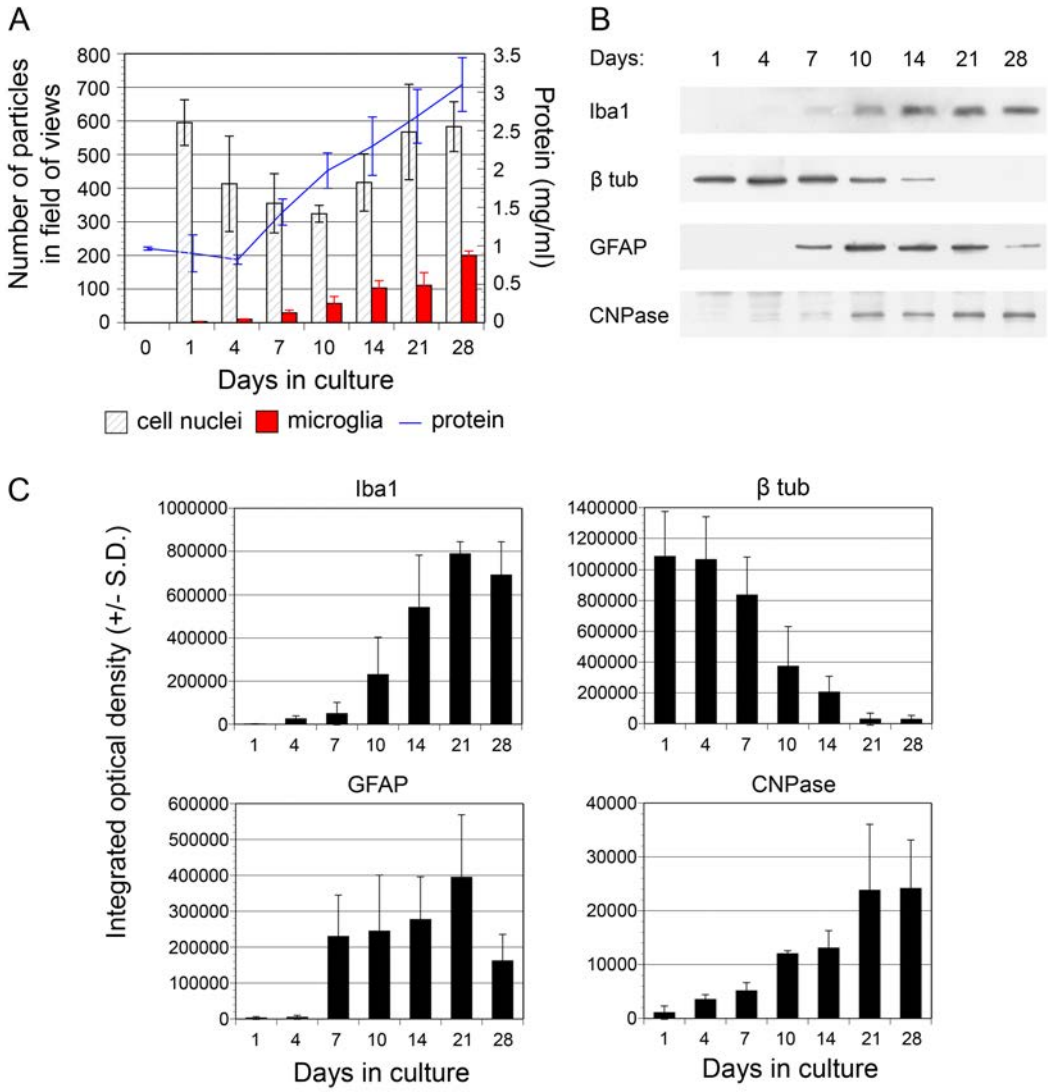

Fig. 3. Quantitative analysis of the cellular composition, the protein content and the amount of selected biomarkers during culturing.
(A) The numbers of cell nuclei (open bars) and Iba1-positive (microglial) cells (solid bars) and the protein content (solid line) were quantitative analyzed in primary cortical cultures (DIV1-DIV28). The methods of counting cell nuclei and anti-Iba1-immunolabeled cells are described in the Experimental procedures section. Error bars indicate means ± S.D. **(B)** Representative Western blot pictures of Iba1, β tubulin III, GFAP and CNPase immunoreactivities in primary cortical cultures (DIV1-DIV28). **(C)** Quantitative Western blot analysis of Iba1, β tubulin III, GFAP and CNPase immunoreactivities in cell cultures between DIV1 and DIV28. Iba1: ionized calcium binding adaptor molecule 1, β tub: β tubulin III, GFAP: glial fibrillar acidic protein, CNPase: 2', 3'-cyclic nucleotide 3'-phosphodiesterase. Error bars indicate means ± S.D.

The microglia were situated in a scattered manner in younger cultures (before and around DIV 14; Fig. 2A-E), but when they increased in abundance as the cultures grew older, they became more clumped and grouped together around other cells, as seen between DIV 21 and DIV28 (Fig. 2F, G). Typical relative distributions of neuronal and microglial cells during

culturing may be seen in Fig. 2H-J. The microglial cell content originally amounted to less than 0.5% of the total cell number at the time of seeding, but steadily rose during culturing. On DIV 4 and DIV7, progressively more microglial cells appeared, accounting for 2% and 8% of the total cell number, respectively (Fig. 3A). On DIV10, the overall morphological diversity of the microglial cells in the culture was similar to that on DIV7; at this time, the cultures contained barely 50% of the total cell number seen on DIV1, and the microglial cells comprised around 18% of the total cell population (see Fig. 2D for comparison). From this time onward, most of the gains in the number of total cell counts could be attributed to microglial cell proliferation (Fig. 3A). On DIV14, as the majority of the microglia had started to differentiate toward the ramified form, approximately 20% of all the cells were microglia. The proportion of microglial cells reached 33.7% by DIV28 (Fig. 3A, see Fig. 2G also for comparison). This massive, roughly 67-fold multiplication of the microglial cell type was also demonstrated by Western blot analysis (Fig. 3B, C). The Iba1 immunoreactivities detected in the blots steadily increased some 750-fold between DIV1 and DIV28. The β tubulin III, GFAP and CNPase immunoreactivities, quantified by Western blot analyses, demonstrated the evolution of other cellular components during culturing (Fig. 3B, C): while the amount of the neuronal marker β tubulin III steadily decreased, the immunoreactivity of the oligodendrocyte marker CNPase constantly rose between DIV1 and DIV28. A decrease in GFAP immunoreactivity at DIV28 was also observed in the cultures (Fig. 3C).

4.3. Mixed microglial populations exist in primary forebrain cultures

Diverse morphological forms of microglial cells developed and were present throughout the culturing (Fig. 4). At one end of the morphological spectrum, on DIV1, the microglial cells were virtually exclusively ameboid, frequently with smooth-surfaced spherical cell bodies, although ovoid or fusiform cells with a few microspikes could also be seen (Fig. 4A-D). As the cultures grew older (DIV7-DIV10), the microglia became more ramified. They acquired larger somata bearing typically one or two, but rarely more, large processes (Fig. 4E-H). One large, stubby lamellipoda usually formed first, but by DIV10 further processes, or the more ramified morphology of a single large lamellipoda could be observed (Fig. 4G-H). After DIV10, the microglial cells became more heterogeneous, as a constantly increasing microglia population characterized by relatively even cellular processes and enlarging somata accompanied the ameboid form (Fig. 4I-K, M). Microglial process formation became widespread by DIV14. Incidentally, this was the first time at which the ramified microglia (demonstrating morphology similar to that of the resting microglia in the adult rodent CNS)

predominated in the cultures (Fig. 4I, J). The Iba1-positive microglial cells were characterized morphologically by larger somata with a few long, relatively thin and sparsely ramified processes. As the cultures grew older, on both DIV21 and DIV28, the characteristic microglial morphology was a ramified form with several axes of symmetry along the processes (Fig. 4K, M), albeit ameboid cells were also present (Fig. 4L, N). The typical microglial morphology during the later stages of in vitro culturing also included cells with elongated, slightly curved somata emanating a few processes of mixed lengths. It must be noted that islands of densely grown ameboid microglial cells were persistently present throughout culturing.

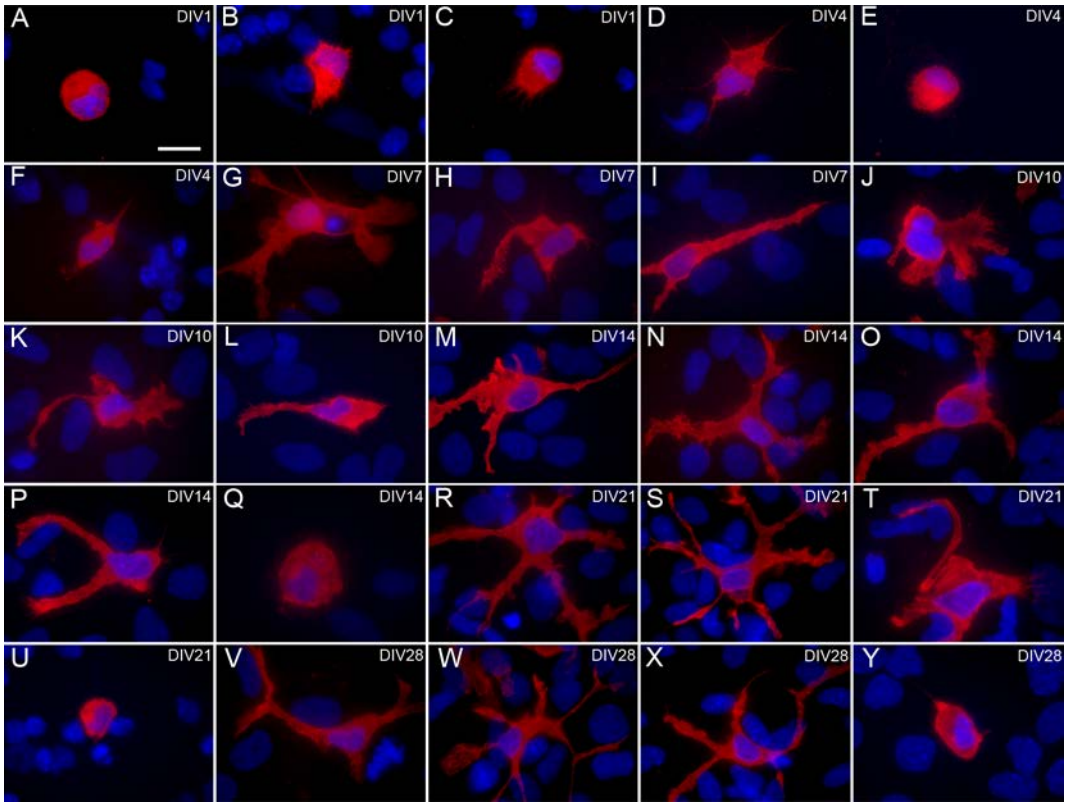

Fig. 4. Development of the morphology of the microglia in the primary cultures (DIV1-DIV28). The microglial cells (red) were first labeled with the anti-Iba1 primary antibody, and then with the Alexa Fluor 568 fluorochrome-conjugated goat anti-rabbit secondary antibody, while the cell nuclei (blue) were stained with Hoechst 33258. On day 1 **(A, B)**, all the microglial cells had an ameboid appearance, with round or slightly ovoid cell forms. Very few, if any, microspikes or lamellipodae could be seen **(B)**. On day 4 **(C, D)**, some of the microglial cells had become more asymmetric or rod-shaped, and some of these cells possessed more pronounced lamellipodae **(C)**. At later stages, from day 7 **(E, F)**, the microglia became more ramified. Usually only a few, heavier branches appeared at this stage of microglial differentiation **(F)**. From this stage on, the cultures were characterized by two distinctly polarized populations, representing the two extremes of the morphological continuum displayed by the microglial cells in the cultures, i.e. the ameboid and the ramified microglial cells. From day 14 **(I, J)**, the microglia became truly ramified as they usually had 3-4 strongly developed branches, but 6-7 equally strong and long branches could sometimes be seen from day 21 **(K, M)**. At these times, ameboid forms were also still quite frequent **(L, N)**. Scale bar in **A** (for A-Y): 10 µm.

4.4. Cultured microglia populations can be evaluated by their TI values

The time course of the morphological changes in the microglia was analyzed on binary silhouettes, as depicted in Fig. 5. Quantitative analysis based on the TI value, a dimensionless number that is an indicator for identification of the degree of morphological differentiation (e.g. the degree of process extension) of a cell, revealed a continuum of the microglial phenotype between the ameboid and the extremely ramified morphologies of the microglia. Throughout the experiments, microglial cells with TI < 3 were considered ameboid (Fig. 6A-G; circles). While younger cultures displayed predominantly ameboid cell forms with a regular, round outline reflecting the expanding microglia population (Figs. 5 and 6A-D), older cultures presented a more heterogeneous morphological repertoire, concurrently involving cells with ameboid (proliferating) and ramified (resting) forms, the majority being ramified (Figs. 5 and 6E-G). The ramified, resting microglia that developed later during the culturing could be characterized by a TI value as high as 81 (Fig. 6H). The ameboid, proliferating microglial cells, predominant in the early stages but always present throughout culturing, had TI values of less than 3, independently of the age of the culture (Fig. 6H; below dashed line), and were always Ki67-positive (Fig. 7). The Ki67 immunoreactivity observed in the ameboid microglial nuclei usually exhibited a distinct dotlike pattern representative of the S/G2 phase (Fig. 7A-D) unless it was associated with the periphery of the condensed chromosomes of the M-phase (Fig. 7E-H).

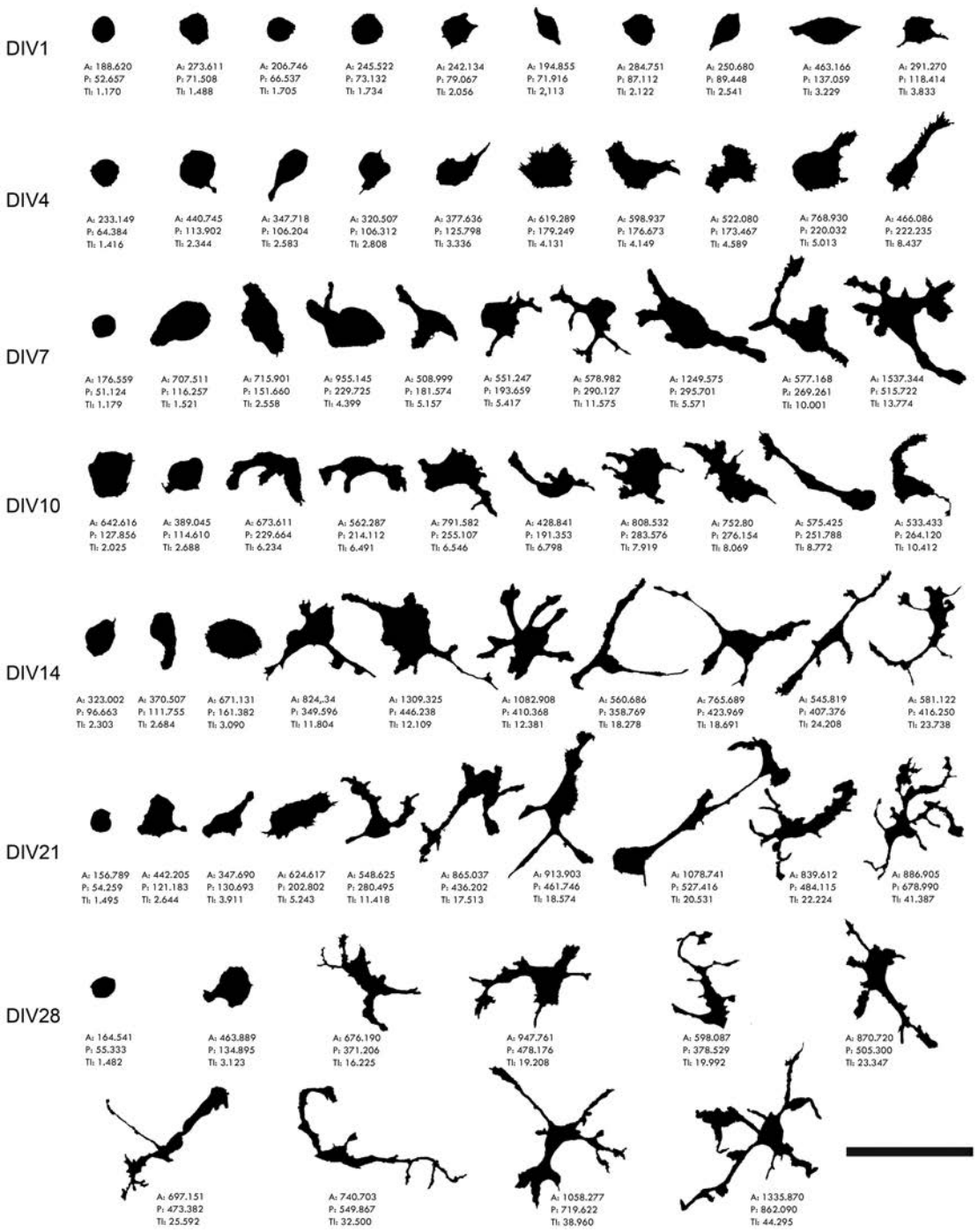

Fig. 5. Morphological heterogeneity of microglial cells after different culturing times.
The Iba1-positive microglial cells were photographed, digitized and quantitatively analyzed according to their morphological characteristics. Area (A), perimeter (P) and transformation index (TI) are indicated for each digitized cell. Ten representative cells are shown at each culturing time. While younger cultures exhibited predominantly ameboid cell forms with TI < 3, older cultures were morphologically heterogeneous, as they developed a continuum of populations with two distinct populations of microglial cells at the extrema: the ameboid cell population (TI < 3) and the ramified cell population (TI > 3). Younger cultures exhibited predominantly ameboid cell forms, while older cultures displayed more ramified forms, but also proliferating ameboid populations (see the few ameboid microglia among the mainly heterogeneous microglial cells at DIV28.

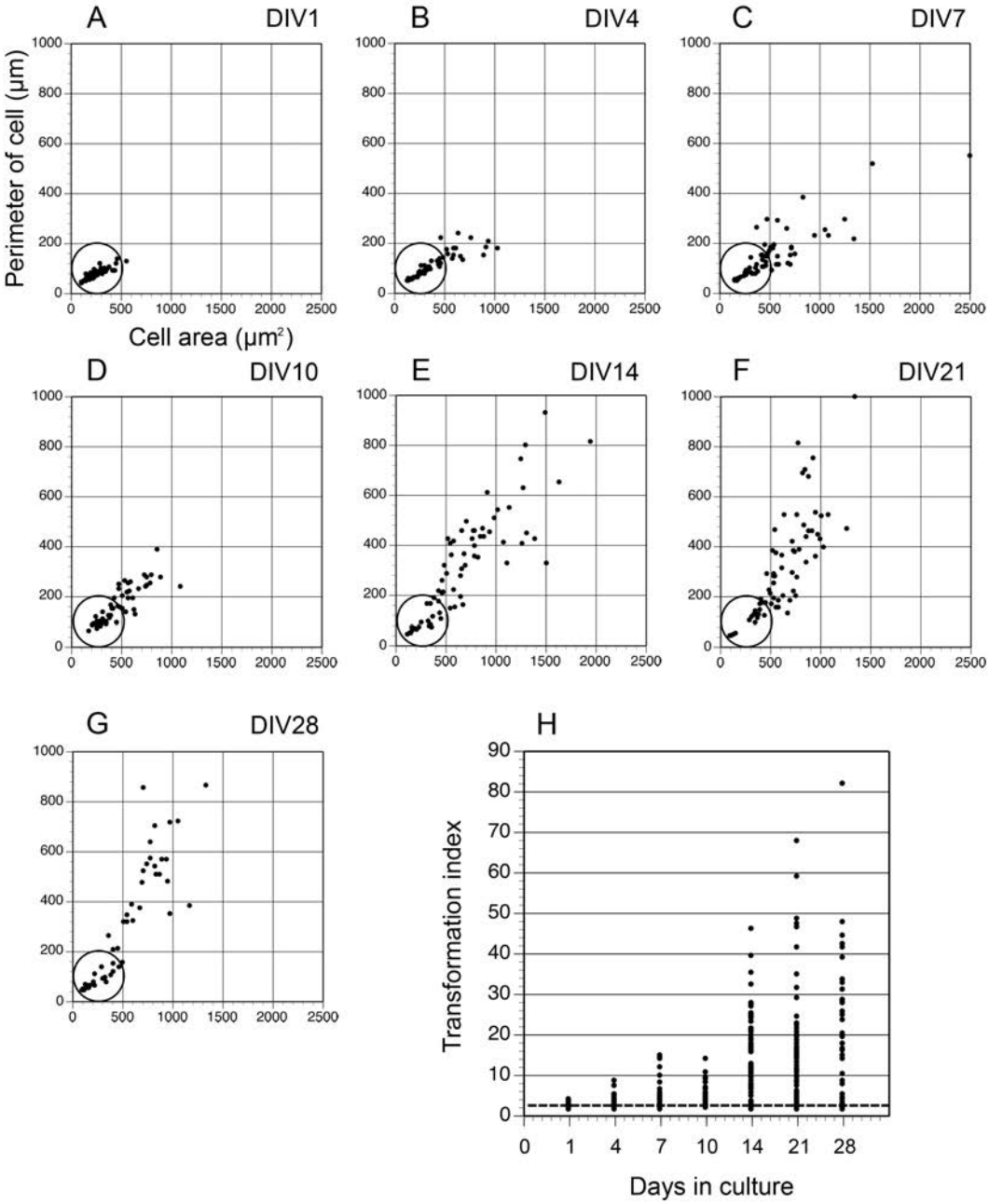

Fig. 6. Evolution of morphometric parameters of the microglial cells during culturing.
(A-G) Relationship between the perimeter of the microglial cell and its cell surface area. Cell area and perimeter values were measured by using the computer program ImageJ, and TI values were calculated as [perimeter of cell (µm)]^2/4π[cell area (µm^2)]. Each dot represents a digitized microglial cell. Some of the dots overlap at this resolution. Dots within the circles almost always indicate a cell with TI < 3 and a cell surface area < 500 µm^2. The less differentiated microglial cell populations (TI < 3) are marked with circles. **(H)** Distribution of TI values as a function of the culturing time. Microglial cells with TI < 3 are located below the dashed line. As may be seen here, there are microglial cells with extremely high TI values on DIV21 and DIV28.

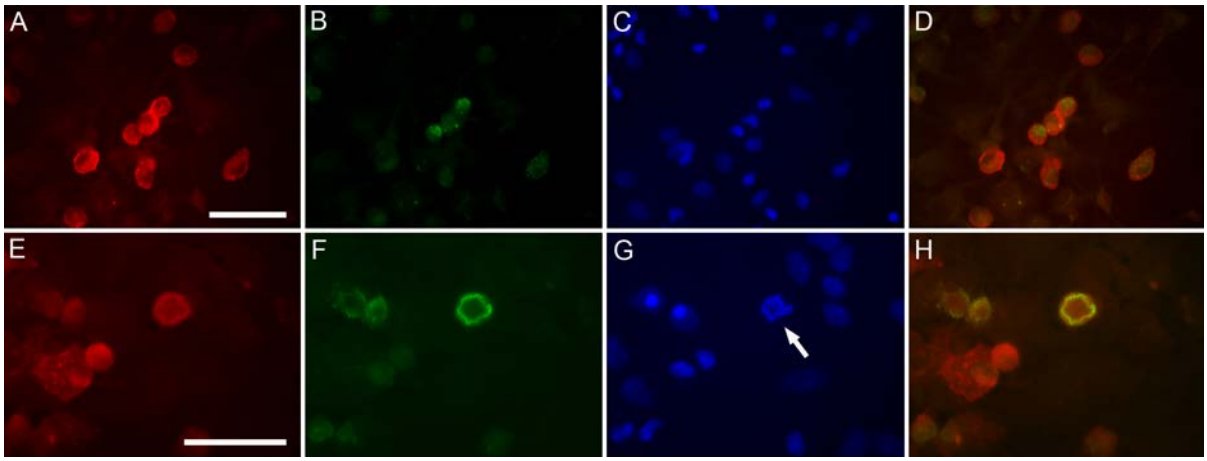

Fig. 7. Relationship between proliferation, ameboid morphology and Ki67 immunoreactivity. Representative immunocyochemical pictures of Ki67-positive ameboid microglial cells in DIV7 cultures. Fluorescent microphotographs of the cultures were taken through the red **(A, E)**, green **(B, F)** and blue **(C, G)** channels and displayed in this sequence. CD11b/c-positive microglia **(A, E)**, Ki67-positive cells **(B, F)** and Hoechst 33258-labeled cell nuclei **(C, G)** are depicted. The merged pictures of CD11b/c- and Ki67-immunolabeled microglial cells are also shown **(D, H)**. The presence of some non-microglial and non-dividing cells is indicated by the Hoechst 33258 stain at the upper right corner of the pictures. A group of CD11b/c-positive microglial cells is located at the bottom left corner of the pictures. Proliferating CD11b/c-positive microglial cells are located in the middle of the pictures. Arrow points to the condensed chromatin in an M phase microglia **(G)**. Scales for all pictures: 50 µm.

4.5. Phagocytosis is predominant in ameboid microglia in culture

Ameboid and ramified microglial cell populations in culture could be differentiated through their ability to phagocytose (Fig. 8). Unstimulated microglia readily phagocytosed fluorescent microbeads. On DIV14, when mixed populations of ameboid and ramified microglia were present in the cultures in about equal numbers, microbeads were significantly more preferred by the ameboid forms (characterized by low TI values; Fig. 8A), while the ramified microglia (with higher TI values; Fig. 8B) were less active in phagocytosing microbeads. On average, microglia with TI < 3 phagocytosed 11.08 ± 8.6 beads per cell (average ± S.D., n = 39), while microglia with TI > 3 engulfed 3.16 ± 3.6 beads per cell (n = 81); the difference was statistically significant ($p < 0.001$; Mann-Whitney Rank Sum test). When the number of phagocytosed microbeads per microglia was plotted as a function of TI under unstimulated/unchallenged conditions, the physiologically distinct populations of ameboid and ramified microglia could be readily demonstrated (Fig. 8C).

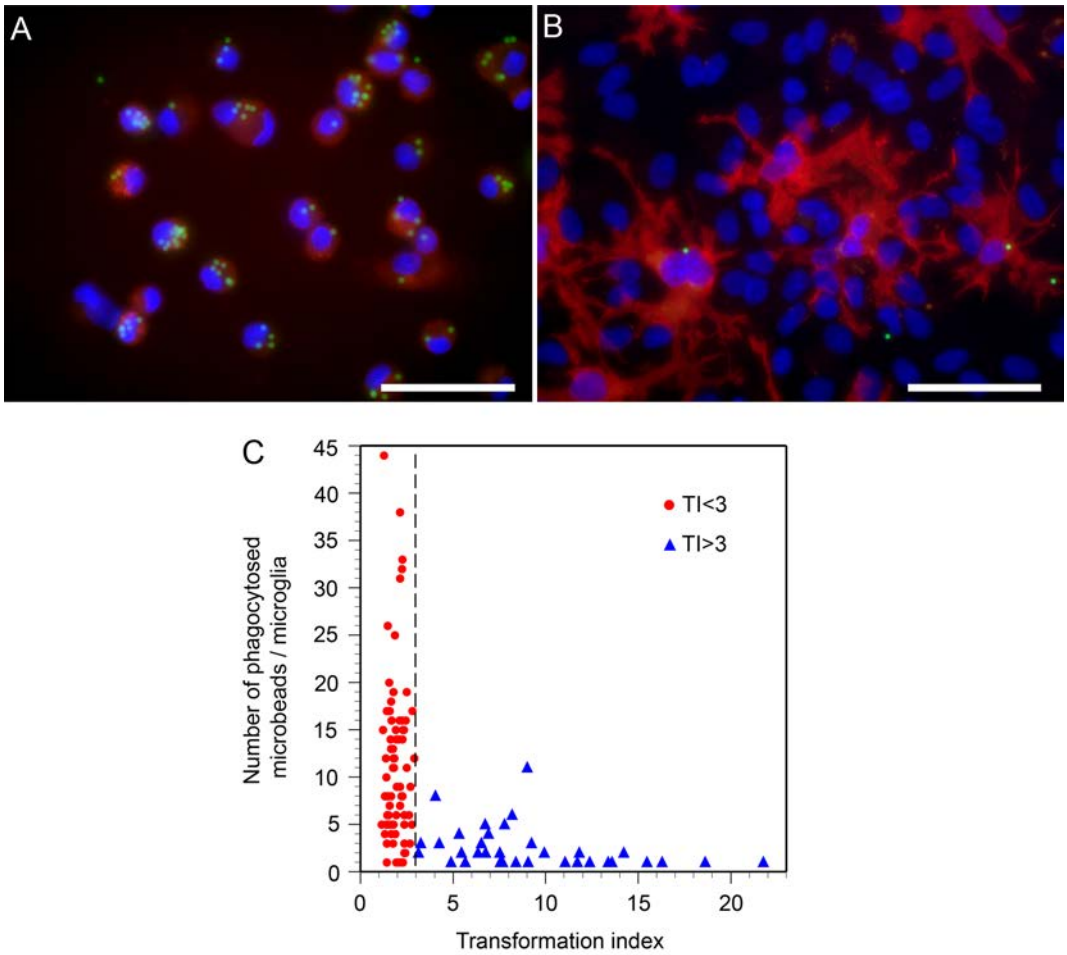

Fig. 8. Phagocytic activity of unstimulated microglial cells in a primary culture (DIV14). **(A, B)** Representative immunocyochemical pictures showing the unstimulated phagocytic capability of microglial cells (red) as a function of the TI value from the same 14-day-old culture. Fluorescent dye-coated latex microbeads (green; d = 2 µm) were added to the medium and phagocytosed by microglia. Microglial cells with TI < 3 **(A)**, i.e. ameboid forms with 11.08 ± 8.6 beads per cell, were about 3.5-times more likely to phagocytose the microbeads than cells with TI > 3 **(B)**, i.e. ramified forms with 3.16 ± 3.6 beads per cell. Non-phagocytosed microbeads were very rare in the cultures (a solitary bead can be seen in both **A** and **B**). Scale bar: 50 µm. **(C)** Distribution of unstimulated microglial cells with phagocytosed microbeads as a function of the TI value. The vertical dashed line separates the functionally different microglial populations (TI < 3 as ameboid, phagocytosing and proliferating, and TI > 3 as ramified, resting microglia).

4.6. Immunocytochemistry reveals microglial populations displaying changing molecular phenotypes during culturing

Double immunofluorescent microscopy revealed that Iba1-labeled microglial cells occasionally also expressed the HLA DP, DQ, DR antigens, exclusively in young cultures (Fig. 9A, B). HLA DP, DQ, DR-positive Iba1-expressing microglial cells were always ameboid, with TI < 3 (Fig. 9A, B). They were sporadically present from seeding up to DIV10, but disappeared completely from the cultures thereafter. Cultures older than DIV10 did not

express this antigen, even when they had an ameboid shape and proliferated, indicating that the HLA antigen expression can be uncoupled from the ameboid morphology.

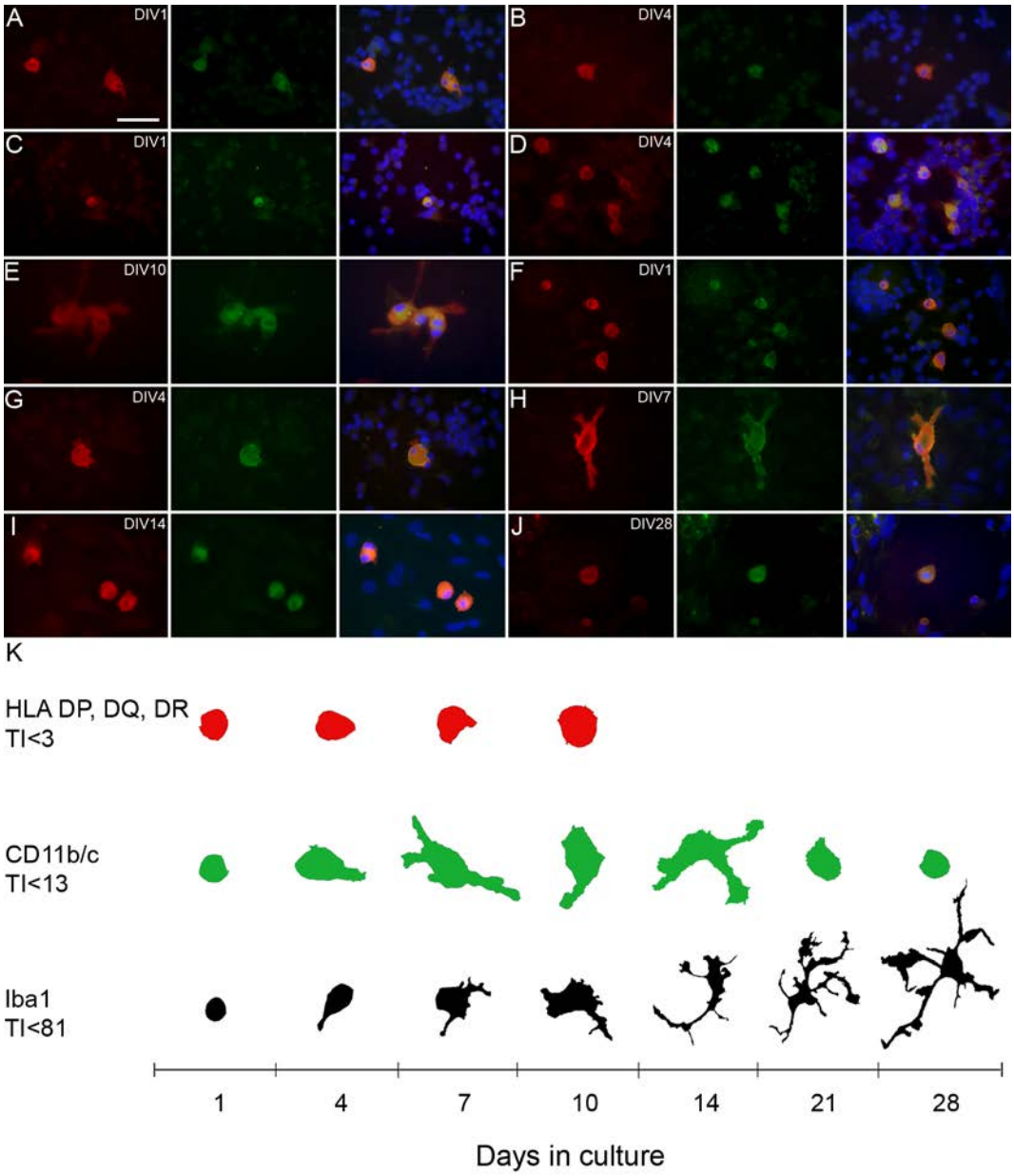

Fig. 9. Colocalizations of specific microglial markers during culturing.
Representative fluorescent microphotographs of double-immunopositive microglial cells of the cultures were taken through the red, green and blue channels and displayed in this sequence together with their merged pictures. Cell nuclei (blue) were stained with Hoechst 33258. Culturing times are indicated at the upper right corners for each triad. **(A, B)** Double-immunopositive microglial cells for the coexpression of Iba1 and HLA DP, DQ, DR antigens at DIV1 **(A)** and DIV4 **(B)**. These antigens are colocalized only in microglial cells of young cultures (up to DIV10), but solely in those that are truly ameboid or have low TI values. **(C-D)** Double-immunopositive microglial cells for the coexpression of CD11b/c and HLA DRα antigens at DIV4 **(C)** and DIV10 **(D)**. These antigens are colocalized exclusively in the young cultures and only in microglia with typical ameboid morphology. The CD11b/c-positive microglia are no longer able to express HLA antigens in older cultures. **(E-F)**

Double-immunopositive microglial cells for the coexpression of CD11b/c and Iba1 antigens at DIV7 **(E)** and DIV28 **(F)**. These antigens are colocalized only in ameboid, proliferating cells with low TI values in both young and old cultures. Iba1-immunopositive microglial cell were morphologically heterogenous as both ameboid and ramified forms were labeled throughout culturing. Scale bar for all fluorescent microscopic pictures: 50 μm. **(G)** Relationship between TI values and microglia-specific markers. During culturing, only the less differentiated, ameboid microglia (TI < 3) express HLA antigens; these cells will eventually die out or differentiate to more ramified morphologies (TI > 3) that do not express HLA antigens. CD11b/c-positive cells can be observed throughout culturing, but they never become fully ramified (TI < 13).

Microglial cells with typical ameboid morphology and doubly immunopositive for the CD11b/c and HLA DRα antigens were also found in young cultures (Fig. 9C, D). The last day on which these markers were colocalized was DIV10. CD11b/c-positive microglia in cultures older than DIV10 were no longer able to express any of these HLA antigens. CD11b/c-positive microglial cells, however, were present throughout culturing (Fig. 9C-F). CD11b/c could be colocalized with the Iba1 antigen in both young and old cultures, but only in cells with ameboid (i.e. activated, proliferating) or slightly ramified forms with TI < 13 (Fig. 9E). The Iba1-immunopositive cells predominated throughout culturing, their morphology ranging from ameboid (Fig. 9A, B) to the ramified forms (Fig. 6E). Morphologically, Iba1-positive microglia were the most heterogeneous with TI values from the whole spectrum during the culturing.

The relationship between TI values and myeloid/microglial cell-specific markers in cultured microglial cells is shown in Fig. 9G. We observed that microglial cells either lose some of their macrophage characteristics (e.g. HLA DP, DQ, DR or HLA DRα antigens) during culturing or restrict them to their less differentiated forms (e.g. CD11b/c), even though they retain this latter phenotype for subsequent generations. During culturing, only the less differentiated, ameboid microglial cells (TI < 3) expressed HLA DP, DQ, DR (or HLA DRα) antigens; these cells will either die out or differentiate to more ramified morphologies with TI > 3. CD11b/c-positive cells can be observed throughout culturing, but they never become fully ramified, and their TI values are always < 13.

4.7. CaM is differentially localized in ameboid and ramified microglia both in mixed and pure cultures

The quantity and cell type-specific localization of the CaM protein was first established in mixed primary cultures under unstimulated and untreated (control) conditions. Fluorescent immunocytochemistry (Fig. 10A-P) and Western blot analysis (Fig. 10Q, R) demonstrated

that a high concentration of CaM protein was characteristic of the mixed cultures throughout culturing. In young cultures (DIV1-DIV7), when only a few cells double-positive for the Iba1 (Fig. 10A, E) and CaM (Fig. 10B, F) antigens existed (Fig. 10A-H), most of the CaM immunoreactivity was associated with non-microglial, e.g. mainly neuronal, cell forms, as demonstrated earlier (Szabo and Gulya, 2013). From DIV14 (up to DIV28), as more Iba1-positive microglia populated the cultures (Fig. 10I, M), the proportion of CaM immunoreactivity associated with the microglia (Fig. 10J, N) also grew steadily. Both ameboid (Fig. 10A, E) and ramified microglia (a few cells in Fig. 10I, M) expressed CaM immunoreactivity. As the cultures aged, the CaM immunoreactivity localized to microglia became predominant (compare Fig. 10I, M with Fig. 10K, O). Similarly, Western blot studies confirmed the increase in Iba1 immunoreactivity during culturing (Fig. 10Q), during which time the CaM content of the cultures remained unchanged (Fig. 10R). Thus, by DIV14, the microglia had become the main CaM-expressing cell type in the mixed primary forebrain culture.

Subsequent experiments were performed on pure microglial cultures (subDIV4; Fig. 11). In these microglial cells the Iba1 immunoreactivity was most intense in the lamellipodia of the ameboid forms (Fig. 12A, D, G), followed by the perinuclear region (Fig. 12D, G). The strongest CaM immunoreactivity was always observed in the ameboid microglia, where the cell somata, and especially the perinuclear area, were the most intensely labeled (Fig. 12B, E, H). In ameboid microglia, the CaM and Iba1 immunoreactivities were distributed in a complementary manner, as the Iba1 protein tending to localize in the cell cortex and lamellipodia (Fig. 12A, B, C). The ramified microglia displayed an almost homogenous cytoplasmic Iba1 distribution (Fig. 12J) with a considerably lower CaM content typically localized around the nucleus; the branches had only traces of CaM immunoreactivity (Fig. 12K, L).

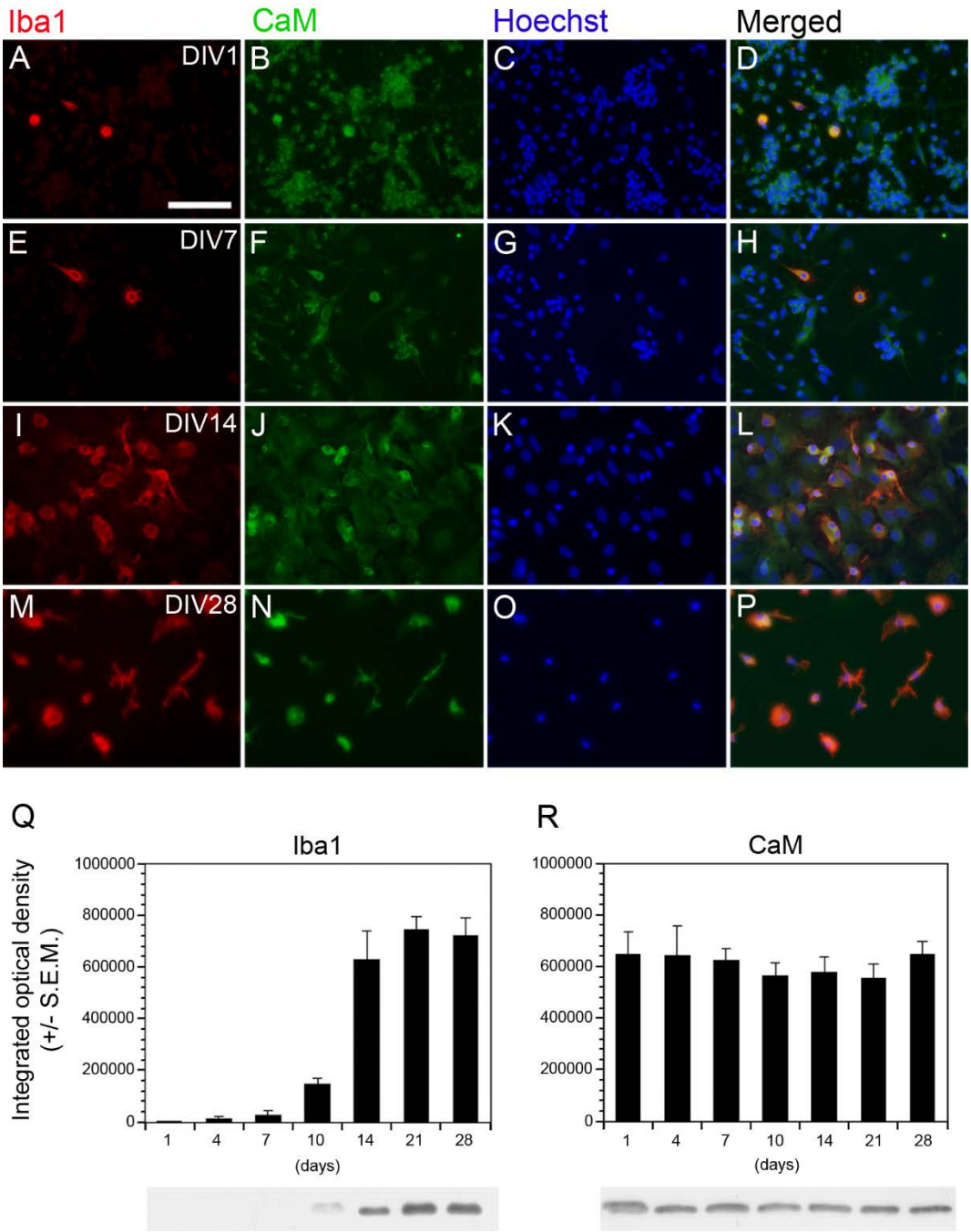

Fig. 10. Development of Iba1 and CaM immunoreactivities in primary cultures (DIV1-DIV28). At early culturing times (DIV1 **(A-D)** and DIV7 **(E-H)**), all seeded cells displayed CaM immunoreactivity (green), but only a few of them were Iba1-positive microglia (red). The cell nuclei (blue) were labeled with Hoechst 33258. Since most of the cells present early in the culturing are neurons (Szabó and Gulya, 2013), most of the CaM immunoreactivity seen at DIV1-DIV7 is of neuronal origin. At DIV14 **(I-L)**, a large number of Iba1-positive cells showed CaM positivity, a number of them were ramified. At DIV28 **(M-P)**, the predominant cell type in the culture was the CaM-positive microglia. Note the visibly different Iba1 **(M)** and CaM contents **(N)** of the ameboid and ramified microglia at this culturing time. The merged pictures show cells double-positive for Iba1 and CaM **(D, H, L, P)**. The development of Iba1 **(Q)** and CaM **(R)** immunoreactivities during culturing (DIV1-DIV28) was quantitatively analyzed on Western blots. Protein samples from primary cultures were separated by gel electrophoresis, transferred to nitrocellulose membranes and probed with either

the Iba1 (**Q**) or CaM (**R**) antibody. Gray scale digital images of the immunoblots were acquired by scanning the autoradiographic films with a desktop scanner. The images were scanned and processed at identical settings to allow comparisons between the Western blots from different samples. Error bars indicate integrated optical density values (mean ± S.E.M.). Representative Western blot pictures are shown below the graphs. During culturing (DIV1-DIV28), a massive increase in the number of cells with microglial phenotype was observed in the mixed primary cultures, while the CaM content of the cultures remained constant. Most of the gain in Iba1 content occurred between DIV10 and DIV14. Culturing times are indicated at the upper right corners **(A, E, I, M)**. Scale bar in **A** for all pictures: 50 µm.

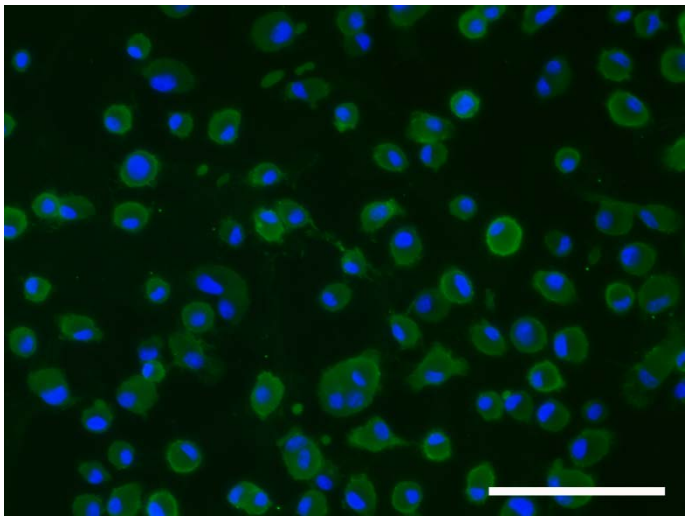

Fig. 11. Localization of Iba1 immunoreactivity in pure microglial cell cultures (subDIV4). Representative photomicrograph of Iba1 imunoreactive microglial cells in culture. The purity of this culture is close to 100%, since every Hoechst 33258-labeled cell nuclei (blue) is surrounded by Iba1 immunopositive cytoplasm (green). Scale bar: 100 µm.

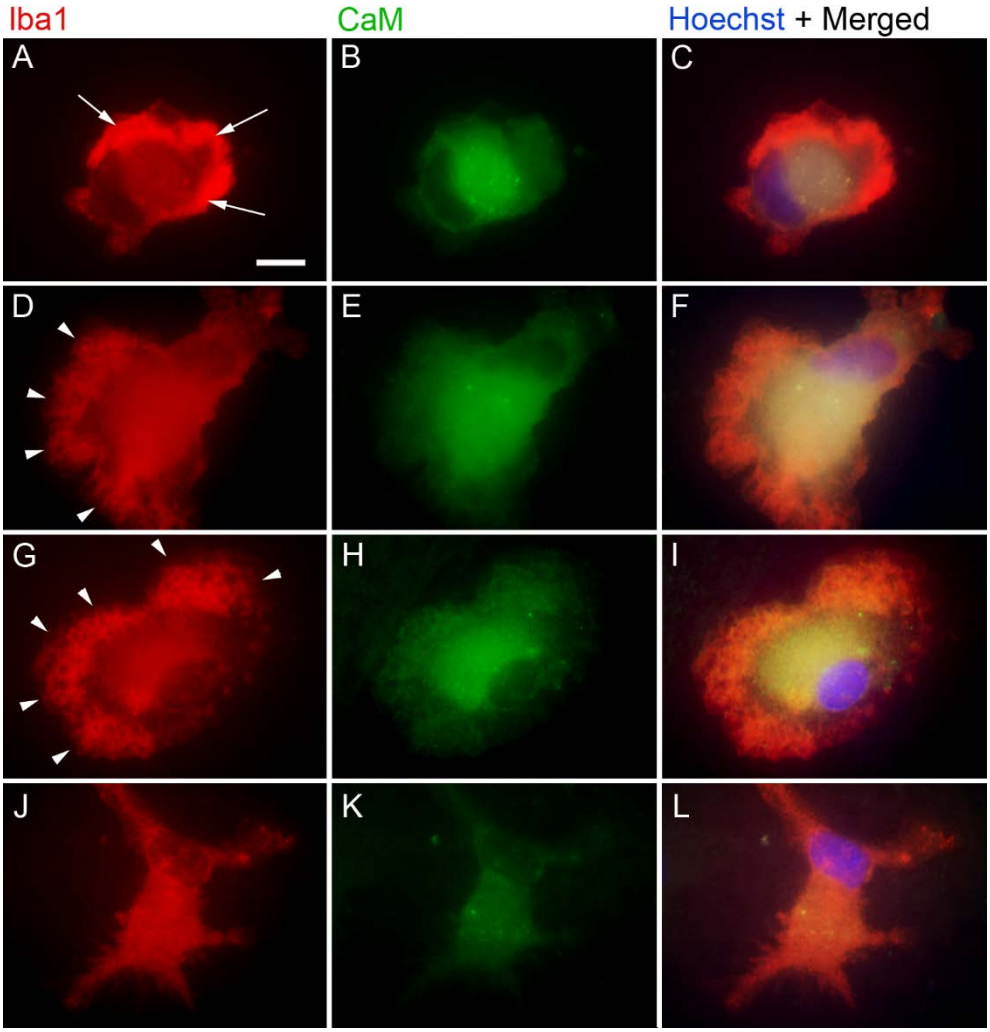

Fig. 12. Distribution of Iba1 and CaM immunoreactivities in pure microglial cells (subDIV4). In pure microglial cultures (subDIV4), the majority of the unchallenged cells were ameboid or slightly ramified. While the Iba1 immunoreactivity (red) could be localized into two subcellular compartments, the perinuclear and the cell cortex domains **(A, D, G, J)**, the CaM immunoreactivity (green) was largely confined to the perinuclear region **(B, E, H, K)**, with the cell cortex having a considerably smaller CaM content, which progressively diminished deeper into the branches. Merged pictures **(C, F, I, L)** show the cell nuclei (blue) and the overlapping Iba1 and CaM immunoreactivities predominantly localized to the perinuclear area. Ameboid microglia have predominantly cortically localized Iba1 immunoreactivity in the leading edges of large lamellipodia (**A**, arrows), a cytoplasmic domain largely devoid of CaM immunoreactivity (**B**). Arrowheads **(D, G)** point to large lamellipodia. Scale bar in **A** for all pictures: 10 µm.

4.8. CaM inhibition affects cell morphology and actin cytoskeleton reorganization

The microglial morphology in the control and experimental groups was analyzed through binary silhouettes (Fig. 13). The quantitative analysis was based on the area, perimeter and TI, the latter being a dimensionless number that is an indicator for the degree of process extension of a cell.

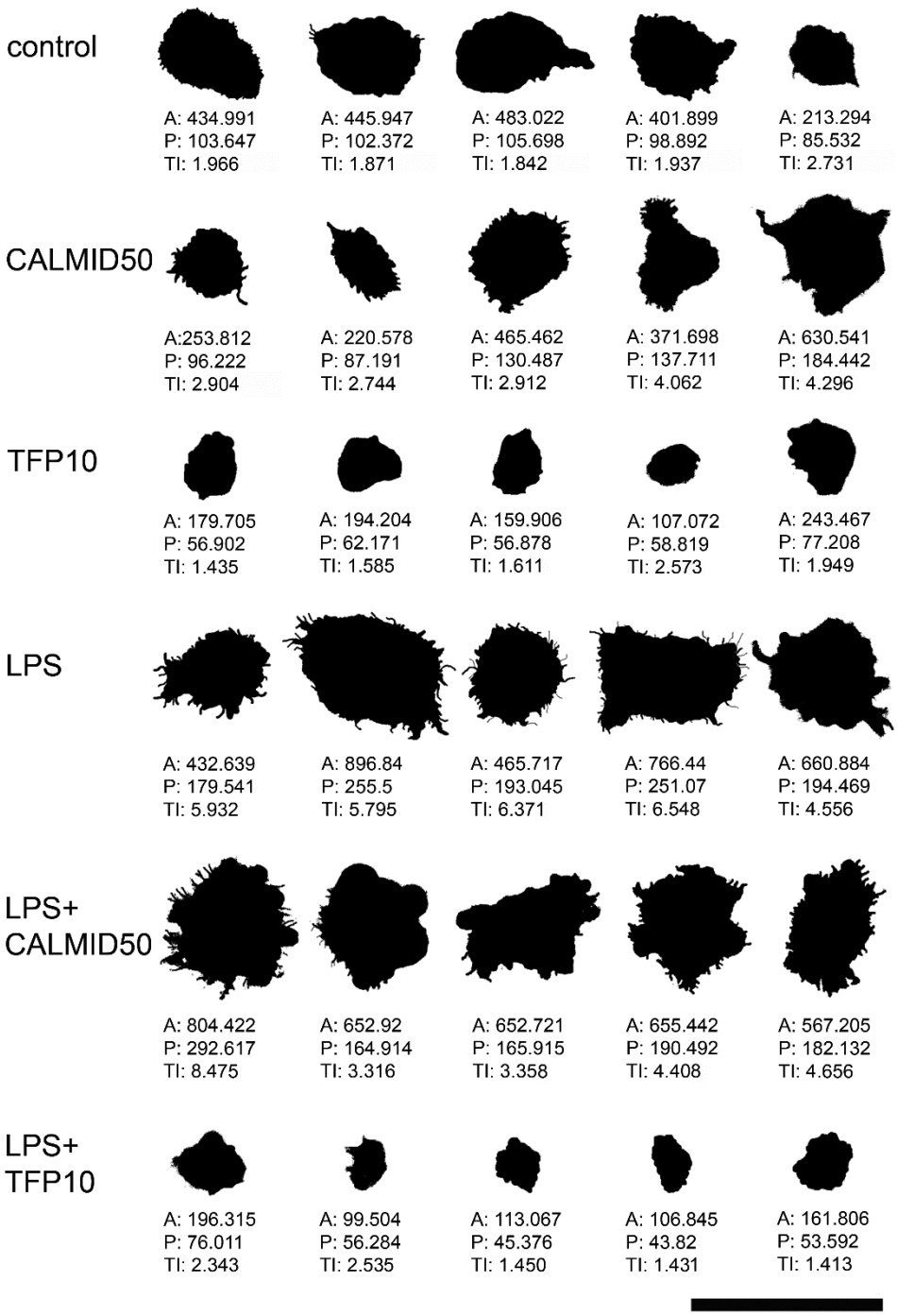

Fig. 13. Representative binary silhouettes from pure microglial cultures after different treatment regimens.

Iba1-positive microglial cells from pure microglial cultures (subDIV4) were photographed, digitized and quantitatively analyzed according to their morphological characteristics. Five representative binary silhouettes are shown at each culturing time. CALMID50, in either control or LPS-challenged microglia, increased the number of filipodia, while the complete absence of filipodia was seen both in TFP10 and in LPS+TFP10-treated microglia. Area (A) in μm^2, perimeter (P) in µm, and TI values (calculated as $[\text{perimeter of cell } (\mu m)]^2/4\pi[\text{cell area } (\mu m^2)]$) are indicated for each digitized cell. LPS: 100 ng/ml; CALMID50: 50 nM CALMID; TFP10: 10 µM TFP. Scale bar for all silhouettes: 50 µm.

Throughout the experiments, microglial cells with TI < 3 were considered ameboid. The unchallenged, untreated 4-day-old pure microglia culture (subDIV4) consisted mainly of ameboid cells (Fig. 13, control row; see also controls in Figs. 15, 16) with an average area of 412.91 ± 27.2 μm^2, perimeter of 100.73 ± 5.4 μm and a TI of 2.02 ± 0.1 (Fig. 14). When administered alone, CALMID and TFP affected TI and the microglial cell surface area and perimeter differently. For example, both CALMID5 and CALMID50 resulted in increased area, perimeter and TI, whereas TFP alone strongly inhibited these characteristics. When challenged with LPS, the microglia became enlarged and acquired significantly larger perimeter and TI (A = 777.23 ± 40.1 μm^2, P = 238.97 ± 8.6 μm, TI = 6.14 ± 0.4), consistent with these cells becoming activated (Figs. 13, 14 and Fig. 15D-F). Interestingly, CALMID5 or CALMID50 alone was not effective but when used in combination with LPS, they significantly increased the cell surface area, perimeter and TI (Fig. 13, Fig. 14A, C, E, Fig. 15G-I). TFP sigificantly inhibited the expansion of cell surface area and perimeter both in unchallenged and LPS-challenged cells (Fig. 14B, D). As an example, the cell surface area was decreased substantially after TFP or LPS+TFP treatment, to 46.4 or 44.5% of the unchallenged or LPS-challenged control value, respectively. TFP treatment was also very effective in decreasing TI, to 25.53% of the LPS-challenged value (Fig. 13, 14).

CaM inhibition affected the microglial morphology through reorganization of the actin cytoskeleton (Fig. 15). In unchallenged and untreated (control) cultures, the Iba1- and phalloidin-related fluorescence signals largely overlapped in the cell cortex of the mainly ameboid microglia, often in lamellipodia (Fig. 15A-C) as expected, since they both bind to the actin cytoskeleton. When treated with LPS, the microglia that became activated and enlarged displayed a phalloidin distribution much fuzzier than that in the case of Iba1, probably due to the rapid association of fibrous actin, to which phalloidin preferentially binds (Fig. 15D-F). However, spot-like concentrations of phalloidin fluorescence resembling podosomes were often visible in LPS-treated cells (Fig. 15E, arrow). CaM inhibitors affected the Iba1 and phalloidin distributions in different ways. CALMID50 treatment resulted in phalloidin fluorescence that was clearly distributed in two distinct concentric rings in the cytoplasm, one ring in the cell cortex, and the other as a perinuclearly localized cytoplasmic streaming of freshly synthesized fibrous actin (Fig. 15H, K, arrows). Phalloidin-containing filipodia were also obvious in these cells. Similar, albeit less dense, Iba1 distribution was observed after CALMID50 treatments (Fig. 15G). TFP treatment resulted in an overlapping and almost homogenous distribution of both Iba1 immunoreactivity and phalloidin fluorescence

(Fig.15M-O) in the surviving cells. While the Iba1 immunoreactivity remained relatively intact (Fig. 15M), most of the phalloidin fluorescence intensity was lost in TFP-treated microglia (Fig. 15N) indicating that TFP affected actin polymerization.

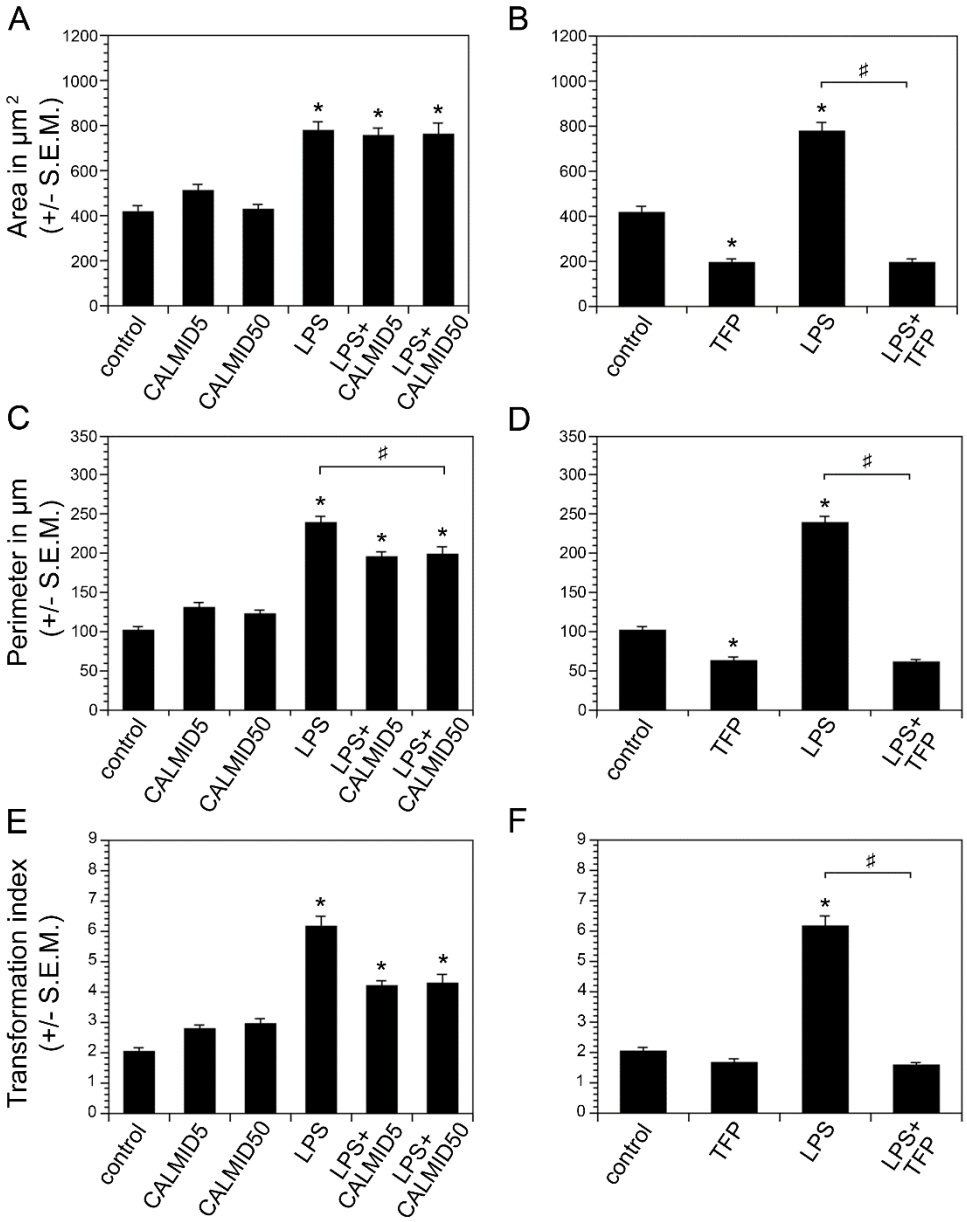

Fig. 14. Effects of CaM inhibitors on selected morphological parameters of pure microglial cells. Surface area **(A, B)** in µm^2, perimeter **(C, D)** in µm, and TI values **(E, F)** of the microglia for CALMID **(A, C, E)** and TFP **(B, D, F)** were analyzed in pure unchallenged and LPS-challenged microglial cell cultures. All statistical comparisons were made by using SigmaPlot (v. 12.3, Systat Software Inc., Chicago, IL, USA) and analyzed with Kruskal-Wallis one-way analysis of variance, followed by Dunn's method for pairwise multiple comparison procedures for statistically significant differences between the groups. Values (mean ± S.E.M.) were computed from at least three independent culturing experiments. *Statistically significant from control ($p<0.05$); #statistically significant from LPS-treated cells. LPS: 100 ng/ml; CALMID5: 5 nM CALMID; CALMID50: 50 nM CALMID; TFP10: µM TFP.

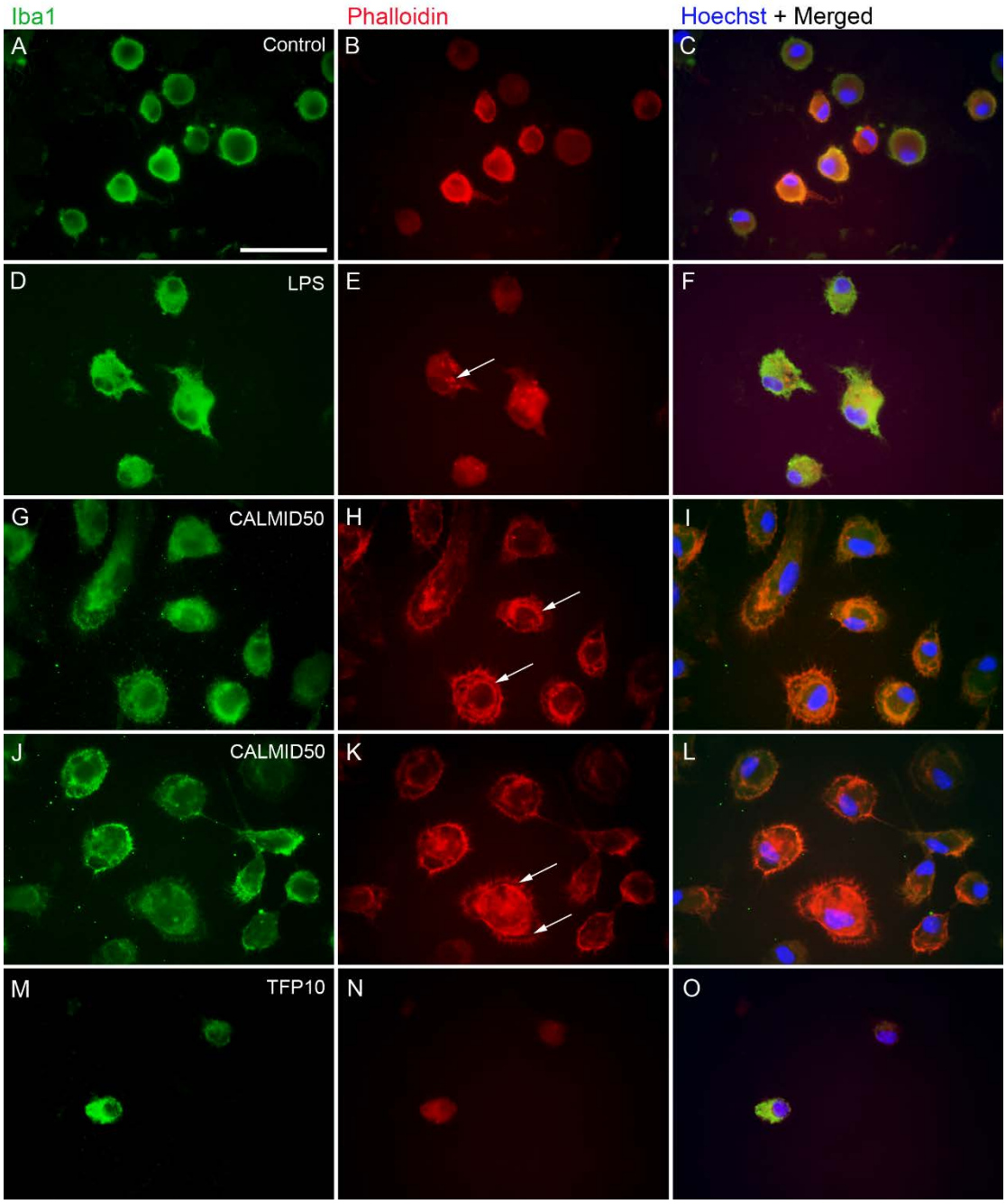

Fig. 15. Immunocytochemical localization of actin-binding proteins in pure microglial cells. Iba1 immunoreactivity **(A, D, G, J, M**; shown here in green**)** and phalloidin fluorescence **(B, E, H, K, N**; shown in red**)** were colocalized in unchallenged and untreated (control) cells and in microglia treated with LPS or CaM inhibitors in pure microglial cultures (subDIV4). Merged pictures **(C, F, I, L, O)** show the Hoechst 33258-labeled cell nuclei (blue) and the colocalization of Iba1 immunoreactivity and phalloidin fluorescence. Filamentous actin often forms continuous ring-like lamellipodia in unchallenged microglia **(B)**. In LPS-challenged microglial cells, lamellipodia were less dominant, but the toxin stimulated podocyte formation, as indicated by several puncta delineated by phalloidin fluorescence **(**arrow, **E)**. When CALMID50 was used, strong lamellipodia formation was observed, often accompanied by a perinuclear cytoplasmic streaming of filamentous actin **(**arrows, **H, K)**, giving a double-ringed appearance of these cells. TFP treatment abolished the formation of filamentous actin bundles as detected by phalloidin fluorescence microscopy **(N)**. LPS: 100 ng/ml; CALMID50: 50 nM CALMID; TFP10: 10 µM TFP. Scale bar in panel **A** for all pictures: 50 µm.

4.9. CaM inhibitors differentially alter the intracellular localization of CaM, and affect the Iba1 and CaM protein expressions

CaM inhibitors altered the intracellular localization of CaM protein (Fig. 16). Both unchallenged and untreated cells (Fig. 16A-C) and LPS-challenged cells (Fig. 16D-F) displayed high CaM content primarily localized in the perinuclear compartment and to a much lesser extent with that in the cell cortex (Fig. 16A, B). Some of the cells with larger TI had CaM immunoreactivity that progressively diminished toward the cell cortex (Fig. 16C). Interestingly, cells treated with CALMID50 alone displayed a more heterogenously translocated CaM immunoreactivity often cortically localized in lamellipodia (Fig. 16J-L, arrowheads). In TFP10-treated cells, the CaM immunoreactivity was very weak and homogenously distributed in the cytoplasm (Fig. 16M-O).

CaM antagonists inhibited Iba1 and CaM protein expressions with different efficacies (Fig. 17). In general, CALMID was less potent than TFP in affecting Iba1 and CaM protein expressions. CALMID, either alone or in combination with LPS, was not able to alter the Iba1 expression significantly (Fig. 17A). TFP was more potent as TFP10 and TFP20 inhibited Iba1 protein expression in a dose-dependent manner both in unchallenged and LPS-challenged cells (Fig. 17C). Similarly to their effects on the Iba1 expression, CALMID and TFP antagonized the CaM protein expression with different efficacy (Fig. 17B, D). When CALMID was used, the CaM immunoreactivity was observed to decrease somewhat dose-dependently in the unchallenged microglia as CALMID50 significantly inhibited the CaM protein expression to 38.6% of the control level (Fig. 17B). Again, TFP20 had a more profound effect on the CaM protein expression (Fig. 17D), as it exhibited a strong inhibition both in the unchallenged and in the LPS-activated microglia (20.8% and 23.4% of the control value, respectively).

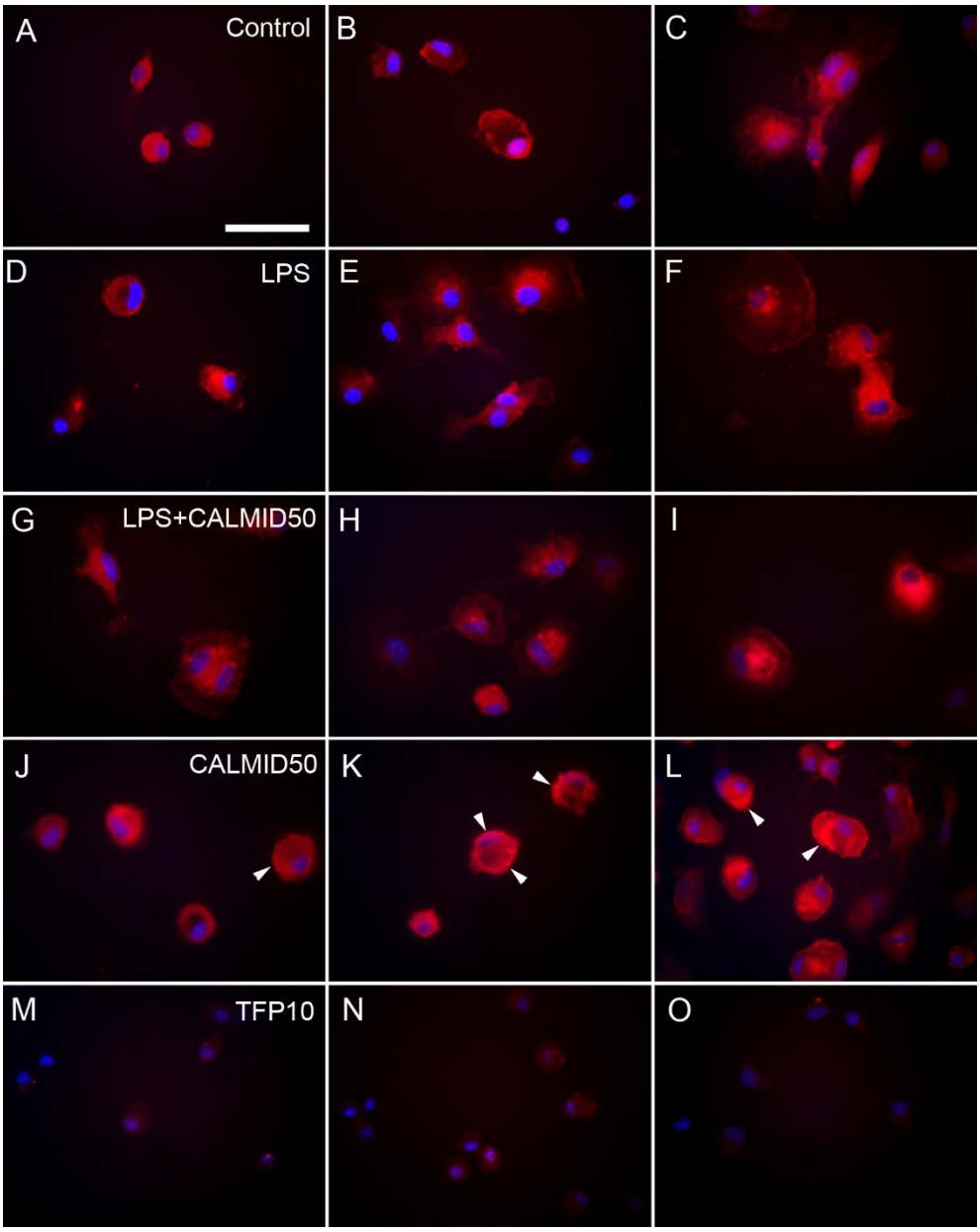

Fig. 16. Effects of CaM inhibitors on the intracellular localization of CaM immunoreactivity in pure microglial cells.

Representative immunocytochemical pictures showing the intracellular distribution of CaM immunopositivity (red) in pure microglia cells (subDIV4). The merged pictures show the cell nuclei (blue) that were stained with Hoechst 33258. The unchallenged and untreated (control) microglia (**A-C**) and LPS-challenged cells (**D-F**) showed mainly perinuclearly localized CaM immunoreactivity. LPS-challenged and treated cells (**G-I**), and more typically CALMID50-treated microglia (**J-L**) displayed CaM distribution often more targeted to the cell cortex and developing lamellipodia (arrowheads). TFP treatment resulted in a significant cell death (see Figure 4) and a homogenous cytoplasmic distribution of CaM immunoreactivity in the surviving microglia (**M-O**). LPS: 100 ng/ml; CALMID50: 50 nM CALMID; TFP10: 10 μM TFP. Scale bar in panel **A** for all pictures: 50 μm.

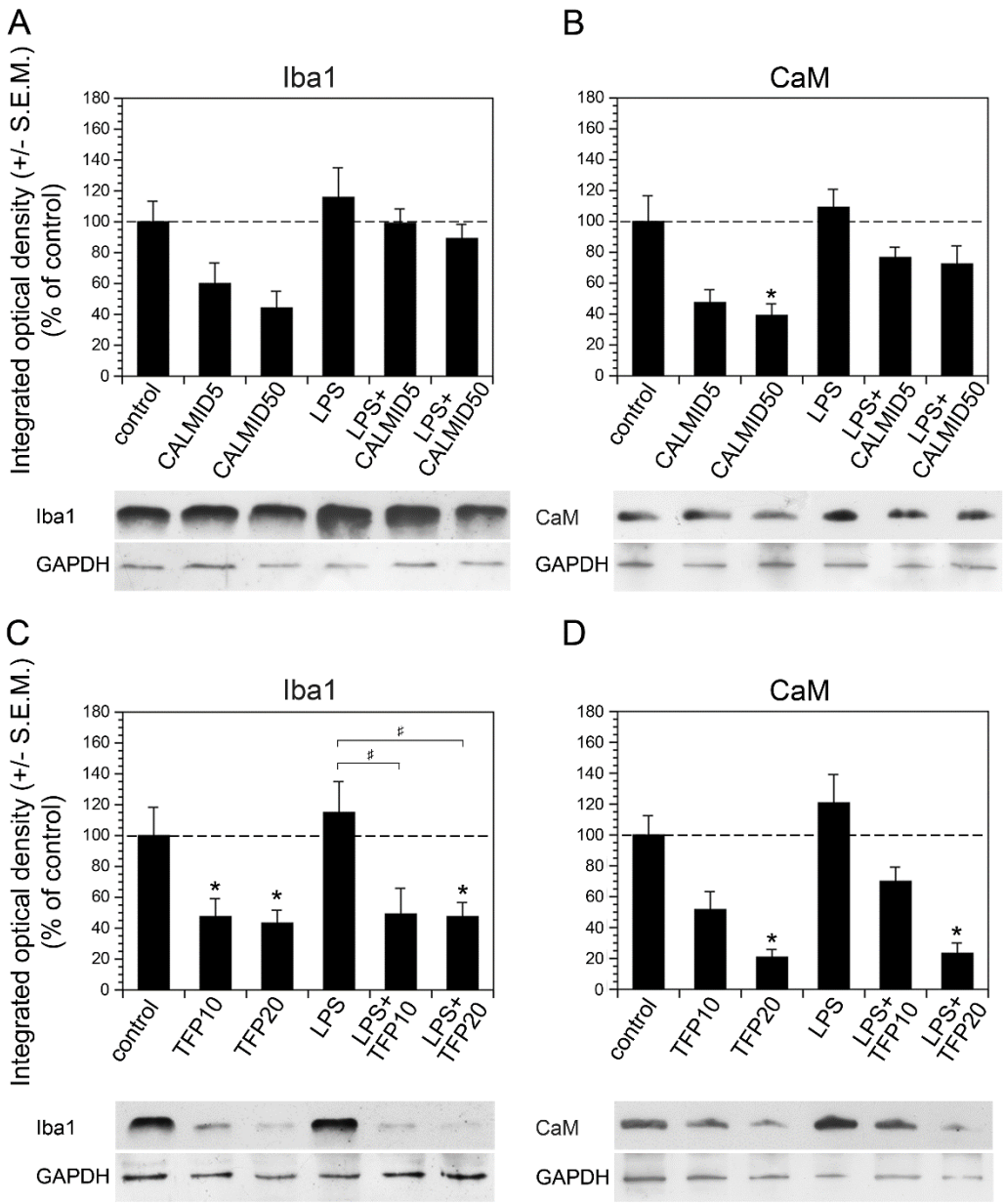

Fig. 17. Effects of CaM inhibitors on Iba1 and CaM protein expression in pure microglial cells, as detected by Western blot analysis.

Quantitative Western blot analysis of Iba1 (**A, C**) and CaM (**B, D**) immunoreactivities in pure microglial cell cultures (subDIV4). Representative Western blot pictures of the respective immunoreactivities are shown below the graphs together with the GAPDH immunoreactive bands that served as inner standards in the same gel. Protein samples were collected from 3 separate culturings, each involving plating on at least 6 Petri dishes, electrophoresed and quantitatively analyzed as described in the Materials and methods section. The integrated optical density data (mean ± S.E.M.), normalized to GAPDH immunoreactivities, were analyzed with Kruskal-Wallis one-way ANOVA on ranks, followed by pairwise multiple comparisons (Dunn's method). *Statistically significant from control ($p<0.05$); #statistically significant from LPS-treated cells. Iba1: ionized calcium-binding adaptor molecule 1; CaM: calmodulin; LPS: 100 ng/ml; CALMID5 and CALMID50: 5 and 50 nM CALMID; TFP10 and TFP20: 10 and 20 μM TFP; GAPDH: glyceraldehyde 3-phosphate dehydrogenase.

5. DISCUSSION

Ramified microglial cells, the most common form of microglial cells in the normal adult brain, are derived from macrophage-like cells of mesodermal origin (Dalmau et al., 1997; Gehrmann et al., 1995; Ling and Wong, 1993). Many lines of evidence have recently demonstrated that these "true" resident microglial cells can be distinguished from other myeloid monocytic cells in the CNS from the aspects of their location, origin, specific cell surface antigens, other biochemical markers, their functions and their turnover with the periphery. Adult resting microglia with ramified forms reside in the parenchyma of the CNS, their position often being juxtavascular (Davalos et al., 2005; Ginhoux et al., 2010). They express a defined set of markers differently from other myeloid cell populations of the CNS (including, for example, CD11b, F4/80, the chemokine receptor CX3CR1 and Iba1), and function as local immune surveyors and scavengers of cell debris; the true, resident microglia population does not participate in exchange with the circulation (Prinz et al., 2011). Myeloid cell populations of the CNS with specific patroling functions include the perivascular, the meningeal and the choroid plexus macrophages, which possess slightly different sets of markers, but always take part in extensive exchange with the myeloid cells of the circulation (Bechmann et al., 2001a, b; Chinnery et al., 2010; Hawkes and McLaurin, 2009; Kim et al., 2006; Vallières and Sawchenko, 2003) and the vessel-patroling resident monocytes and inflammatory monocytes that originate from and display a high turnover with the bone marrow (Auffray et al., 2009; Geissmann et al., 2003).

Discrimination between the different myeloid monocytic cell forms with uniquely important in vivo functions was beyond the scope of this study when cells were collected for the primary culture. Previous studies on the preparation of tissue slices (Hailer et al., 1996, 1997; Stence et al., 2001) and primary cultures (Floden and Combs, 2006) indicated that physical damage to cells during tissue handling and cell harvesting (tissue removal from the embryo, sectioning, cell isolation procedure, etc.) can alter the microglial morphology, marker expression and function, and the resulting molecular characteristics seen in vitro may not necessarily reflect the in vivo phenotype. It is possible, therefore, that the cells we harvested from E18 rat forebrains and later identified as Iba1-positive included many of the myeloid monocytic cell populations described above, but the prolonged culturing led to the development of molecular and functional phenotypes quite different from those seen in vivo, and perhaps even sparser, less differentiated myeloid-derived cell populations when cultured.

Earlier attempts to characterize microglial cells in vitro frequently employed culturing times of less than a week (Becher and Antel, 1996; Otani et al., 2011; Tanaka et al., 1998),

when changes in microglial population dynamics were not always apparent. Microglia cultured from the embryonic or from the adult brain were also found to differ in many important ways. Microglia prepared from the adult rat brain became progressively de-differentiated and acquired a phenotype reminiscent of that of activated microglia in vivo over a period of 7 days in culture (Slepko and Levi, 1996). The differences between microglia acutely isolated from the CNS and cultured microglia derived from mixed glial cultures were most clearly seen in their differential proliferative capacity and cytokine responsiveness (Ford et al., 1995; Frei et al., 1994). Unlike microglia from cultures, microglial cells from adults were not stimulated by transforming growth factor (Rozovsky et al., 1998), nor did they proliferate in response to granulocyte- or macrophage colony-stimulating factor (Ford et al., 1995). While the concept of M1/M2 macrophage heterogeneity has gained momentum in recent years, there is considerable uncertainty as to the extent to which this notion could be extrapolated to microglial cells. For example, in a recent study, Durafourt et al. (2012) found that M1 and M2 subtypes of macrophages and those of the microglial cells not only differentially expressed a number of genes, but phagocytosed myelin quite differently, indicating that the expression of similar biomarkers by macrophages and microglia does not necessarily mean that they have the same function.

Our results showed that microglia prepared from embryonic tissue and maintained for up to 4 weeks displayed multiple phenotypes with different immunologic, proliferative and phagocytic characteristics. While the number of total cells did not vary significantly during culturing, their composition exhibited a dramatic change. The number of microglial cells rose steadily during culturing, by a factor of 67-fold. The selected microglial antigenic and functional (proliferation and phagocytosis) properties in primary mixed cultures of E18 rat forebrain tissues revealed a marked morphological and antigenic differentiation during culturing.

Morphometric analysis on binary silhouettes of microglial cells revealed that ameboid forms were dominant in the early stages of in vitro differentiation, while older cultures were characterized by mixed populations of ameboid and ramified cells, the latter being the dominant form. The ameboid microglia, characterized by TI < 3, was the mitotically active, Ki67-immunopositive population even in older cultures where it formed a core of proliferating cells. The feasibility of a quantitative assessment of different microglial populations (resting vs. activated microglia) through morphological features alone was recently demonstrated (Kozlowski and Weimer, 2012); the sensitivity of this automated method was reported to be comparable to that of immunohistochemical methods.

While the morphology of the cultured microglial cells was very similar to that in the normal rat brain, their antigenic markers specific for the monocyte/macrophage/microglial cell line were distinctly different and exhibited a more restricted immunological phenotypic repertoire from those seen in vivo. We found that microglial cell populations in culture, without the presence of recruited hematogenous macrophages from the periphery through the blood-brain barrier, were more similar to those in the normal adult (or physiologically aging) brain (e.g. showing no signs of significant neurodegeneration and therefore almost no turnover for the microglial cells with the periphery) than to those in the neuropathologic brain (e.g. in Alzheimer's disease). The large flux of HLA DP, DQ, DR-positive macrophages that entered the E18 brain through the blood-brain barrier soon died or differentiated further in the culture. As a consequence, cultured microglial cells that were doubly positive for Iba1 and HLA DP, DQ, DR antigens were absent from cultures older than DIV10. This is in contrast with earlier reports of an upregulation of HLA class II proteins upon phagocytosis (Becher and Antel, 1996; Beyer et al., 2000; Smith, 2001), a function displayed by ameboid microglial cells throughout the entire culturing, although they were negative for the HLA DP, DQ, DR antigens after DIV10.

The loss of a large number of cells, which peaked on DIV10, concomitantly with the formation of neuronal clumps in the culture, could be coupled causatively to microglial activation and proliferation in two ways: either the massive neuronal death triggered microglia proliferation or, conversely, the proliferating microglial cells adversely influenced and eventually killed some other cells in the culture. This neuronal loss, most prominent around DIV10, was documented by Western analysis and was accompanied by an increase in the phagocytic activity of these cells. Interestingly, microglia proliferation could also be linked to the observed increase in CNPase activity during culturing. Similar phenomenon was observed in neonatal mouse brain cultures (Amur-Umarjee et al., 1990). Such microglia-oligodendrocyte interactions could be due to factors secreted by activated microglia that promote oligodendrocyte proliferation and differentiation (Deierborg et al., 2010).

One of the main roles of microglia is phagocytosis, a process that is critical for the uptake and degradation of infectious agents and senescent cells, and which contributes to the immune response and inflammation (Aderem and Underhill, 1999; Marín-Teva et al., 2004). As reviewed by Neumann et al. (2009), the recent evidence suggests that the phagocytic clearance by the microglia plays a fundamental role in facilitating the reorganization of neuronal circuits and triggering repair mechanisms. For example, there are substantial differences in microglial phagocytosis during the restructuring of neuronal connections

(Marín-Teva et al., 2004), in acute CNS injury (Cullheim and Thams, 2007), in multiple sclerosis (Takahashi et al., 2007), in normal development and ageing (Streit, 2006) or in Alzheimer's disease (Meyer-Luehmann et al., 2008), and the insufficient level of clearance seen in certain neurodegenerative diseases might be associated with an inadequate regenerative response such as that in Alzheimer's disease.

We used unstimulated microglial cells to measure phagocytic activity for two reasons: 1) certain immunomodulatory functions could be reduced in stimulated microglia (Magnus et al., 2004), and 2) there could be a differential expression of a number of microglial enzymes and markers upon stimulation (Imamura et al., 1991). Both such effects could lead to the ameboid microglial phenotype being favored, which could interfere with our statistical analysis. The fact that unstimulated ramified microglia do not proliferate (Imamura et al., 1991) ruled out the possibility that the conversion to the ameboid form would be induced, thereby biasing the actual composition of the microglial pool. We found that unstimulated microglial phagocytosis was tightly coupled to the ameboid morphology, as cells with low TI values exhibited much higher phagocytic activity. The ameboid morphology was also related to the proliferation of the microglial cells, as low TI values were always present in the cultures.

As microglial cells participate in both protective and pathogenic mechanisms in the healthy and in the diseased CNS, further correlative morphological, molecular and functional characterizations of cultured rat microglial cell populations similar to that presented here could provide further information concerning the specific roles of the different microglia cells in the physiology and the pathophysiology of the CNS. In vitro phenotyping of these cells could also be important in providing detailed information on how different signals may activate the microglial cell populations, on their relation to each other and their origin, on the regulation of their migration, etc. Furthermore, therapeutic approaches through which to modify the microglial responses could also benefit from in vitro studies similar to that presented here.

One of the most ubiquitous Ca^{2+}-sensing proteins is CaM. Its distributions in the developing and the adult rodent brain have been well documented (Caceres et al., 1983; Seto-Ohshima et al., 1983). It is encoded by three different genes in mammals (Palfi et al., 2002; Toutenhoofd and Strehler, 2000). The expression patterns corresponding to the three CaM genes display a broad differential distribution in the developing (Kortvely et al., 2002) and the adult rat CNS under both physiological (Kovacs and Gulya, 2002, 2003; Palfi et al., 1999; Solá et al., 1996) and pathophysiological conditions (Palfi et al., 2001; Palfi and Gulya, 1999;

Vizi et al., 2000). Quantitative analysis of the expression patterns of these genes indicated a differential dendritic targeting of the CaM mRNAs (Kortvely et al., 2003; Palfi et al., 1999, 2005); differential intracellular targeting of selected CaM mRNA populations could serve for the local translation of the necessary CaM proteins that regulate the numerous target proteins in that particular cytoplasmic compartment (Kortvely and Gulya, 2004).

CaM expression could be regulated by a number of different physiological and pathophysiological cues. Although its gene expression is generally very stable (Kortvely and Gulya, 2004; Palfi et al., 2002), we have identified many factors that could differentially affect the expressions of the individual CaM genes in neurons with distinct phenotypes from different brain regions (Orojan et al., 2006; Palfi et al., 1999, 2002; Bakota et al., 2005), e.g. inflammation (Orojan et al., 2008), ischemia (Palfi et al., 2001), dehydration (Palfi and Gulya, 1999), and chronic ethanol treatment and withdrawal (Vizi et al., 2000). Apart from the neurons, the microglia display a considerable amount of CaM. This CaM expression, however, is strongly dependent on the phenotype. After a kainic acid challenge, CaM immunoreactivity was earlier demonstrated in reactive microglia of the hippocampus (Solá et al., 1997), where the thickened and shortened microglial processes accumulated CaM protein.

In our studies, CaM was localized both in developing microglial cells of primary cortical cultures established from E18 wild-type rat embryos maintained for up to 28 days (DIV1-28) and in pure microglial cells subcultured from DIV7 cultures for 4 days (subDIV4). Moreover, the presence of CaM protein was demonstrated not only in reactive microglia (treated with LPS alone or in combination with one of the CaM inhibitors), but also, at a lower protein level, in unchallenged proliferating ameboid or even ramified, microglial cells. We observed morphologically and functionally different microglial populations within the range from weak to strong levels of CaM expression during culturing, as evidenced by their quantitative assessment by fluorescent immunocytochemical and Western blotting methods. In mixed primary cortical cultures, ameboid microglia, the predominant form in the early stages but always present (in much smaller numbers) during culturing (Szabo and Gulya, 2013), expressed strong CaM immunoreactivity throughout the cytoplasm, while ramified microglia, the typical form in the later stages of microglial development, showed a weaker and more evenly distributed CaM immunoreactivity. A similar intracellular distribution of CaM protein expression was observed in pure microglial cultures. In unchallenged and LPS-challenged cultures, most of the microglia was ameboid and had strong CaM immunoreactivity throughout the cytoplasm. Treatments with CaM inhibitors, both in

unchallenged and LPS challenged cells, resulted in a weaker and more homogenously localized CaM immunoreactivity.

We found that the intracellular localization of CaM immunoreactivity described above was closely related, and typically complementary, to the filamentous actin cytoskeleton, comprised mainly of branched F-actin (Rotty et al., 2013). F-actin was visualized in our studies by the distributions of an actin-binding protein, Iba1, and phalloidin, a bicyclic heptapeptide that recognizes F-actin only, e.g. the form that possesses cellular functionality. Iba1 is an intracellular Ca^{2+}-binding protein that plays an important role in regulation of the intracellular actin dynamics through the direct binding of actin, enhances membrane ruffling and participates in phagocytosis and cell motility (Ohsawa et al., 2000, 2004), functions that require large amounts of cortical F-actin. Our immunocytochemical observations showed that ramified cells (characterized by larger TI values) that displayed minimal or no ruffling at all had only modest quantities of CaM proteins in the cell cortex as compared with ameboid or reactive microglia. Coincidentally, the amount of cortical F-actin was likewise less in ramified microglia, and the reorganization of the actin cytoskeleton determined the intracellular distribution of CaM. Concomitantly increased levels of Iba1 and CaM protein expression, however, were evident both in unchallenged ameboid and in LPS- or LPS and CaM inhibitor-challenged, e.g. activated/reactive microglia. Our observations relating to the intracellularly redistributed CaM *vs.* F-actin are consistent with the findings in mast cells in previous studies. For example, Sullivan et al. (2000) demonstrated that CaM promoted the disassembly of cortical F-actin, while Psatha et al. (2004) found that the disassembly of the actin cytoskeleton eliminated CaM localization.

LPS activation renders microglia ameboid, induces several pro- and anti-inflammatory signaling molecules (Lim et al., 2015; Zhu et al., 2014) and neurotoxic substances through binding to the CD14/MD-2/Toll-like receptor 4-complex (Fricker et al., 2012; Tokes et al., 2011), and gives rise, among others, to cell spreading by interfering with the organization of the actin cytoskeleton through the alteration of integrin clustering (Abram and Lowell, 2009). Microglia activation was shown to involve the signaling pathways nuclear factor κB and p38 mitogen-activated protein kinase (Bachstetter et al., 2007; Cao et al., 2014; Kaushal et al., 2007). It must be noted, however, that the activation of microglial cells by LPS is not proliferative (Suzumura et al., 1991).

In our studies, LPS challenge resulted in significant cell spreading, documented in increases in cell surface, perimeter and TI, and in a repositioning of intracellular actin

filaments toward podosome and filipodia formation. In spite of this lack of interaction between the LPS challenge and CaM protein expression, some of the effects of LPS are mediated through CaM-related phenomena in macrophages (Sweet and Hume, 1996). An LPS challenge, for example, elevated the intracellular Ca^{2+} concentration in brain macrophages via the activation of phosphatidylinositol (3,4,5)-trisphosphate-sensitive stores that, in turn, activated the actin cytoskeleton (Bader et al., 1994). Such an inflammatory response was recently identified as one developed through the activation of CaM-dependent kinase kinase 2 via Toll-like receptors (Racioppi et al., 2012). Thus, the effects of LPS could be attributed, at least in part, to CaM-related phenomena regulating the actin cytoskeleton without directly affecting the CaM protein expression. In another study, CaM was involved in spontaneous microglial ramification and the activation of proliferation from quiescence as it inhibited the spontaneous ramification and decreased the proliferation of these cells (Casal et al., 2001). The loss of ramification was reported to be induced by the elevation of intracellular Ca^{2+} via direct or indirect routes (Kalla et al., 2003) that eventually resulted in CaM activation and/or accumulation in the cell cortex.

The ability of CaM to activate many target proteins depends on its highly flexible conformation, enabling it to interact with a wide variety of proteins (Yamniuk and Vogel, 2004). We hypothesize that this conformational flexibility is limited to different degrees when CaM inhibitors are applied; consequently, many of the CaM-regulated effects will be differentially affected by CaM inhibition. Thus, given the number of CaM-interacting target proteins and their participation in the various intracellular signaling pathways involved in, for example, the remodeling of the actin cytoskeleton during lamellipodia, filipodia or podosome formation (Evans et al., 2003; Murphy and Courtneidge, 2011; Sunagawa et al., 2000; Vincent et al., 2012), it is difficult at present to give an accurate explanation as to how different CaM antagonists might interfere with the outcome of the signaling processes. It seems clear, however, that CaM inhibition interferes strongly with both morphological and functional aspects of the microglial cells. Future experiments may shed light on whether the effects of CaM inhibition seen in selected morphological and functional properties of microglia are uniquely characteristic of these cells or may perhaps be typical of other cell types too, and may promote an understanding of the cell type-specific roles of CaM.

6. CONCLUSION

In our studies, selected morphological, immunocytochemical and functional aspects of various microglial cell populations were characterized in mixed neuronal/glial and pure microglial

cultures. The mixed primary cortical cultures were prepared from the forebrains of embryonic (E18) rats and maintained for up to 28 days (DIV1–DIV28) using routine culturing techniques. The pure microglial cells were subcloned (subDIV4) from the mixed primary cultures and maintained for up to 7 days (DIV7). During culturing, expansion of the microglial cells was observed, as evidenced by quantitative assessment of selected monocyte/macrophage/microglial cell-specific markers (HLA DP, DQ, DR, CD11b/c and Iba1) via immunocyto- and -histochemistry and Western blot analysis. The Iba1 immunoreactivity in Western blots steadily increased about 750-fold, and the number of Iba1-immunoreactive cells rose at least 67-fold between DIV1 and DIV28. Morphometric analysis on binary (digital) silhouettes of the microglia revealed their evolving morphology during culturing. Microglial cells were mainly ameboid in the early stages of in vitro differentiation, while mixed populations of ameboid and ramified cell morphologies were characteristic of older cultures as the average transformation index (TI) increased from 1.96 (DIV1) to 15.17 (DIV28). Multiple immunofluorescence labeling of selected biomarkers revealed different microglial phenotypes during culturing. For example, while HLA DP, DQ, DR immunoreactivity was present exclusively in ameboid microglia (TI < 3) between DIV1 and DIV10, CD11b/c- and Iba1-positive microglial cells were moderately (TI < 13) and progressively (TI < 81) more ramified, respectively, and always present throughout culturing. Regardless of the age of the cultures, proliferating microglia were Ki67-positive and characterized by low TI values (TI < 3). The microglial function was assessed by an in vitro phagocytosis assay. Unstimulated microglia with low TI values were significantly more active in phagocytosing fluorescent microspheres than the ramified forms. In vitro studies on microglial population dynamics combined with phenotypic characterization can be of importance when different in vivo pathophysiological situations are modeled in vitro.

The roles of CaM, a multifunctional intracellular calcium receptor protein, as concerns selected morphological and functional characteristics of pure microglial cells were investigated through use of the CaM antagonists calmidazolium (CALMID) and trifluoperazine (TFP). The intracellular localization of the CaM protein relative to phalloidin, a bicyclic heptapeptide that binds only to filamentous actin, and the Iba1 protein was determined by immunocytochemistry, with quantitative analysis by immunoblotting. In unchallenged and untreated (control) microglia, high concentrations of CaM protein were found mainly perinuclearly in ameboid microglia, while the cell cortex had a smaller CaM content that diminished progressively deeper into the branches in the ramified microglia. The amounts and intracellular distributions of both Iba1 and CaM proteins were altered after

lipopolysaccharide (LPS) challenge in activated microglia. CALMID and TFP exerted different, sometimes opposing, effects on many morphological, cytoskeletal and functional characteristics of the microglial cells. They influenced the CaM and Iba1 protein expressions and their intracellular localizations differently, and differentially affected the reorganization of the actin cytoskeleton in the microglial cell cortex, influencing lamellipodia, filipodia and podosome formation.

Acting on many target proteins, CaM is a key factor in the regulation of a number of morphological aspects of the microglia through the modulation of the actin cytoskeleton that affects the formation and maintenance of lamellipodia, filipodia and podosomes of these cells. CALMID and TFP, two prototypical CaM antagonists acting through different molecular mechanisms on the CaM protein, have differential effects on these morphological and certain fuctional aspects, including Iba1 and CaM protein expression, when tested both in unchallenged and LPS-challenged pure microglial cells. In general, TFP was more potent in provoking these structural alterations. Deciphering the roles of CaM in microglial functions, perhaps through use of different CaM-specific inhibitors, could be important in understanding the roles and modes of action of microglia in health and disease.

In summary, the main findings of our studies are:

1) In mixed primary cultures, TI values revealed the evolving microglial morphology and functions during culturing as microglia with TI < 3 were more active in phagocytosing than the ramified forms characterized with TI > 3.
2) The macrophage/microglia markers labelled different microglial phenotypes in culture: HLA DP, DQ, DR-positive microglia were exclusively ameboid, while CD11b/c-labeled microglia were typically less ramified than the Iba1-labeled cells.
3) When CaM inhibitors were tested in unchallenged and in LPS-challenged pure microglia, they affected many morphological and functional aspects of microglial cells. CALMID and TFP differentially affected the intracellular distributions of CaM and Iba1, and the actin cytoskeleton reorganization.

7. ACKNOWLEDGMENTS

I thank Professor Karoly Gulya for his help. I am also grateful to my coworkers Miss Karolina Dulka, Mrs. Susan Ambrus and Mrs. Olga Daranyi. This work was supported by program project grants to the University of Szeged from the Ministry of National Resources (TÁMOP-

4.2.1.B-09/1/KONV-2010-0005 and TÁMOP-4.2.2.A-11/1/KONV-2012-0052) through the European Union Cohesion Fund. I dedicate this work to my family for their help and love.

8. REFERENCES

Abram CL, Lowell CA (2009) The ins and outs of leukocyte integrin signaling. Annu Rev Immunol 27:339–362.

Abràmoff MD, Magalhães PJ, Ram SJ (2004) Image Processing with ImageJ. Biophotonics Internat 11:36-42.

Aderem A, Underhill DM (1999) Mechanisms of phagocytosis in macrophages. Annu Rev Immunol 17:593-623.

Amur-Umarjee SG, Dasu RG, Campagnoni AT (1990) Temporal expression of myelin-specific components in neonatal mouse brain cultures: evidence that 2',3'-cyclic nucleotide 3'-phosphodiesterase appears prior to galactocerebroside. Dev Neurosci 12:251-262.

Auffray C, Sieweke MH, Geissmann F (2009) Blood monocytes: development, heterogeneity, and relationship with dendritic cells. Annu Rev Immunol 27:669-692.

Bachstetter AD, Xing B, de Almeida L, Dimayuga ER, Watterson DM, Van Eldik LJ (2011) Microglial p38α MAPK is a key regulator of proinflammatory cytokine up-regulation induced by toll-like receptor (TLR) ligands or beta-amyloid (Aβ). J Neuroinflammation 8:79.

Bader MF, Taupenot L, Ulrich G, Aunis D, Ciesielski-Traska J (1994) Bacterial endotoxin induces [Ca2+]i transients and changes the organization of actin in microglia. Glia 11:336–344.

Bakota L, Orojan I, Gulya K (2005) Intranuclear differences in calmodulin gene expression in the trigeminal nuclei of the rat. Acta Biol Szeged 49:9-14.

Banerjee A, Roach MC, Trcka P, Ludueña RF (1990) Increased microtubule assembly in bovine brain tubulin lacking the type III isotype of beta-tubulin. J Biol Chem 265:1794-1799.

Becher B, Antel JP (1996) Comparison of phenotypic and functional properties of immediately ex vivo and cultured human adult microglia. Glia 18:1-10.

Bechmann I, Kwidzinski E, Kovac AD, Simbürger E, Horvath T, Gimsa U, Dirnagl U, Priller J, Nitsch R (2001a) Turnover of rat brain perivascular cells. Exp Neurol 168:242-249.

Bechmann I, Priller J, Kovac A, Böntert M, Wehner T, Klett FF, Bohsung J, Stuschke M, Dirnagl U, Nitsch R (2001b) Immune surveillance of mouse brain perivascular spaces by blood-borne macrophages. Eur J Neurosci 14:1651-1658.

Berger JV, Dumont AO, Focant MC, Vergouts M, Sternotte A, Calas AG, Goursaud S, Hermans E (2012) Opposite regulation of metabotropic glutamate receptor 3 and metabotropic glutamate receptor 5 by inflammatory stimuli in cultured microglia and astrocytes. Neuroscience 205:29-38.

Berridge MJ, Lipp P, Bootman MD (2000) The versatility and universality of calcium signalling. Nature Rev Mol Cell Biol 1:11-21.

Beyer M, Gimsa U, Eyüpoglu IY, Hailer NP, Nitsch R (2000) Phagocytosis of neuronal or glial debris by microglial cells: upregulation of MHC class II expression and multinuclear giant cell formation in vitro. Glia 31:262-266.

Borsa J, Einspenner M, Sargent MD, Hickie RA (1986) Selective cytotoxicity of calmidazolium and trifluoperazine for cycling versus noncycling C3H10T1/2 cells in vitro. Cancer Res 46:133-136.

Caceres A, Bender P, Snavely L, Rebhun LI, Steward O (1983) Distribution and subcellular localization of calmodulin in adult and developing brain tissue. Neuroscience 10:449-461.

Cao H, Zang KK, Han M, Zhao ZQ, Wu GC, Zhang YQ (2014) Inhibition of p38 mitogen-activated protein kinase activation in the rostral anterior cingulate cortex attenuates pain-related negative emotion in rats. Brain Res Bull 107:79-88.

Casal C, Tusell JM, Serratosa J (2001) Role of calmodulin in the differentiation/activation of microglial cells. Brain Res 902:101-107.

Chinnery HR, Ruitenberg MJ, McMenamin PG (2010) Novel characterization of monocyte-derived cell populations in the meninges and choroid plexus and their rates of replenishment in bone marrow chimeric mice. J Neuropathol Exp Neurol 69:896-909.

Clapham DE (2007) Calcium signaling. Cell 131:1047-1058.

Cullheim S, Thams S (2007) The microglial networks of the brain and their role in neuronal network plasticity after lesion. Brain Res Rev 55:89-96.

Dalmau I, Finsen B, Tønder N, Zimmer J, González B, Castellano B (1997) Development of microglia in the prenatal rat hippocampus. J Comp Neurol 377:70-84.

Dalmau I, Finsen B, Zimmer J, González B, Castellano B (1998) Development of microglia in the postnatal rat hippocampus. Hippocampus 8:458-474.

Dalmau I, Vela JM, González B, Finsen B, Castellano B (2003) Dynamics of microglia in the developing rat brain. J Comp Neurol 458:144-157.

Davalos D, Grutzendler J, Yang G, Kim JV, Zuo Y, Jung S, Littman DR, Dustin ML, Gan WB (2005) ATP mediates rapid microglial response to local brain injury in vivo. Nat Neurosci 8:752-758.

Deierborg T, Roybon L, Inacio AR, Pesic J, Brundin P (2010) Brain injury activates microglia that induce neural stem cell proliferation ex vivo and promote differentiation of neurosphere-derived cells into neurons and oligodendrocytes. Neuroscience 171:1386-1396.

Drew PD, Chavis JA (2000) Inhibition of microglial cell activation by cortisol. Brain Res Bull 52:391-396.

Durafourt BA, Moore CS, Zammit DA, Johnson TA, Zaguia F, Guiot MC, Bar-Or A, Antel JP (2012) Comparison of polarization properties of human adult microglia and blood-derived macrophages. Glia 60:717-727.

Eglitis MA, Mezey E (1997) Hematopoietic cells differentiate into both microglia and macroglia in the brains of adult mice. Proc Natl Acad Sci USA 94:4080-4085.

Erondu NE, Kennedy MB (1985) Regional distribution of type II Ca^{2+}/calmodulin-dependent protein kinase in rat brain. J Neurosci 5:3270-3277.

Evans JG, Correia I, Krasavina O, Watson N, Matsudaira P (2003) Macrophage podosomes assemble at the leading lamella by growth and fragmentation. J Cell Biol 161:697-705.

Färber K, Kettenmann H (2006) Functional role of calcium signals for microglial function. Glia 54:656-665.

Floden AM, Combs CK (2006) Beta-amyloid stimulates murine postnatal and adult microglia cultures in a unique manner. J Neurosci 26:4644-4648.

Ford AL, Goodsall AL, Hickey WF, Sedgewick JD (1995) Normal adult ramified microglia separated from other central nervous system macrophages by flow cytometric sorting. J Immunol 154:4309-4321.

Frei K, Lins H, Schwerdel C, Fontana A (1994) Antigen presentation in the central nervous system: The inhibitory effect of IL-10 on MHC class II expression and production of cytokines depends on the inducing signals and the types of cell analyzed. J Immunol 152:2720-2728.

Fricker M, Oliva-Martín MJ, Brown GC (2012) Primary phagocytosis of viable neurons by microglia activated with LPS or Aβ is dependent on calreticulin/LRP phagocytic signalling. J Neuroinflammation 9:196.

Fujita H, Tanaka J, Toku K, Tateishi N, Suzuki Y, Matsuda S, Sakanaka M, Maeda N (1996) Effects of GM-CSF and ordinary supplements on the ramification of microglia in culture: A morphometrical study. Glia 18:269-281.

Gehrmann J (1996) Microglia: a sensor to threats in the nervous system? Res Virology 147:79-88.

Gehrmann J, Matsumoto Y, Kreutzberg GW (1995) Microglia: intrinsic immunoeffector cell of the brain. Brain Res Rev 20:269-287.

Geissmann F, Jung S, Littman DR (2003) Blood monocytes consist of two principal subsets with distinct migratory properties. Immunity 19:71-82.

Geissmann F, Manz MG, Jung S, Sieweke MH, Merad M, Ley K (2010) Development of monocytes, macrophages, and dendritic cells. Science 327:656-61. (Erratum in Science 330:1319.)

Ginhoux F, Greter M, Leboeuf M, Nandi S, See P, Gokhan S, Mehler MF, Conway SJ, Ng LG, Stanley ER, Samokhvalov IM, Merad M (2010) Fate mapping analysis reveals that adult microglia derive from primitive macrophages. Science 330:841-845.

Gordon S (2003) Alternative activation of macrophages. Nat Rev Immunol 3:23–35.

Greenberg S (1995) Signal transduction of phagocytosis. Trends Cell Biol 5:93-99.

Guillemin G, Boussin FD, Croitoru J, Franck-Duchenne M, Le Grand R, Lazarini F, Dormont D (1997) Obtention and characterization of primary astrocyte and microglial cultures from adult monkey brains. J Neurosci Res 49:576-591.

Hailer NP, Heppner FL, Haas D, Nitsch R (1997) Fluorescent dye prelabelled microglial cells migrate into organotypic hippocampal slice cultures and ramify. Eur J Neurosci 9:863-866.

Hailer NP, Jarhult JD, Nitsch R (1996) Resting microglial cells in vitro: analysis of morphology and adhesion molecule expression in organotypic hippocampal slice cultures. Glia 18:319-331.

Hawkes CA, McLaurin J (2009) Selective targeting of perivascular macrophages for clearance of beta-amyloid in cerebral amyloid angiopathy. Proc Natl Acad Sci USA 106:1261-1266.

Hickey WF, Kimura H (1988) Perivascular microglial cells of the CNS are bone marrow-derived and present antigen in vivo. Science 239:290-292.

Horejsí V, Němec M, Angelisová P, Kristofová H, Gorga JC, Hilgert I (1986) Characterization of seven new monoclonal antibodies against human DR, DR + DP and DQ1 + DQ3 antigens. Tissue Antigens 28:288-297.

Ikura M (1996) Calcium binding and conformational response in EF-hand proteins. Trends Biochem 21:14-17.

Imai Y, Ibata I, Ito D, Ohsawa K, Kohsaka S (1996) A novel gene iba1 in the major histocompatibility complex class III region encoding an EF hand protein expressed in a monocytic lineage. Biophys Biochem Res Commun 224:855-862.

Imamura K, Suzumura A, Sawada M, Marunouchi T, Takahashi A (1991) Functional and immunohistochemical studies of cultured rat microglia. Rinsho Shinkeigaku 31:127-134.

Ito D, Imai Y, Ohsawa K, Nakajima K, Fukuuchi Y, Kohsaka S (1998) Microglia-specific localisation of a novel calcium binding protein Iba1. Mol Brain Res 57:1-9.

Kalla R, Bohatschek M, Kloss CU, Krol J, Von Maltzan X, Raivich G (2003) Loss of microglial ramification in microglia-astrocyte cocultures: involvement of adenylate cyclase, calcium, phosphatase, and Gi-protein systems. Glia 41:50-63.

Kaushal V, Koeberle PD, Wang Y, Schlichter LC (2007) The Ca2+-activated K+ channel KCNN4/KCa3.1 contributes to microglia activation and nitric oxide-dependent neurodegeneration. J Neurosci 27:234-244.

Kennedy MB (1989) Regulation of neuronal function by calcium. Trends Neurosci 12:417-420.

Kim WK, Alvarez X, Fisher J, Bronfin B, Westmoreland S, McLaurin J, Williams K (2006) CD163 identifies perivascular macrophages in normal and viral encephalitic brains and potential precursors to perivascular macrophages in blood. Am J Pathol 168:822-834.

Kortvely E, Varszegi S, Palfi A, Gulya K (2003) Intracellular targeting of calmodulin mRNAs in primary hippocampal cells. J Histochem Cytochem 51:541-544.

Kortvely E, Gulya K (2004) Calmodulin, and various ways to regulate its activity. Life Sci 74:1065-1070.

Kortvely E, Palfi A, Bakota L, Gulya K (2002) Ontogeny of calmodulin gene expression in rat brain. Neuroscience 114:301-316.

Kovacs B, Gulya K (2002) Differential expression of multiple calmodulin genes in cells of the white matter of the rat spinal cord. Mol Brain Res 102:28-34.

Kovacs B, Gulya K (2003) Calmodulin gene expression in the neural retina of the adult rat. Life Sci 73:3213-3224.

Kozlowski C, Weimer RM (2012) An automated method to quantify microglia morphology and application to monitor activation state longitudinally in vivo. PLoS One 7(2):e31814.

Kreutzberg GW (1996) Microglia: A sensor for pathological events in the CNS. Trends Neurosci 19:312-318.

Ladeby R, Wirenfeldt M, Garcia-Ovejero D, Fenger C, Dissing-Olesen L, Dalmau I, Finsen B (2005) Microglial cell population dynamics in the injured adult central nervous system. Brain Res Rev 48:196-206.

Libich DS, Harauz G (2008) Backbone dynamics of the 18.5 kDa isoform of myelin basic protein reveals transient alpha-helices and a calmodulin-binding site. Biophys J 94:4847-4866.

Lim HW, Park JI, More SV, Park JY, Kim BW, Jeon SB, Yun YS, Park EJ, Yoon SH, Choi DK (2015) Anti-neuroinflammatory effects of DPTP, a novel synthetic clovamide derivative in in vitro and in vivo model of neuroinflammation. Brain Res Bull 112:25-34.

Ling EA, Kaur LC, Yick TY, Wong WC (1990) Immunocytochemical localization of CR3 complement receptors with OX-42 in amoeboid microglia in postnatal rats. Anat Embryol (Berl). 182:481-486.

Ling EA, Wong WC (1993) The origin and nature of ramified and amoeboid microglia: A historical review and current concepts. Glia 7:9-18.

Liu B, Du L, Kong LY, Hudson PM, Wilson BC, Chang RC, Abel HH, Hong JS (2000) Reduction by naloxone of lipopolysaccharide-induced neurotoxicity in mouse cortical neuron-glia co-cultures. Neuroscience 97:749-756.

Lowry OH, Rosebrough NJ, Farr AL, Randall RJ (1951) Protein measurement with the Folin phenol reagent. J Biol Chem 193:265-275.

Magnus T, Korn T, Jung S (2004) Chronically stimulated microglial cells do no longer alter their immune functions in response to the phagocytosis of apoptotic cells. J Neuroimmunol 155:64-72.

Marín-Teva JL, Dusart I, Colin C, Gervais A, van Rooijen N, Mallat M (2004) Microglia promote the death of developing Purkinje cells. Neuron 41:535-547.

Matsushima N, Hayashi N, Jinbo Y, Izumi Y (2000) Ca^{2+}-bound calmodulin forms a compact globular structure on binding four trifluoperazine molecules in solution. Biochem J 347:211-215.

Meyer-Luehmann M, Spires-Jones TL, Prada C, Garcia-Alloza M, de Calignon A, Rozkalne A, Koenigsknecht-Talboo J, Holtzman DM, Bacskai BJ, Hyman BT (2008) Rapid appearance and local toxicity of amyloid-beta plaques in a mouse model of Alzheimer's disease. Nature 451:720-724.

Milligan CE, Cunningham TJ, Levitt P (1991a) Differential immunochemical markers reveal the normal distribution of brain macrophages and microglia in the developing rat brain. J Comp Neurol 314:125-135.

Milligan CE, Levitt P, Cunningham TJ (1991b) Brain macrophages and microglia respond differently to lesions of the developing and adult visual system. J Comp Neurol 314:136-146.

Mitchison TJ, Cramer LP (1996) Actin-based cell motility and cell locomotion. Cell 84:371-379.

Mosser DM, Edwards JP (2008) Exploring the full spectrum of macrophage activation. Nat Rev Immunol 8:958-969. Erratum in Nat Rev Immunol (2010) 10:460.

Murphy DA, Courtneidge SA (2011) The 'ins' and 'outs' of podosomes and invadopodia: characteristics, formation and function. Nature Rev Mol Cell Biol 12:413-426.

Myllykoski M, Itoh K, Kangas SM, Heape AM, Kang S.U., Lubec G, Kursula I, Kursula P (2012) The N-terminal domain of the myelin enzyme 2',3'-cyclic nucleotide 3'-phosphodiesterase: direct molecular interaction with the calcium sensor calmodulin. J Neurochem 123:515-524.

Neumann H, Kotter MR, Franklin RJ (2009) Debris clearance by microglia: an essential link between degeneration and regeneration. Brain 132:288-295.

Ohsawa K, Imai Y, Kanazawa H, Sasaki Y, Kohsaka S (2000) Involvement of Iba1 in membrane ruffling and phagocytosis of macrophages/microglia. J Cell Sci 113:3073-3084.

Ohsawa K, Imai Y, Sasaki Y, Kohsaka S (2004) Microglia/macrophage-specific protein Iba1 binds to fimbrin and enhances its actin-bundling activity. J Neurochem 88:844-856.

Orłowski D, Sołtys Z, Janeczko K (2003) Morphological development of microglia in the postnatal rat brain. A quantitative study. Int J Dev Neurosci 21:445-450.

Orojan I, Bakota L, Gulya K (2006) Differential calmodulin gene expression in the nuclei of the rat midbrain-brain stem region. Acta Histochem 108:455-462.

Orojan I, Bakota L, Gulya K (2008) Trans-synaptic regulation of calmodulin gene expression after experimentally induced orofacial inflammation and subsequent corticosteroid treatment in the principal sensory and motor trigeminal nuclei of the rat. Neurochem Int 52:265-271.

Otani Y, Yamaguchi Y, Sato Y, Furuichi T, Ikenaka K, Kitani H, Baba H (2011) PLD4 is involved in phagocytosis of microglia: expression and localization changes of PLD4 are correlated with activation state of microglia. PLoS One 6(11):e27544.

Palfi A, Kortvely E, Fekete E, Gulya K (2005) Multiple calmodulin mRNAs are selectively transported to functionally different neuronal and glial compartments in the rat hippocampus. An electron microscopic in situ hybridization study. Life Sci 77:1405-1415.

Palfi A, Gulya K (1999) Water deprivation upregulates the three calmodulin genes in exclusively the supraoptic nucleus of the rat brain. Mol Brain Res 74:111-116.

Palfi A, Kortvely E, Fekete E, Kovacs B, Varszegi S, Gulya K (2002) Differential calmodulin gene expression in the rodent brain. Life Sci 70:2829-2855.

Palfi A, Simonka JA, Pataricza M, Tekulics P, Lepran I, Papp G, Gulya K (2001) Postischemic calmodulin gene expression in the rat hippocampus. Life Sci 68:2373-2381.

Palfi A, Vizi S, Gulya K (1999) Differential distribution and intracellular targeting of mRNAs corresponding to the three calmodulin genes in rat brain: a quantitative in situ hybridization study. J Histochem Cytochem 47:583-600.

Priller J, Flügel A, Wehner T, Boentert M, Haas CA, Prinz M, Fernández-Klett F, Prass K, Bechmann I, de Boer BA, Frotscher M, Kreutzberg GW, Persons DA, Dirnagl U (2001) Targeting gene-modified hematopoietic cells to the central nervous system: use of green fluorescent protein uncovers microglial engraftment. Nature Med 7:1356-1361.

Prinz M, Mildner A (2011) Microglia in the CNS: immigrants from another world. Glia 59:177-187.

Prinz M, Priller J, Sisodia SS, Ransohoff RM (2011) Heterogeneity of CNS myeloid cells and their roles in neurodegeneration. Nature Neurosci 14:1227-1235.

Prinz M, Priller J (2014) Microglia and brain macrophages in the molecular age: from origin to neuropsychiatric disease. Nature Rev Neurosci 15:300-312.

Psatha M, Koffer A, Erent M, Moss SE, Bolsover S (2004) Calmodulin spatial dynamics in RBL-2H3 mast cells. Cell Calcium 36:51-59.

Racioppi L, Noeldner PK, Lin F, Arvai S, Means AR (2012) Calcium/calmodulin-dependent protein kinase kinase 2 regulates macrophage-mediated inflammatory responses. J Biol Chem 287:11579-11591.

Raivich G, Bohatschek M, Kloss CUA, Werner A, Jones LL, Kreutzberg GW (1999) Neuroglial activation repertoire in the injured brain: graded response, molecular mechanisms and cues to physiological function. Brain Res Rev 30:77-105.

Robinson AP, White TM, Mason DW (1986) Macrophage heterogeneity in the rat as delineated by two monoclonal antibodies MRC OX-41 and MRC OX-42, the latter recognizing complement receptor type 3. Immunology 57:239-247.

Rotty JD, Wu C, Bear JE (2013) New insights into the regulation and cellular functions of the ARP2/3 complex. Nature Rev Mol Cell Biol 14:7-12.

Rozovsky I, Finch CE, Morgan TE (1998) Age-related activation of microglia and astrocytes: in vitro studies show persistent phenotypes of aging, increased proliferation, and resistance to down-regulation. Neurobiol Aging 19:97-103.

Sack DB, Porter SE, Ladenson JH, McDonald JM (1991) Monoclonal antibody to calmodulin: development, characterization, and comparison with polyclonal anti-calmodulin antibodies. Anal Biochem 194:369-377.

Saijo K, Glass CK (2011) Microglial cell origin and phenotypes in health and disease. Nature Rev Immunol 11:775-787.

Sanabria H, Digman MA, Gratton E, Waxham MN (2008) Spatial diffusivity and availability of intracellular calmodulin. Biophys J 95:6002-6015.

Scott IS, Heath TM, Morris LS, Rushbrook SM, Bird K, Vowler SL, Arends MJ, Coleman N (2004) A novel immunohistochemical method for estimating cell cycle phase distribution in ovarian serous neoplasms: implications for the histopathological assessment of paraffin-embedded specimens. Br J Cancer 90:1583-1590.

Seto-Ohshima A, Kitajima S, Sano M, Kato K, Mizutani A (1983) Immunohistochemical localization of calmodulin in mouse brain. Histochemistry 79:251-257.

Sezgin M, Sankur B (2004) Survey over image thresholding techniques and quantitative performance evaluation. J Electronic Imaging 13:146-165.

Siddiqui TA, Lively S, Vincent C, Schlichter LC (2012) Regulation of podosome formation, microglial migration and invasion by $Ca(^{2+})$-signaling molecules expressed in podosomes. J Neuroinflammation 9:250.

Slepko N, Levi G (1996) Progressive activation of adult microglial cells in vitro. Glia 16:241-246.

Smith ME (2001) Phagocytic properties of microglia in vitro: implications for a role in multiple sclerosis and EAE. Microsc Res Tech 54:81-94.

Solá C, Tusell JM, Serratosa J (1996). Comparative study of the pattern of expression of calmodulin messenger RNAs in the mouse brain. Neuroscience 75, 245-256.

Solá C, Tusell JM, Serratosa J (1997) Calmodulin is expressed by reactive microglia in the hippocampus of kainic acid-treated mice. Neuroscience 81:699-705.

Song XY, Hu JF, Sun MN, Li ZP, Zhu ZX, Song LK, Yuan YH, Liu G, Chen NH (2014) IMM-H004, a novel coumarin derivative compound, attenuates the production of inflammatory mediatory mediators in lipopolysaccharide-activated BV2 microglia. Brain Res Bull 106:30-38.

Starborg M, Gell K, Brundell E, Höög C (1996) The murine Ki-67 cell proliferation antigen accumulates in the nucleolar and heterochromatic regions of interphase cells and at the periphery of the mitotic chromosomes in a process essential for cell cycle progression. J Cell Sci 109:143-153.

Stence N, Waite M, Dailey ME (2001) Dynamics of microglial activation: a confocal time-lapse analysis in hippocampal slices. Glia 33:256-266.

Strack S, Wadzinski BE, Ebner FF (1996) Localization of the calcium/calmodulin-dependent protein phosphatase, calcineurin, in the hindbrain and spinal cord of the rat. J Comp Neurol 375:66-76.

Streit WJ (2006) Microglial senescence: does the brain's immune system have an expiration date? Trends Neurosci 29:506-510.

Streit WJ, Graeber MB, Kreutzberg GW (1989) Expression of Ia antigens on perivascular and microglial cells after sublethal and lethal neuronal injury. Exp Neurol 105:115-126.

Streit WJ, Walter SA, Pennel NA (1999) Reactive microgliosis. Progr Neurobiol 57:563-581.

Sullivan R, Burnham M, Török K, Koffer A (2000) Calmodulin regulates the disassembly of cortical F-actin in mast cells but is not required for secretion. Cell Calcium 28:33-46.

Sunagawa M, Kosugi T, Nakamura M, Sperelakis N (2000) Pharmacological actions of calmidazolium, a calmodulin antagonist, in cardiovascular system. Cardiovasc Drug Rev 18:211-221.

Suzumura A, Marunouchi T, Yamamoto H (1991) Morphological transformation of microglia in vitro. Brain Res 545:301–306.

Sweet MJ, Hume DA (1996) Endotoxin signal transduction in macrophages. J Leukoc Biol 60:8-26.

Szabo M, Gulya K (2013) Development of the microglial phenotype in culture. Neuroscience 241:280-295.

Szabo M, Dulka K, Gulya K (2016) Calmodulin inhibition regulates morphological and functional changes related to the actin cytoskeleton in microglial cell cultures. Brain Res Bull 120:41-57.

Takahashi K, Prinz M, Stagi M, Chechneva O, Neumann H (2007) TREM2- transduced myeloid precursors mediate nervous tissue debris clearance and facilitate recovery in an animal model of multiple sclerosis. PLoS Med 4:e124.

Tanaka J, Toku K, Matsuda S, Sudo S, Fujita H, Sakanaka M, Maeda N (1998) Induction of resting microglia in culture medium devoid of glycine and serine. Glia 24:198-215.

Tokes T, Eros G, Bebes A, Hartmann P, Várszegi S, Varga G, Kaszaki J, Gulya K, Ghyczy M, Boros M (2011) Protective effects of a phosphatidylcholine-enriched diet in lipopolysaccharide-induced experimental neuroinflammation in the rat. Shock 36:458-465.

Toutenhoofd SL, Strehler EE (2000) The calmodulin multigene family as a unique case of genetic redundancy: multiple levels of regulation to provide spatial and temporal control of calmodulin pools? Cell Calcium 28:83-96.

Town T, Nikolic V, Tan J (2005) The microglial "activation" continuum: from innate to adaptive responses. J Neuroinflammation 2:24.

Ulvestad E, Williams K, Bjerkvig R, Tiekotter K, Antel J, Mørk S (1994a). Human microglial cells have phenotypic and functional characteristics in common with both macrophages and dendritic antigen-presenting cells. J Leukoc Biol 56:732-740.

Ulvestad E, Williams K, Bø L, Trapp B, Antel J, Matre R (1994b) HLA class II molecules (HLA-DR, -DP, -DQ) on cells in the human CNS studied in situ and in vitro. Immunology 82:535-541.

Vallières L, Sawchenko PE (2003) Bone marrow-derived cells that populate the adult mouse brain preserve their hematopoietic identity. J Neurosci 23:5197-5207.

Vandonselaar M, Hickie RA, Quail JW, Delbaere LT (1994) Trifluoperazine-induced conformational change in $Ca(^{2+})$-calmodulin. Nature Struct Biol 1:795-801.

Vertessy BG, Harmat V, Bocskei Z, Naray-Szabo G, Orosz F, Ovadi J (1998) Simultaneous binding of drugs with different chemical structures to Ca^{2+}-calmodulin: crystallographic and spectroscopic studies. Biochemistry 37:15300-15310.

Vincent C, Siddiqui TA, Schlichter LC (2012) Podosomes in migrating microglia: components and matrix degradation. J Neuroinflammation 9:190.

Vizi S, Palfi A, Gulya K (2000) Multiple calmodulin genes exhibit systematically differential responses to chronic ethanol treatment and withdrawal in several regions of the rat brain. Mol Brain Res 83:63-71.

Wang CC, Wu CH, Shieh JY, Wen CY, Ling EA (1996) Immunohistochemical study of amoeboid microglial cells in fetal rat brain. J Anat 189:567-574.

Werry EL, Liu GJ, Lovelace MD, Nagarajah R, Hickie IB, Bennett MR (2011) Lipopolysaccharide-stimulated interleukin-10 release from neonatal spinal cord microglia is potentiated by glutamate. Neuroscience 175:93-103.

Wirenfeldt M, Dissing-Olesen L, Babcock AA, Nielsen M, Meldgaard M, Zimmer J, Azcoitia I, Leslie RG, Dagnaes-Hansen F, Finsen B (2007) Population control of resident and immigrant microglia by mitosis and apoptosis. Am J Pathol 171:617-631.

Wong R, Schlichter LC (2014) PKA reduces the rat and human KCa3.1 current, CaM binding, and Ca2+ signaling, which requires Ser332/334 in the CaM-binding C terminus. J Neurosci 34:13371-13383.

Wu Y, Wu M, He G, Zhang X, Li W, Gao Y, Li Z, Wang Z, Zhang C (2012) Glyceraldehyde-3-phosphate dehydrogenase: a universal internal control for Western blots in prokaryotic and eukaryotic cells. Anal Biochem 423:15-22.

Xu Y, Qian L, Zong G, Ma K, Zhu X, Zhang H, Li N, Yang Q, Bai H, Ben J, Li X, Xu Y, Chen Q (2012) Class A scavenger receptor promotes cerebral ischemic injury by pivoting microglia/macrophage polarization. Neuroscience 218:35-48.

Yamada M, Ohsawa K, Imai Y, Kohsaka S, Kamitori S (2006) X-ray structures of the microglia/macrophage-specific protein Iba1 from human and mouse demonstrate novel molecular conformation change induced by calcium binding. J Mol Biol 364:449-457.

Yamniuk AP, Vogel HJ (2004) Calmodulin's flexibility allows for promiscuity in its interactions with target protein and peptides. Mol Biotechnol 27:33–57.

Zhang L, Chopp M, Zhang RL, Wang L, Zhang J, Wang Y, Toh Y, Santra M, Lu M, Zhang ZG (2010) Erythropoietin amplifies stroke-induced oligodendrogenesis in the rat. PLoS One 5(6):e11016.

Zhu MD, Zhao LX, Wang XT, Gao YJ, Zhang ZJ (2014) Ligustilide inhibits microglia-mediated proinflammatory cytokines production and inflammatory pain. Brain Res Bull 109:54-60.

9. COPIES OF PUBLICATIONS

ARTICLE I.

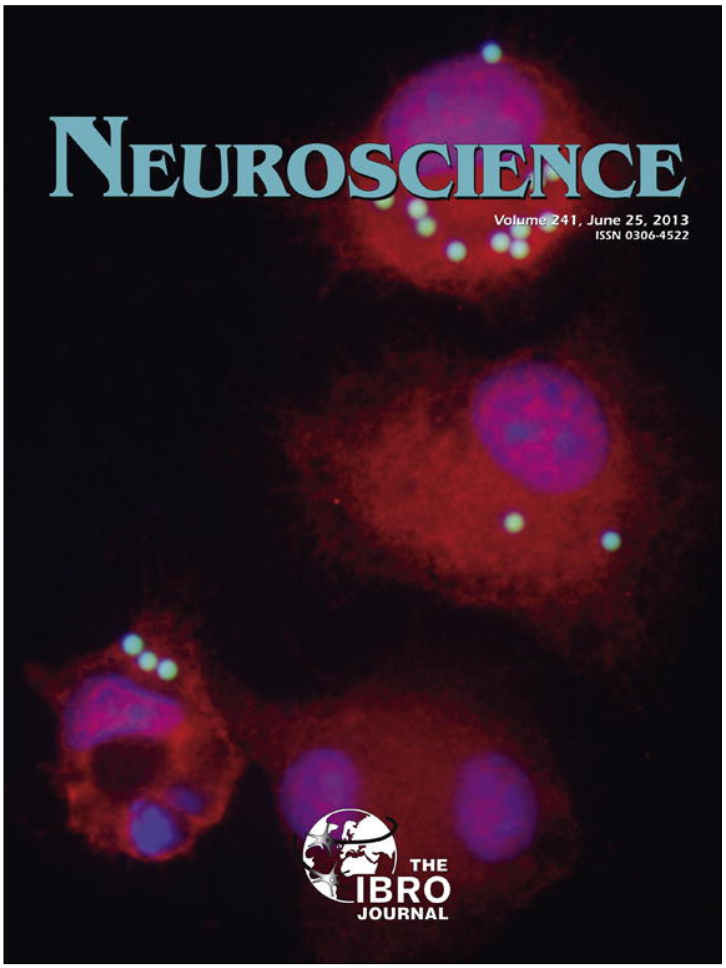

Neuroscience 241 (2013) 280–295

DEVELOPMENT OF THE MICROGLIAL PHENOTYPE IN CULTURE

M. SZABO AND K. GULYA *

Department of Cell Biology and Molecular Medicine, University of Szeged, Szeged, Hungary

Abstract—Selected morphological, molecular and functional aspects of various microglial cell populations were characterized in cell cultures established from the forebrains of E18 rat embryos. The mixed primary cortical cultures were maintained for up to 28 days using routine culturing techniques when the microglial cells in the culture were not stimulated or immunologically challenged. During culturing, expansion of the microglial cell populations was observed, as evidenced by quantitative assessment of selected monocyte/macrophage/microglial cell-specific markers (human leukocyte antigen (HLA) DP, DQ, DR, CD11b/c and Iba1) via immunocyto- and histochemistry and Western blot analysis. The Iba1 immunoreactivity in Western blots steadily increased about 750-fold, and the number of Iba1-immunoreactive cells rose at least 67-fold between one day *in vitro* (DIV1) and DIV28. Morphometric analysis on binary (digital) silhouettes of the microglia revealed their evolving morphology during culturing. Microglial cells were mainly ameboid in the early stages of *in vitro* differentiation, while mixed populations of ameboid and ramified cell morphologies were characteristic of older cultures as the average transformation index (TI) increased from 1.96 (DIV1) to 15.17 (DIV28). Multiple immunofluorescence labeling of selected biomarkers revealed different microglial phenotypes during culturing. For example, while HLA DP, DQ, DR immunoreactivity was present exclusively in ameboid microglia (TI < 3) between DIV1 and DIV10, CD11b/c- and Iba1-positive microglial cells were moderately (TI < 13) and progressively (TI < 81) more ramified, respectively, and always present throughout culturing. Regardless of the age of the cultures, proliferating microglia were Ki67-positive and characterized by low TI values (TI < 3). The microglial function was assessed by an *in vitro* phagocytosis assay. Unstimulated microglia with low TI values were significantly more active in phagocytosing fluorescent microspheres than the ramified forms. *In vitro* studies on microglial population dynamics combined with phenotypic characterization can be of importance when different *in vivo* pathophysiological situations are modeled *in vitro*.

Key words: immunocytochemistry, microglia, phagocytosis, primary culture, transformation index, Western blotting.

INTRODUCTION

Microglial cells, the resident immune cells of the central nervous system (CNS), share a number of phenotypic characteristics and lineage properties with other bone marrow-derived myeloid cell populations, and are regarded as members of the monocyte/macrophage lineage (Gehrmann et al., 1995; Kreutzberg, 1996; Geissmann et al., 2003, 2010; Ginhoux et al., 2010; Prinz and Mildner, 2011; Prinz et al., 2011). Recent *in vivo* lineage-tracing studies demonstrated that adult microglial cells originate from primitive myeloid progenitors that arise early in embryonic development, and constitute an ontogenetically distinct population in the mononuclear phagocyte system (Ginhoux et al., 2010). Microglia are highly plastic and, by virtue of their location and current role in the nervous tissue, are able to undergo a variety of morphological and functional changes in response to various stimuli. In their non-activated or resting state, they display a ramified morphology characterized by numerous, fine-branched processes with relatively small somata and subdued macrophage-like functional properties. In response to neural injury, infection and inflammatory or other signals, however, microglial cells become activated and undergo a series of morphological, molecular and functional changes in proportion to the severity of the damage to the neuronal tissue (Ling and Wong, 1993; Kreutzberg, 1996). Shortly after their initial activation, microglial cells become progressively less ramified and quickly develop an enlarged cell body with several short, thickened processes (activated microglia) that may eventually completely retract (phagocytic microglia). This morphological transformation parallels microglial proliferation, homing and adhesion to damaged cells (Raivich et al., 1999; Streit et al., 1999). The development of the ameboid appearance and phagocytic nature of the microglial cells coincides with their antigen presentation ability and cytotoxic and inflammation-mediating signalization (Ling and Wong, 1993; Kreutzberg, 1996; Town et al., 2005; Werry et al., 2011).

As regards origin, there are two populations of microglial cells in the CNS at any given time. The

*Corresponding author. Address: Department of Cell Biology and Molecular Medicine, University of Szeged, 4 Somogyi u., Szeged H-6720, Hungary. Tel: +36-62-544-570; fax: +36-62-544-569.
E-mail address: gulyak@bio.u-szeged.hu (K. Gulya).

Abbreviations: CD11b/c, cluster of differentiation 11b/c, the rat CR3 complement receptor; CNPase, 2′,3′-cyclic nucleotide 3′-phosphodiesterase; CNS, central nervous system; DIV, days *in vitro*; DMEM, Dulbecco's Modified Eagle's Medium; EDTA, ethylenediamminetetraacetate; GFAP, glial fibrillar acidic protein; HLA, human leukocyte antigen; Iba1, ionized calcium-binding adaptor molecule 1; Ki67, proliferation marker antigen identified by the monoclonal antibody Ki67; MHC, major histocompatibility complex; PBS, phosphate-buffered saline; RT, room temperature; SD, standard deviation; TBS, Tris-buffered saline; TI, transformation index.

0306-4522/13 $36.00
http://dx.doi.org/10.1016/j.neuroscience.2013.03.033

resident microglia comprise a distinct pool of cells that respond to stimuli and proliferate accordingly, and regulate their population dynamics in a manner dependent on the severity of the tissue damage. They are distributed more or less evenly throughout the nervous tissue (Milligan et al., 1991a) and exhibit an extremely slow turnover with the bone marrow or the peripheral blood under normal conditions. The resting microglia with ramified morphology lack the major histocompatibility complex (MHC) class I/MHC class II proteins, interferon-γ, cytokines, CD45 antigens and many other surface receptors required to serve in the antigen-presenting, phagocytic and cytotoxic roles characteristic of the normal macrophage functions. Another population of cells, however, among which the perivascular microglial cells are prominent in number, is located in the close vicinity of blood vessels, and can be replaced regularly by bone marrow-derived precursor cells (Hickey and Kimura, 1988; Eglitis and Mezey, 1997) that express MHC class II antigens, indicating their monocyte/macrophage origin (Streit et al., 1989; Gehrmann et al., 1995). In cases of extreme damage to the CNS, as in infection or stroke, the blood–brain barrier may weaken considerably, and hematogenous, bone marrow-derived cells, such as myeloid progenitor cells and macrophages, may enter the brain (Priller et al., 2001). Once the damage has abated, the peripheral and central systems are disconnected for the recovery and regrowth period (Gehrmann, 1996). Although macrophages and microglia may have similar roles, the populations of resident microglia and recently migrated hematogenous myeloid progenitors/macrophages differ in many important respects (Geissmann et al., 2003; Ladeby et al., 2005; Wirenfeldt et al., 2007).

Similar to the extensive studies on the origin and the morphological and functional development of the microglial phenotype *in vivo* (Ling et al., 1990; Milligan et al., 1991a,b; Ling and Wong, 1993; Dalmau et al., 1997, 1998, 2003; Streit et al., 1999; Orłowski et al., 2003; Geissmann et al., 2010), a large body of information is available on the characteristics of the different microglial populations maintained in cell cultures. However, as a variety of proinflammatory factors are produced by activated microglial cells on the one hand (see Kreutzberg, 1996, for references), and activation of microglial cells by a number of agents has been demonstrated on the other (Liu et al., 2000; Werry et al., 2011; Berger et al., 2012), characterization of the activated microglial cells in response to an *in vitro* stimulation/challenge predominates in the literature. Recent studies have demonstrated, for example, that under specific polarization conditions microglial cells, in a similar way to peripheral macrophages, develop into different inflammation-related phenotypes, termed M1 and M2 (Gordon, 2003; Mosser and Edwards, 2008).

Under physiological conditions, the vast majority of the resident microglial cells in the CNS are certainly unstimulated and characterized by ramified morphology. Despite the recent *in vivo* experimental approaches that unveiled new aspects of the functional, developmental and lineage characteristics of the microglial cell populations (Geissmann et al., 2003, 2010; Auffray et al., 2009; Ginhoux et al., 2010; Durafourt et al., 2012; Xu et al., 2012), only limited data are available on the development of the microglial phenotype *in vitro* under unstimulated/immunologically unchallenged conditions. In an attempt to shed more light on the nature of the unstimulated microglia *in vitro*, we set out to characterize selected morphological, molecular and functional aspects of such cells, partially by quantitative techniques, in rat primary cortical cell cultures maintained routinely up to DIV28, in order to monitor the "normal" development of their phenotype. We analyzed the population dynamics of the microglial cells in terms of their percentage of the total number of cells during culturing, quantitatively characterized the different microglial populations according to their transformation indices, and differentially localized some of the canonical microglial markers to these distinct morphologies. As far as we are aware, a similarly detailed study for a period of up to 28 days on the characteristics of the *in vitro* development of unstimulated and unchallenged microglial cells of embryonic origin has not been reported previously.

EXPERIMENTAL PROCEDURES

Animals

All animal experiments were carried out in strict compliance with the European Council Directive (86/609/EEC) and EC regulations (O.J. of EC No. L 358/1, 18/12/1986) regarding the care and use of laboratory animals for experimental procedures, and followed the relevant Hungarian and local legislation requirements. The experimental protocols were approved by the Institutional Animal Welfare Committee of the University of Szeged (I-74-II/2009/MÁB). The pregnant Sprague–Dawley rats (170–190 g; one animal per cage) were kept under standard housing conditions and fed *ad libitum*.

Antibodies

The antibodies used in our immunohistochemical, immunocytochemical and Western blot studies are listed in Table 1. For a thorough characterization of different microglial phenotypes developed *in vitro*, antibodies against the ionized calcium-binding adaptor molecule 1 (Iba1), the human leukocyte antigen (HLA) class II genes HLA DP, DQ, DR and cluster of differentiation 11b/c, the rat CR3 complement receptor (CD11b/c) were used in our immunohistochemical and Western blot analyses. The anti-Iba1 antibody recognizes the Iba1 protein, an intracellular Ca^{2+}-binding protein expressed in the CNS specifically in macrophages and microglia (Imai et al., 1996), and has been used to detect both resting and activated microglial phenotypes (Ito et al., 1998). The HLA class II genes are composed of three closely linked subregions encoding the polymorphic HLA class II molecules HLA DP, DQ, DR. The anti-HLA DP, DQ, DR antibody reacts with the α and β-chains of all products of these subregions and recognizes numerous antigen-presenting cells that express these molecules, including the reactive and the resting microglia, the perivascular microglial cells, many macrophages and most monocytes in the CNS (Horejsí et al., 1986; Ulvestad et al., 1994b). The anti-HLA DRα antibody recognizes the α subunit of the class II MHC complex antigen HLA DR, a transmembrane glycoprotein

Table 1. Antibodies used in immunohistochemistry, immunocytochemistry and Western blot analysis

Primary antibody, abbrev. name	Primary antibody, full name	Final dilution	Company	Secondary antibody with fluorochrome, full name	Company	Final dilution
Antibodies used in immunohistochemistry and immunocytochemistry						
Iba1	Rabbit anti-Iba1 polycl. ab.	1/300	Wako, Osaka, Japan	Alexa Fluor 568 goat anti-rabbit	Invitrogen, Carlsbad, CA, USA	1/1000
CD11b/c (OX42)	Mouse anti-CD11b/c equivalent monocl. ab., clone OX42	1/200	Abcam, Cambridge, England	Alexa Fluor 488 goat anti-mouse or Alexa Fluor 568 goat anti-mouse	Invitrogen, Carlsbad, CA, USA	1/1000
HLA DP, DQ, DR	Mouse anti-HLA-DP, DQ, DR, monocl. ab., clone CR3/43	1/100	Dako, Glostrup, Denmark	Alexa Fluor 488 goat anti-mouse	Invitrogen, Carlsbad, CA, USA	1/1000
HLA DRα	Rabbit anti-HLA-DRα, FL-254, polycl. ab., SC-25614	1/50	Santa Cruz Biotechnol., Inc., Santa Cruz, CA, USA	Alexa Fluor 488 goat anti-rabbit	Invitrogen, Carlsbad, CA, USA	1/1000
β Tubulin III	Mouse anti-tubulin, β-III, monocl. ab., clone TU-20	1/400	Abcam, Cambridge, England	Alexa Fluor 488 goat anti-mouse	Invitrogen, Carlsbad, CA, USA	1/1000
Ki67	Rabbit anti-Ki67, monocl. ab., clone SP6	1/200	Thermo Scientific, Fremonz, CA, USA	Alexa Fluor 488 goat anti-rabbit	Invitrogen, Carlsbad, CA, USA	1/1000
Antibodies used in Western blot studies						
Iba1	Rabbit anti-Iba1 polycl. ab.	1/1000	Wako, Osaka, Japan	Anti-rabbit IgG, peroxidase conjug.	Sigma, St. Louis, MO, USA	1/1000
β Tubulin III	Mouse anti-tubulin, β-III, monocl. ab., clone TU-20	1/1000	Abcam, Cambridge, England	Anti-mouse IgG, peroxidase conjug.	Sigma, St. Louis, MO, USA	1/3000
GFAP	Rabbit anti-GFAP polycl. ab.	1/5000	Abcam, Cambridge, England	Anti-rabbit IgG, peroxidase conjug.	Sigma, St. Louis, MO, USA	1/2000
CNPase	Mouse anti-CNPase, monocl. ab., clone 11–5B	1/500	Abcam, Cambridge, England	Anti-mouse IgG, peroxidase conjug.	Sigma, St. Louis, MO, USA	1/3000

constitutively expressed by microglia (Ulvestad et al., 1994a). The anti-CD11b/c antibody recognizes a common epitope shared between CD11b and CD11c (integrin α_M and α_X chains), reacts with all monocytes and macrophages (Robinson et al., 1986; Wang et al., 1996), and is commonly used as a resident microglial marker in the CNS (Imai et al., 1996). The anti-β tubulin III (Banerjee et al., 1990) antibody has been used to detect neurons, the anti-glial fibrillar acidic protein (GFAP) antibody (Guillemin et al., 1997) to label astrocytes, and the anti-2′,3′-cyclic nucleotide 3′-phosphodiesterase (CNPase) antibody (Zhang et al., 2010) to detect oligodendrocytes. The anti-Ki67 antibody has been used to detect proliferating cells. Ki67 is a nuclear protein expressed in all active phases of the cell cycle from the late G1 phase through the end of the M phase but is absent in non-proliferating and early G1 phase cells (Starborg et al., 1996; Scott et al., 2004).

Various dilutions of primary and secondary antibodies, incubation times and blocking conditions for each antibody used were carefully tested for both immunohistochemistry/immunocytochemistry and Western blot analysis. To detect the specificities of the secondary antisera, omission control experiments (staining without the primary antibody) were also performed. In such cases, no fluorescent or Western blot signals were detected.

Paraffin embedding and sectioning

Forebrain samples of embryonic day 18 (E18) rats were carefully removed, fixed by immersion overnight at 4 °C in 0.05 M phosphate-buffered saline (PBS) containing 4% formaldehyde, and then embedded in low-melting point paraffin. Coronal sections (8 μm thick) were cut in a microtome and mounted on slides coated with (3-aminopropyl)triethoxysilane (Menzel, Darmstadt, Germany) to prevent detachment. After deparaffinization and rehydration, the slides were placed in a jar filled with 0.01 M citrate buffer (pH 6.0) and heated three times for 3 min at 800 W in a microwave oven. The sections were then processed for immunohistochemistry.

Cortical cell cultures

Mixed primary cortical cell cultures were established from E18 wild-type rat embryos by the use of general methods described previously (Kortvely et al., 2003). Briefly, 6–8 fetal rats under ether anesthesia were surgically decapitated and the frontal lobe of the cerebral cortex was removed, minced with scissors, incubated for 10 min at 37 °C in 9 ml of Dulbecco's Modified Eagle's Medium (DMEM; Invitrogen, Carlsbad, CA, USA; containing 1 g/l D-glucose, 110 mg/l Na-pyruvate, 4 mM L-glutamine, 3.7 g/l $NaHCO_3$, 10,000 U/ml penicillin G, 10 mg/ml streptomycin sulfate and 25 μg/ml amphotericin B) supplemented with 0.25% trypsin (Invitrogen) and then centrifuged at 1000*g* for 10 min at room temperature (RT). The pellet was resuspended, washed twice in 5 ml of DMEM containing 10% heat-inactivated fetal bovine serum (Invitrogen), and centrifuged for 10 min at 1000*g* at RT. The final pellet was resuspended in 2 ml of the same solution as above, after which the cells were seeded either in poly-L-lysine-coated coverslips (15 × 15 mm; 200,000 cells/coverslip) or in poly-L-lysine-coated Petri dishes (60 mm × 15 mm; 1,000,000 cells/dish) and cultured at 37 °C in a humidified air atmosphere supplemented with 5% CO_2. All experiments were performed with cultures aged 1–28 days (DIV1–DIV28), or occasionally with cultures aged up to 2 months (data not shown). For culturing periods longer than 3 days, the DMEM was changed every 3 days. Apart from the microglial markers, several cell surface and cytoplasmic neuronal, astrocytic and oligodendrocytic markers

were used to characterize the primary cultures. Cell proliferation was assessed by the use of the antibody raised against Ki67.

In vitro phagocytosis assay

The fluid-phase phagocytic capacity of the unstimulated microglial cells was determined via the uptake of fluorescent microspheres (2 μm diameter; Sigma, St. Louis, MO, USA). Cortical cells from E18 rats were plated on coverslips in 35-mm Petri dishes at a density of 200,000 cells/coverslip in 2 ml of DMEM containing 10% heat-inactivated fetal bovine serum as above, and cultured for 14 days. At the end of the culturing period, 1 μl of a 2.5% aqueous suspension of fluorescent microspheres per ml was added to the primary culture, which was then incubated for 60 min at 37 °C. The cells were next washed five times with 2 ml of PBS to remove dish- or cell surface-bound residual fluorescent microspheres, and fixed with 4% formalin in PBS. For measurement of the phagocytotic activity, cells labeled with phagocytosed microbead(s) were counted. Twenty random fields with a total of 120 bead-labeled cells were counted under a fluorescent microscope with a 10× or 20× objective. The number of phagocytosed microbeads (mean ± SD) was analyzed as a function of the transformation index (TI). Statistically significant differences were determined by the Mann–Whitney Rank Sum test.

Immunohistochemistry and -cytochemistry

For immunohistochemistry, primary cortical cells cultured *in vitro* on poly-L-lysine-coated coverslips for 1–28 days (DIV1–DIV28) were used. At different time intervals, the cultured cells on the coverslips were fixed in 4% formaldehyde in 0.05 M PBS (pH 7.4 at RT) for 5 min, and rinsed in 0.05 M PBS for 3 × 5 min. After permeabilization and blocking of the nonspecific sites in 0.05 M PBS solution containing 5% normal goat serum (Sigma), 1% heat-inactivated bovine serum albumin (Sigma) and 0.05% Triton X-100 for 30 min at 37 °C, the cells on the coverslips were incubated overnight at 4 °C with the appropriate primary antibody (Table 1) in the above solution. The cultured cells were washed for 4 × 10 min at RT in 0.05 M PBS, and then incubated with the appropriate Alexa Fluor fluorochrome-conjugated secondary antibody (Table 1) in the above solution, but without Triton X-100, in the dark for 3 h at RT. The cells on the coverslip were washed for 4 × 10 min in 0.05 M PBS at RT, and the nuclei were stained in 0.05 M PBS solution containing 1 mg/ml polyvinylpyrrolidone and 0.5 μl/ml Hoechst 33258 dye (Sigma). The coverslips were rinsed in distilled water for 5 min, air-dried and mounted on microscope slides in a Vectashield mounting medium (Vector Laboratories, Burlingame, CA, USA). Cells were viewed on a Nikon Microphot-FXA epifluorescent microscope (Nikon Corp., Tokyo, Japan) and photographed with a Spot RT Color CCD camera (SPOT RT/ke, Diagnostic Instruments, Inc., Sterling Heights, MI, USA).

Western blot analysis

For Western blotting, the protocols were optimized for each antibody as regards epitope accessibility, polyacrylamide gel separation, antibody dilution and chemiluminescence signal intensity. Cultured primary cells (DIV1–DIV28) were collected through the use of a rubber policeman, homogenized in 50 mM Tris–HCl (pH 7.5) containing 150 mM NaCl, 0.1% Nonidet P40, 0.1% cholic acid, 2 μg/ml leupeptin, 1 μg/ml pepstatin, 2 mM phenylmethylsulfonyl fluoride and 2 mM EDTA, and centrifuged at 10,000*g* for 10 min. The pellet was discarded and the protein concentration of the supernatant was determined (Lowry et al., 1951). For the Western blot analyses of microglial, neuronal, astrocyte or oligodendrocyte immunoreactivities, 5–10 μg of protein was separated on a sodium dodecyl sulfate (SDS)–polyacrylamide gel (4–10% stacking gel/resolving gel), transferred onto Hybond-ECL nitrocellulose membrane (Amersham Biosciences, Little Chalfont, Buckinghamshire, England), blocked for 1 h in 5% nonfat dry milk in Tris-buffered saline (TBS) containing 0.1% Tween 20, and incubated for 1 h with the appropriate primary antibodies. After five washes in 0.1% TBS–Tween 20, the membranes were incubated for 1 h with the appropriate peroxidase-conjugated secondary antibodies (Table 1), and washed five times as before. The enhanced chemiluminescence method (ECL Plus Western blotting detection reagents; Amersham Biosciences) was used to reveal immunoreactive bands according to the manufacturer's protocol.

Digital image processing and image analysis

Gray-scale digital images of the immunoblots were acquired by scanning the autoradiographic films with a desktop scanner (Umax PowerLook III; Umax Data Systems, Inc., Taipei, Taiwan). The images were scanned and processed at identical settings in order to allow comparison between the Western blots from different samples. Digital images were acquired with a Nikon Microphot-FXA epifluorescent microscope (Nikon Corp., Tokyo, Japan), using a Spot RT Color CCD camera and Spot RT software (Spot RT/ke Diagnostic Instruments, Sterling Heights, MI, USA). Color correction and cropping of the digital images were occasionally performed when photomicrographs were made for publication (Adobe Photoshop; Adobe Systems, Inc., San Jose, CA, USA).

Microglial cells and cell nuclei in the cultures were counted with the use of the plugins developed for the computer program ImageJ (version 1.38; developed by W. Rasband at the U.S. National Institutes of Health, and available from the Internet at http://rsb.info.nih.gov/ij). Cell nuclei were counted with the use of the "Nucleus Counter" plugin (Image Processing and Analysis in Java, a collection of plugins and macros) installed under ImageJ (www.macbiophotonics.ca). Briefly, digital images in tagged image file formats (.tif) were opened in ImageJ, and Plugins → Particle Analysis → Nucleus Counter menus were then selected and customized as follows: the smallest and largest particle sizes were set to 50 and 10,000, respectively. "Otsu" was selected for automatic thresholding, and "mean 3 × 3" was chosen for the performance of smooth filtering (Sezgin and Sankur, 2004). After background subtraction, overlapping objects in the resulting binary images were separated, via the menu command "Process/Binary/Watershed" (see Abràmoff et al., 2004, for details, and the documentation web pages for ImageJ at http://rsb.info.nih.gov/ij/docs/index.html). For the counting of microglial cells expressing immunopositivity for the Iba1 antigen, the "Cell Counter" plugin was used (ImageJ for Microscopy). After the appropriate images (.tif) had been opened, Plugins → Particle Analysis → Cell Counter menus were selected, and the output was copied to a Microsoft Excel spreadsheet (Microsoft Corp., Redmond, WA, USA) for statistical analysis.

Microglial cell silhouettes were acquired by transforming the raw digital files of Iba1-immunoreactive cells recorded under fluorescent microscope light to binary files by means of the ImageJ software. The color cell images were transformed into their binary replicas (silhouettes) by using automatic thresholding procedures. After the values of cell perimeter (μm) and cell area (μm^2) had been determined in at least three separate experiments (at least two coverslips in each experiment for each culturing time investigated; around 20 randomly selected cells/coverslip), the TI reflecting the degree of process extension was calculated through the expression $[\text{perimeter of cell } (\mu m)]^2/4\pi$ [cell area (μm^2)] as previously described (Fujita et al., 1996). A total of 398 cell silhouettes were analyzed in this study.

Statistical analysis

For Western blots, values are presented as means ± SD from at least three blots for each of the three independent experiments for each time period examined. For the counting of microglial cells and cell nuclei, at least 10 randomly sampled microscope fields from 2 to 3 coverslips for each culturing time period from each of the three separate cell-culturing experiments were counted. In the computation of semiquantitative cell silhouette characteristics (digital binary pictures), data on 20 cells per coverslip from at least three separate experiments for each culturing time were used. Values are presented as means ± SD. Statistical analyses were carried out with the Mann–Whitney Rank Sum test (SigmaStat 3.11; Systat Software Inc., Chicago, IL, USA).

RESULTS

Microglial cells collected from the forebrains of E18 rats are mainly ameboid

The microglial cells were collected from E18 rat forebrains and maintained in mixed primary neuronal-glial co-cultures. Light microscopic fluorescent immunohistochemistry revealed (Fig. 1) that on E18 the Iba1-labeled microglial cells in the forebrain cortical tissue appeared to be mainly ameboid (arrowheads), though more differentiated forms were also present in smaller numbers. Most of the microglial cells were rounded or slightly ovoid and lacked branching processes; however, rod-like (double-arrowhead) or slightly ramified microglial cells (arrow) were occasionally also seen in the embryonic rat forebrain.

Microglial cells proliferate during *in vitro* culturing of primary forebrain cells

As concerns the cell number and the presence of numerous microglia-specific antigens, fluorescent immunocytochemistry (Fig. 2) and Western analysis (Fig. 3) demonstrated a massive *in vitro* expansion of the microglial cell type between DIV1 and DIV28. The total numbers of cells at the beginning and at the end of the culturing period did not differ significantly. While the total number of cells exhibited a minimum on DIV10, the number of microglia constantly increased from immediately after seeding throughout the entire culturing period. The microglia were situated in a scattered manner in younger cultures (before and around DIV14; Fig. 2A–E), but when they increased in abundance as the cultures grew older, they became more clumped and grouped together around other cells, as seen between DIV21 and DIV28 (Fig. 2F, G). Typical relative distributions of neuronal and microglial cells during culturing may be seen in Fig. 2H–J. The microglial cell content originally amounted to less than 0.5% of the total cell number at the time of seeding, but steadily rose during culturing. On DIV4 and DIV7, progressively more microglial cells appeared, accounting for 2% and 8% of the total cell number, respectively (Fig. 3A). On DIV10, the overall morphological diversity of the microglial cells in the culture was similar to that on DIV7; at this time, the cultures contained barely 50% of the total cell number seen on DIV1, and the microglial cells comprised around 18% of the total cell population (see Fig. 2D for comparison). From this time onward, most of the gains in the number of total cell counts could be attributed to microglial cell proliferation (Fig. 3A). On DIV14, as the majority of the microglia had started to differentiate toward the ramified form, approximately 20% of all the cells were microglia. The proportion of microglial cells reached 33.7% by DIV28 (Fig. 3A, see Fig. 2G also for comparison). This massive, roughly 67-fold multiplication of the microglial cell type was also demonstrated by Western blot analysis (Fig. 3B, C). The Iba1 immunoreactivities detected in the blots steadily increased some 750-fold between DIV1 and DIV28. The β tubulin III, GFAP and CNPase immunoreactivities, quantified by Western blot analyses, demonstrated the evolution of other cellular components during culturing (Fig. 3B, C): while the amount of the neuronal marker β tubulin III steadily decreased, the immunoreactivity of the oligodendrocyte marker CNPase constantly rose between DIV1 and DIV28. A decrease in GFAP immunoreactivity at DIV28 was also observed in the cultures (Fig. 3C).

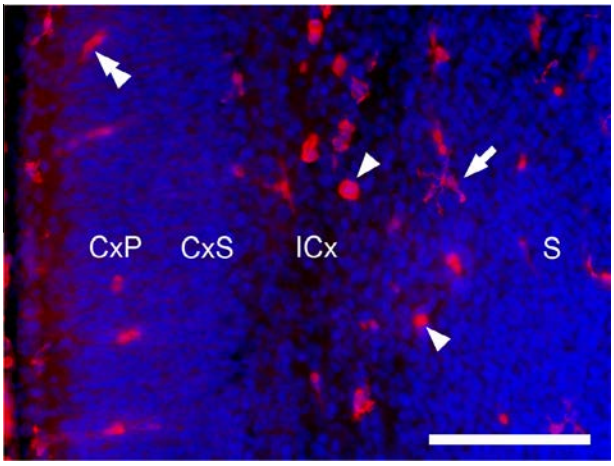

Fig. 1. Microglia in the E18 embryonic rat forebrain. The immunofluorescent detection of microglial cells (red) in 8-μm-thick paraffin-embedded coronal sections of E18 rat forebrains was achieved through the use of anti-Iba1 antibody. Most Iba1-labeled cells displayed ameboid morphology with ovoid (arrowhead) or slightly rod-shaped forms (double-arrowhead), but occasionally more ramified microglia could also be seen (arrow). Cell nuclei were labeled blue with Hoechst 33258. CxP: cortical plate; CxS: cortical subplate; ICx: intermediate cortical layer; S: subiculum. Scale bar = 100 μm. (For interpretation of the references to color in this figure legend, the reader is referred to the web version of this article.)

Mixed microglial populations exist in primary forebrain cultures

Diverse morphological forms of microglial cells developed and were present throughout the culturing (Fig. 4). At one end of the morphological spectrum, on DIV1, the microglial cells were virtually exclusively ameboid, frequently with smooth-surfaced spherical cell bodies, although ovoid or fusiform cells with a few microspikes could also be seen (Fig. 4A–D). As the cultures grew older (DIV7–DIV10), the microglia became more ramified. They acquired larger somata bearing typically one or two, but rarely more, large processes (Fig. 4E–H). One large, stubby lamellipoda usually formed first,

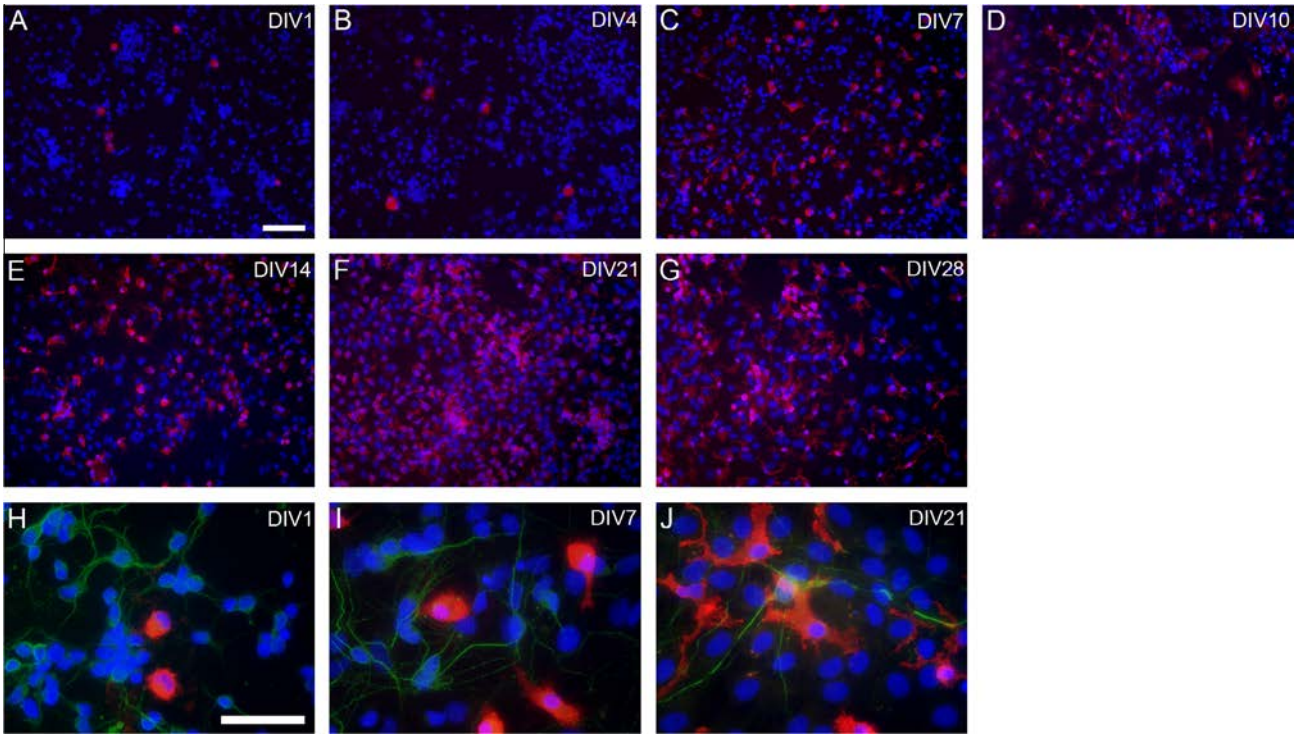

Fig. 2. Development of Iba1 immunoreactivity in primary cortical cultures (DIV1–DIV28). (A–G) The number and composition of the cultured cells are tightly controlled. While the total number of cells remains constant, the microglia proliferate during culturing. The microglial cells (red) were first labeled with the rabbit anti-Iba1 primary (polyclonal) antibody, and then with an appropriate Alexa Fluor fluorochrome-conjugated secondary (Alexa Fluor 568 goat anti-rabbit) antibody, while the cell nuclei (blue) were labeled with Hoechst 33258. Culturing times are indicated at the upper right corners of the pictures. Scale bar in A for A–G = 50 μm. (H–J) Microglial cells in characteristic cellular environments. For the detection of microglial cells and neurons, anti-Iba1 (red) and anti-β tubulin III (green) antibodies, respectively, were used. The cell nuclei (blue) were labeled with Hoechst 33258. (H) On day 1, the Iba1-positive microglial cells (red) were mostly ameboid around the developing β tubulin III-positive neurons (green). (I) On day 7, some of the microglial cells (red) had become ramified around a group of β tubulin III-immunopositive developing neurons (green). (J) On day 21, the culture was characterized by a heterogeneous, albeit mostly ramified population of microglia (red), located around the occasional β tubulin III-positive neurons (green) and many non-neuronal/non-microglial cells indicated by the blue nuclei. Scale bar in H for H–J = 50 μm. (For interpretation of the references to color in this figure legend, the reader is referred to the web version of this article.)

but by DIV10 further processes, or the more ramified morphology of a single large lamellipoda could be observed (Fig. 4G, H). After DIV10, the microglial cells became more heterogeneous, as a constantly increasing microglia population characterized by relatively even cellular processes and enlarging somata accompanied the ameboid form (Fig. 4I–K, M). Microglial process formation became widespread by DIV14. Incidentally, this was the first time at which the ramified microglia (demonstrating morphology similar to that of the resting microglia in the adult rodent CNS) predominated in the cultures (Fig. 4I, J). The Iba1-positive microglial cells were characterized morphologically by larger somata with a few long, relatively thin and sparsely ramified processes. As the cultures grew older, on both DIV21 and DIV28, the characteristic microglial morphology was a ramified form with several axes of symmetry along the processes (Fig. 4K, M), albeit ameboid cells were also present (Fig. 4L, N). The typical microglial morphology during the later stages of *in vitro* culturing also included cells with elongated, slightly curved somata emanating a few processes of mixed lengths. It must be noted that islands of densely grown ameboid microglial cells were persistently present throughout culturing.

Cultured microglia populations can be evaluated by their TI values

The time course of the morphological changes in the microglia was analyzed on binary silhouettes, as depicted in Fig. 5. Quantitative analysis based on the TI value, a dimensionless number that is an indicator for the identification of the degree of morphological differentiation (e.g. the degree of process extension) of a cell, revealed a continuum of the microglial phenotype between the ameboid and the extremely ramified morphologies of the microglia. Throughout the experiments, microglial cells with TI < 3 were considered ameboid (Fig. 6A–G; circles). While younger cultures displayed predominantly ameboid cell forms with a regular, round outline reflecting the expanding microglia population (Figs. 5 and 6A–D), older cultures presented a more heterogeneous morphological repertoire, concurrently involving cells with ameboid (proliferating) and ramified (resting) forms, the majority being ramified (Figs. 5 and 6E–G). The ramified, resting microglia that developed later during the culturing could be characterized by a TI value as high as 81 (Fig. 6H). The ameboid, proliferating microglial cells, predominant in the early stages but always present throughout

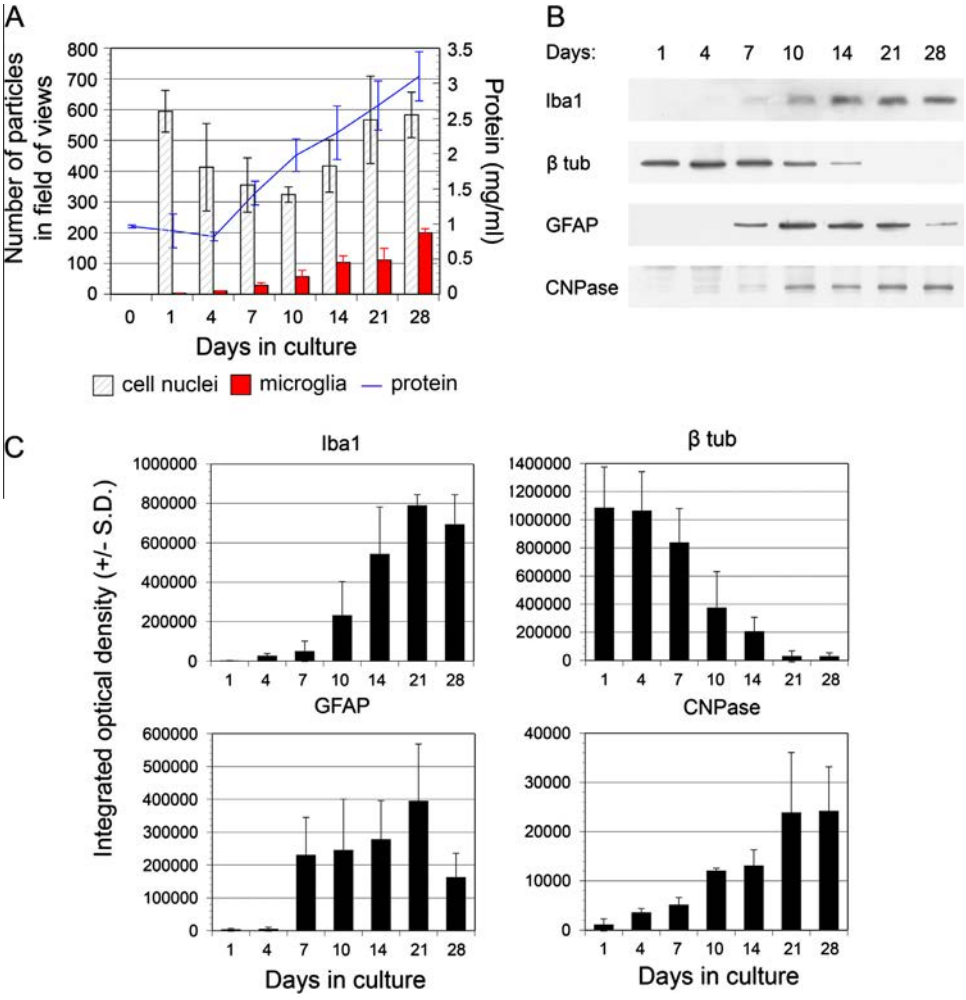

Fig. 3. Quantitative analysis of the cellular composition, the protein content and the amount of selected biomarkers during culturing. (A) The numbers of cell nuclei (striped bars) and Iba1-positive (microglial) cells (solid bars) and the protein content (solid line) were quantitative analyzed in primary cortical cultures (DIV1–DIV28). The methods of counting cell nuclei and anti-Iba1-immunolabeled cells are described in the Experimental procedures section. Error bars indicate means ± SD. (B) Representative Western blot pictures of Iba1, β tubulin III, GFAP and CNPase immunoreactivities in primary cortical cultures (DIV1–DIV28). (C) Quantitative Western blot analysis of Iba1, β tubulin III, GFAP and CNPase immunoreactivities in cell cultures between DIV1 and DIV28. Iba1: ionized calcium-binding adaptor molecule 1, β tub: β tubulin III, GFAP: glial fibrillar acidic protein, CNPase: 2′,3′-cyclic nucleotide 3′-phosphodiesterase. Error bars indicate means ± SD.

culturing, had TI values of less than 3, independently of the age of the culture (Fig. 6H; below dashed line), and were always Ki67-positive (Fig. 7). The Ki67 immunoreactivity observed in the ameboid microglial nuclei usually exhibited a distinct dotlike pattern representative of the S/G2 phase (Fig. 7A–D) unless it was associated with the periphery of the condensed chromosomes of the M-phase (Fig. 7E–H).

Phagocytosis is predominant in ameboid microglia in culture

Ameboid and ramified microglial cell populations in culture could be differentiated through their ability to phagocytose (Fig. 8). Unstimulated microglia readily phagocytosed fluorescent microbeads. On DIV14, when mixed populations of ameboid and ramified microglia were present in the cultures in about equal numbers, microbeads were significantly more preferred by the ameboid forms (characterized by low TI values; Fig. 8A), while the ramified microglia (with higher TI values; Fig. 8B) were less active in phagocytosing microbeads. On average, microglia with TI < 3 phagocytosed 11.08 ± 8.6 beads per cell (average ± SD, $n = 39$), while microglia with TI > 3 engulfed 3.16 ± 3.6 beads per cell ($n = 81$); the difference was statistically significant ($p < 0.001$; Mann–Whitney Rank Sum test). When the number of phagocytosed microbeads per microglia was plotted as a function of TI under unstimulated/unchallenged conditions, the physiologically distinct populations of ameboid and ramified microglia could be readily demonstrated (Fig. 8C).

Immunocytochemistry reveals microglial populations displaying changing molecular phenotypes during culturing

Double immunofluorescent microscopy revealed that Iba1-labeled microglial cells occasionally also expressed

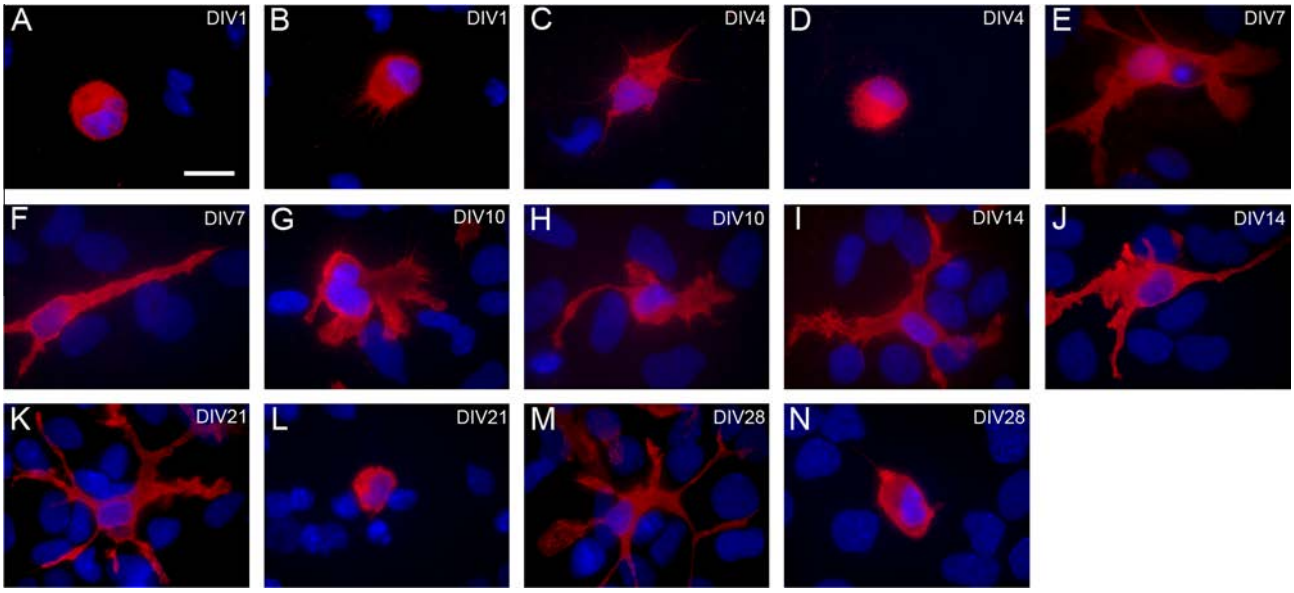

Fig. 4. Development of the morphology of the microglial cells in the primary forebrain cultures (DIV1–DIV28). The microglial cells (red) were first labeled with the anti-Iba1 primary antibody, and then with the Alexa Fluor 568 fluorochrome-conjugated goat anti-rabbit secondary antibody, while the cell nuclei (blue) were stained with Hoechst 33258. On day 1 (A, B), all the microglial cells had an ameboid appearance, with round or slightly ovoid cell forms. Very few, if any, microspikes or lamellipodae could be seen (B). On day 4 (C, D), some of the microglial cells had become more asymmetric or rod-shaped, and some of these cells possessed more pronounced lamellipodae (C). At later stages, from day 7 (E, F), the microglia became more ramified. Usually only a few, heavier branches appeared at this stage of microglial differentiation (F). From this stage on, the cultures were characterized by two distinctly polarized populations, representing the two extremes of the morphological continuum displayed by the microglial cells in the cultures, i.e. the ameboid and the ramified microglial cells. From day 14 (I, J), the microglia became truly ramified as they usually had 3–4 strongly developed branches, but 6–7 equally strong and long branches could sometimes be seen from day 21 (K, M). At these times, ameboid cell forms were also still quite frequent (L, N). Scale bar in A (for all pictures) = 10 μm. (For interpretation of the references to color in this figure legend, the reader is referred to the web version of this article.)

the HLA DP, DQ, DR antigens, exclusively in young cultures (Fig. 9A, B). HLA DP, DQ, DR-positive Iba1-expressing microglial cells were always ameboid, with TI < 3 (Fig. 9A, B). They were sporadically present from seeding up to DIV10, but disappeared completely from the cultures thereafter. Cultures older than DIV10 did not express this antigen, even when they had an ameboid shape and proliferated, indicating that the HLA antigen expression can be uncoupled from the ameboid morphology. Microglial cells with typical ameboid morphology and doubly immunopositive for the CD11b/c and HLA DRα antigens were also found in young cultures (Fig. 9C, D). The last day on which these markers were colocalized was DIV10. CD11b/c-positive microglia in cultures older than DIV10 were no longer able to express any of these HLA antigens. CD11b/c-positive microglial cells, however, were present throughout culturing (Fig. 9C–F). CD11b/c could be colocalized with the Iba1 antigen in both young and old cultures, but only in cells with ameboid (i.e. activated, proliferating) or slightly ramified forms with TI < 13 (Fig. 9E). The Iba1-immunopositive cells predominated throughout culturing, their morphology ranging from ameboid (Fig. 9A, B) to the ramified forms (Fig. 9E). Morphologically, Iba1-positive microglia were the most heterogeneous with TI values from the whole spectrum during the culturing.

The relationship between TI values and myeloid/microglial cell-specific markers in cultured microglial cells is shown in Fig. 9G. We observed that microglial cells either lose some of their macrophage characteristics (e.g. HLA DP, DQ, DR or HLA DRα antigens) during culturing or restrict them to their less differentiated forms (e.g. CD11b/c), even though they retain this latter phenotype for subsequent generations. During culturing, only the less differentiated, ameboid microglial cells (TI < 3) expressed HLA DP, DQ, DR (or HLA DRα) antigens; these cells will either die out or differentiate to more ramified morphologies with TI > 3. CD11b/c-positive cells can be observed throughout culturing, but they never become fully ramified, and their TI values are always < 13.

DISCUSSION

Ramified microglial cells, the most common form of microglial cells in the normal adult brain, are derived from macrophage-like cells of mesodermal origin (Ling and Wong, 1993; Gehrmann et al., 1995; Dalmau et al., 1997). Many lines of evidence have recently demonstrated that these "true" resident microglial cells can be distinguished from other myeloid monocytic cells in the CNS from the aspects of their location, origin, specific cell surface antigens, other biochemical markers, their functions and their turnover with the periphery. Adult resting microglia with ramified forms reside in the parenchyma of the CNS, their position often being juxtavascular (Davalos et al., 2005; Ginhoux

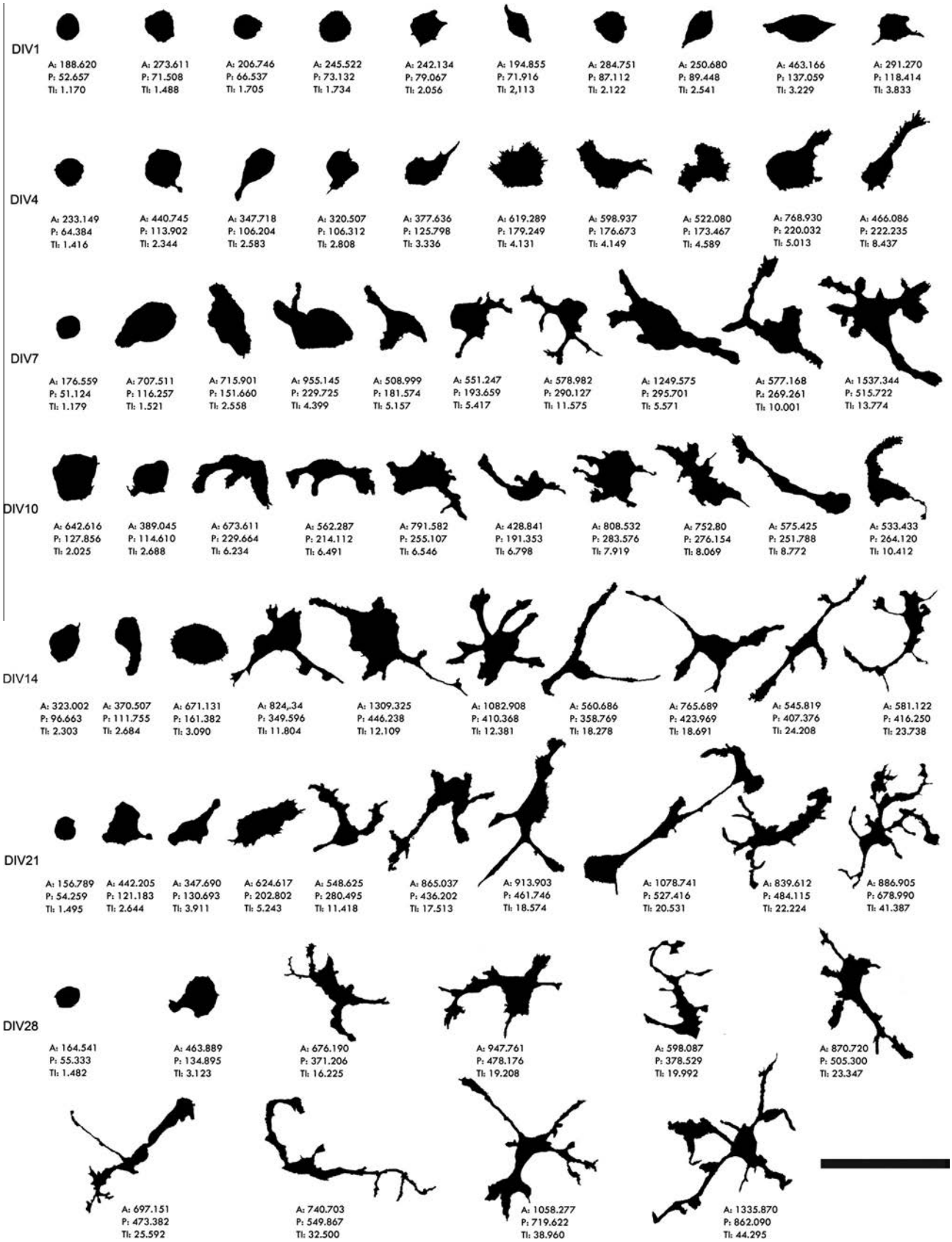

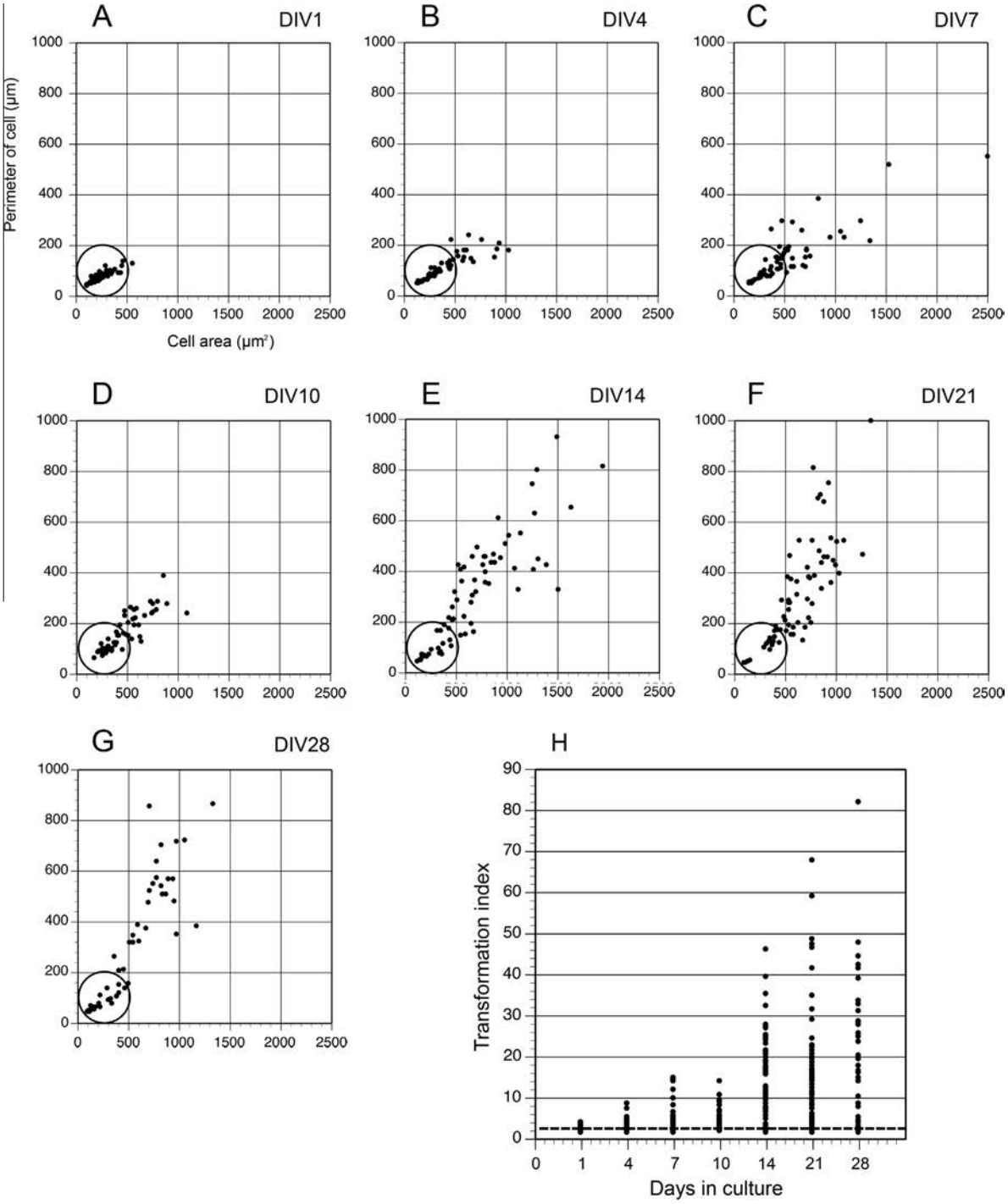

Fig. 6. Evolution of morphometric parameters of the microglial cells during culturing. (A–G) Relationship between the perimeter of the microglial cell and its cell surface area. Cell area and perimeter values were measured by using the computer program ImageJ, and TI values were calculated as [perimeter of cell (μm)]^2/4π [cell area (μm^2)]. Each dot represents a digitized microglial cell. Some of the dots overlap at this resolution. The less differentiated microglial cell populations (TI < 3) are marked with circles. Dots within the circles almost always indicate a cell with TI < 3 and a cell surface area < 500 μm^2. (H) Distribution of TI values as a function of the culturing time. Microglial cells with TI < 3 are located below the dashed line. As may be seen here, there are microglial cells with extremely high TI values on DIV21 and DIV28.

Fig. 5. Morphological heterogeneity of microglial cells after different culturing times. The Iba1-positive microglial cells were photographed, digitized and quantitatively analyzed according to their morphological characteristics. Area (A), perimeter (P) and transformation index (TI) are indicated for each digitized cell. Ten representative cells are shown at each culturing time. While younger cultures exhibited predominantly ameboid cell forms with TI < 3, older cultures were morphologically heterogeneous, as they developed a continuum of populations with two distinct microglial cell populations at the extrema: the ameboid cell population (TI < 3) and the ramified cell population (TI > 3). Younger cultures exhibited predominantly ameboid cell forms, while older cultures displayed more ramified forms, but also proliferating ameboid populations (see the few ameboid microglia among the mainly heterogeneous microglial cells at DIV28.

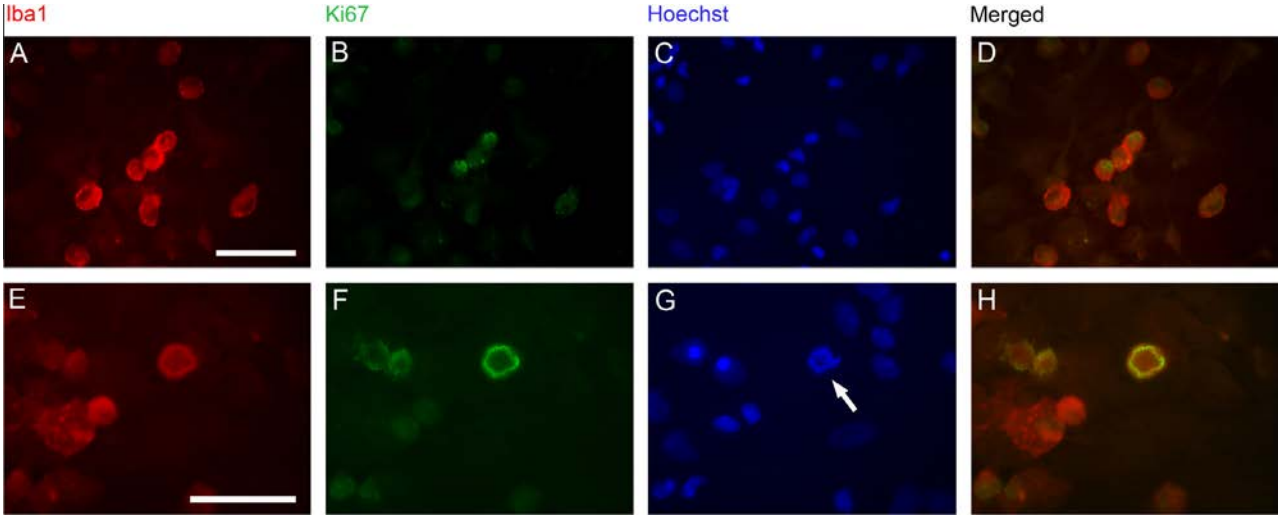

Fig. 7. Relationship between proliferation, ameboid morphology and Ki67 immunoreactivity. Representative immunocyochemical pictures of Ki67-positive ameboid microglial cells in DIV7 cultures. Fluorescent microphotographs of the cultures were taken through the red (A, E), green (B, F) and blue (C, G) channels and displayed in this sequence. CD11b/c-positive microglia (A, E), Ki67-positive cells (B, F) and Hoechst 33258-labeled cell nuclei (C, G) are depicted. The merged pictures of CD11b/c- and Ki67-immunolabeled microglial cells are also shown (D, H). The presence of some non-microglial and non-dividing cells is indicated by the Hoechst 33258 stain at the upper right corner of the pictures. A group of CD11b/c-positive microglial cells is located at the bottom left corner of the pictures. Proliferating CD11b/c-positive microglial cells are located in the middle of the pictures. Arrow points to the condensed chromatin in an M phase microglia (G). Scales for all pictures: 50 μm. (For interpretation of the references to color in this figure legend, the reader is referred to the web version of this article.)

et al., 2010). They express a defined set of markers differently from other myeloid cell populations of the CNS (including, for example, CD11b, F4/80, the chemokine receptor CX3CR1 and Iba1), and function as local immune surveyors and scavengers of cell debris; the true, resident microglia population does not participate in exchange with the circulation (Prinz et al., 2011). Myeloid cell populations of the CNS with specific patroling functions include the perivascular, the meningeal and the choroid plexus macrophages, which possess slightly different sets of markers, but always take part in extensive exchange with the myeloid cells of the circulation (Bechmann et al., 2001a,b; Vallières and Sawchenko, 2003; Kim et al., 2006; Hawkes and McLaurin, 2009; Chinnery et al., 2010) and the vessel-patroling resident monocytes and inflammatory monocytes that originate from and display a high turnover with the bone marrow (Geissmann et al., 2003; Auffray et al., 2009).

Discrimination between the different myeloid monocytic cell forms with uniquely important *in vivo* functions was beyond the scope of this study when cells were collected for the primary culture. Previous studies on the preparation of tissue slices (Hailer et al., 1996, 1997; Stence et al., 2001) and primary cultures (Floden and Combs, 2006) indicated that physical damage to cells during tissue handling and cell harvesting (tissue removal from the embryo, sectioning, cell isolation procedure, etc.) can alter the microglial morphology, marker expression and function, and the resulting molecular characteristics seen *in vitro* may not necessarily reflect the *in vivo* phenotype. It is possible, therefore, that the cells we harvested from E18 rat forebrains and later identified as Iba1-positive included many of the myeloid monocytic cell populations described above, but the prolonged culturing led to the development of molecular and functional phenotypes quite different from those seen *in vivo*, and perhaps even sparser, less differentiated myeloid-derived cell populations when cultured.

Earlier attempts to characterize microglial cells *in vitro* frequently employed culturing times of less than a week (Becher and Antel, 1996; Tanaka et al., 1998; Otani et al., 2011), when changes in microglial population dynamics were not always apparent. Microglia cultured from the embryonic or from the adult brain were also found to differ in many important ways. Microglia prepared from the adult rat brain became progressively de-differentiated and acquired a phenotype reminiscent of that of activated microglia *in vivo* over a period of 7 days in culture (Slepko and Levi, 1996). The differences between microglia acutely isolated from the CNS and cultured microglia derived from mixed glial cultures were most clearly seen in their differential proliferative capacity and cytokine responsiveness (Frei et al., 1994; Ford et al., 1995). Unlike microglia from cultures, microglial cells from adults were not stimulated by transforming growth factor (Rozovsky et al., 1998), nor did they proliferate in response to granulocyte- or macrophage colony-stimulating factor (Ford et al., 1995). While the concept of M1/M2 macrophage heterogeneity has gained momentum in recent years, there is considerable uncertainty as to the extent to which this notion could be extrapolated to microglial cells. For example, in a recent study, Durafourt et al. (2012) found that M1 and M2 subtypes of macrophages and those of the microglial cells not only differentially expressed a number of genes, but phagocytosed myelin

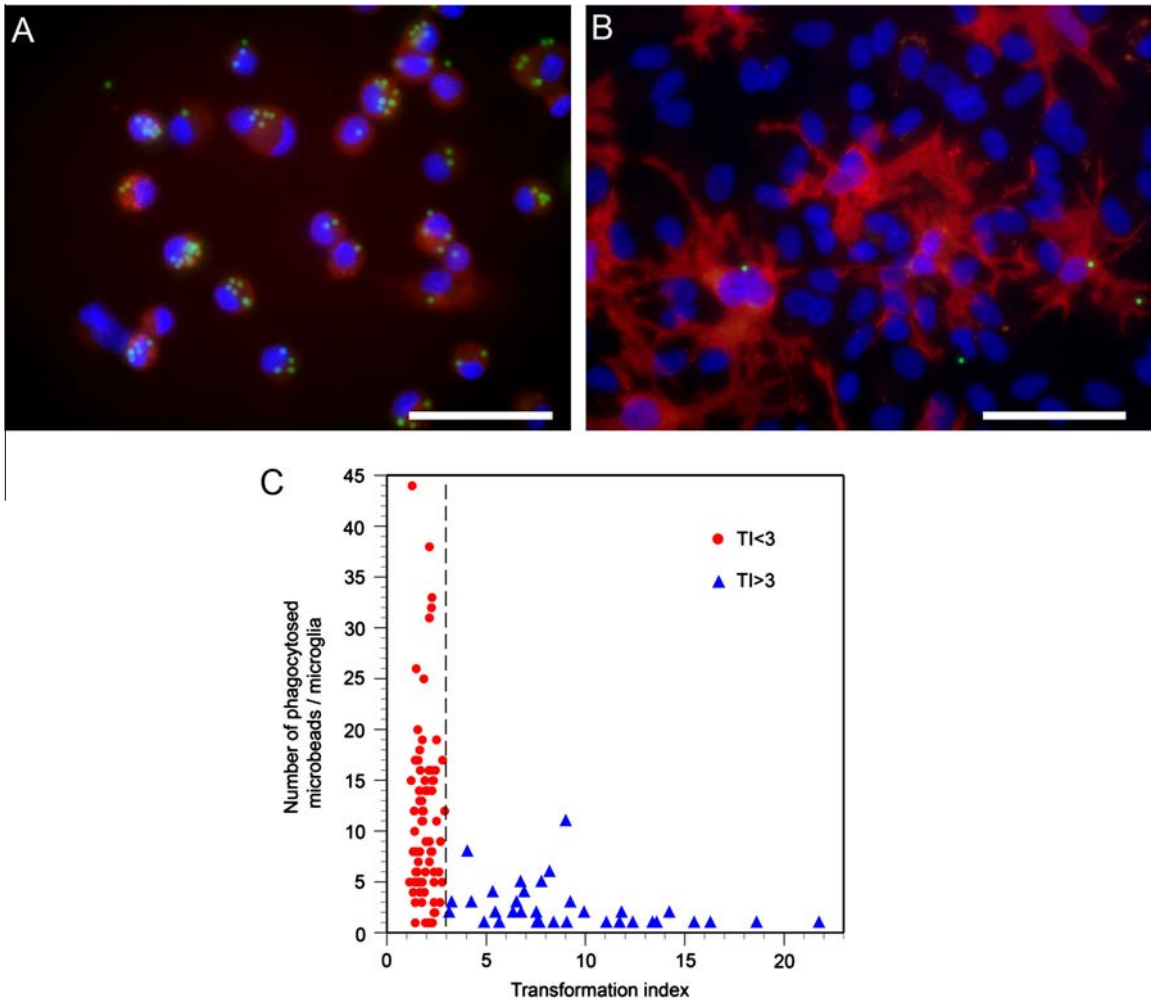

Fig. 8. Phagocytic activity of unstimulated microglial cells in a primary culture (DIV14). (A, B) Representative immunocytochemical pictures showing the unstimulated phagocytic capability of microglial cells (red) as a function of the TI value from the same 14-day-old culture. Fluorescent dye-coated (green) latex microbeads ($d = 2$ μm) were added to the medium and phagocytosed by microglia. Microglial cells with TI < 3 (A), i.e. ameboid forms with 11.08 ± 8.6 beads per cell, were about 3.5-times more likely to phagocytose the microbeads than cells with TI > 3 (B), i.e. ramified forms with 3.16 ± 3.6 beads per cell. Non-phagocytosed microbeads were very rare in the cultures (a solitary bead can be seen in both A and B). Scale bar = 50 μm. (C) Distribution of unstimulated microglial cells with phagocytosed microbeads as a function of the TI value. The vertical dashed line separates the functionally different microglial populations (TI < 3 as ameboid, phagocytosing and proliferating, and TI > 3 as ramified, resting microglia). (For interpretation of the references to color in this figure legend, the reader is referred to the web version of this article.)

quite differently, indicating that the expression of similar biomarkers by macrophages and microglia does not necessarily mean that they have the same function.

Our results showed that microglia prepared from embryonic tissue and maintained for up to 4 weeks displayed multiple phenotypes with different immunologic, proliferative and phagocytic characteristics. While the number of total cells did not vary significantly during culturing, their composition exhibited a dramatic change. The number of microglial cells rose steadily during culturing, by a factor of 67-fold. The selected microglial antigenic and functional (proliferation and phagocytosis) properties in primary mixed cultures of E18 rat forebrain tissues revealed a marked morphological and antigenic differentiation during culturing.

Morphometric analysis on binary silhouettes of microglial cells revealed that ameboid forms were dominant in the early stages of *in vitro* differentiation, while older cultures were characterized by mixed populations of ameboid and ramified cells, the latter being the dominant form. The ameboid microglia, characterized by TI < 3, was the mitotically active, Ki67-immunopositive population even in older cultures where it formed a core of proliferating cells. The feasibility of a quantitative assessment of different microglial populations (resting vs. activated microglia) through morphological features alone was recently demonstrated (Kozlowski and Weimer, 2012); the sensitivity of this automated method was reported to be comparable to that of immunohistochemical methods.

While the morphology of the cultured microglial cells was very similar to that in the normal rat brain, their antigenic markers specific for the monocyte/macrophage/microglial cell line were distinctly different and exhibited a more restricted immunological phenotypic repertoire from those seen *in vivo*. We found that microglial cell populations in culture, without the

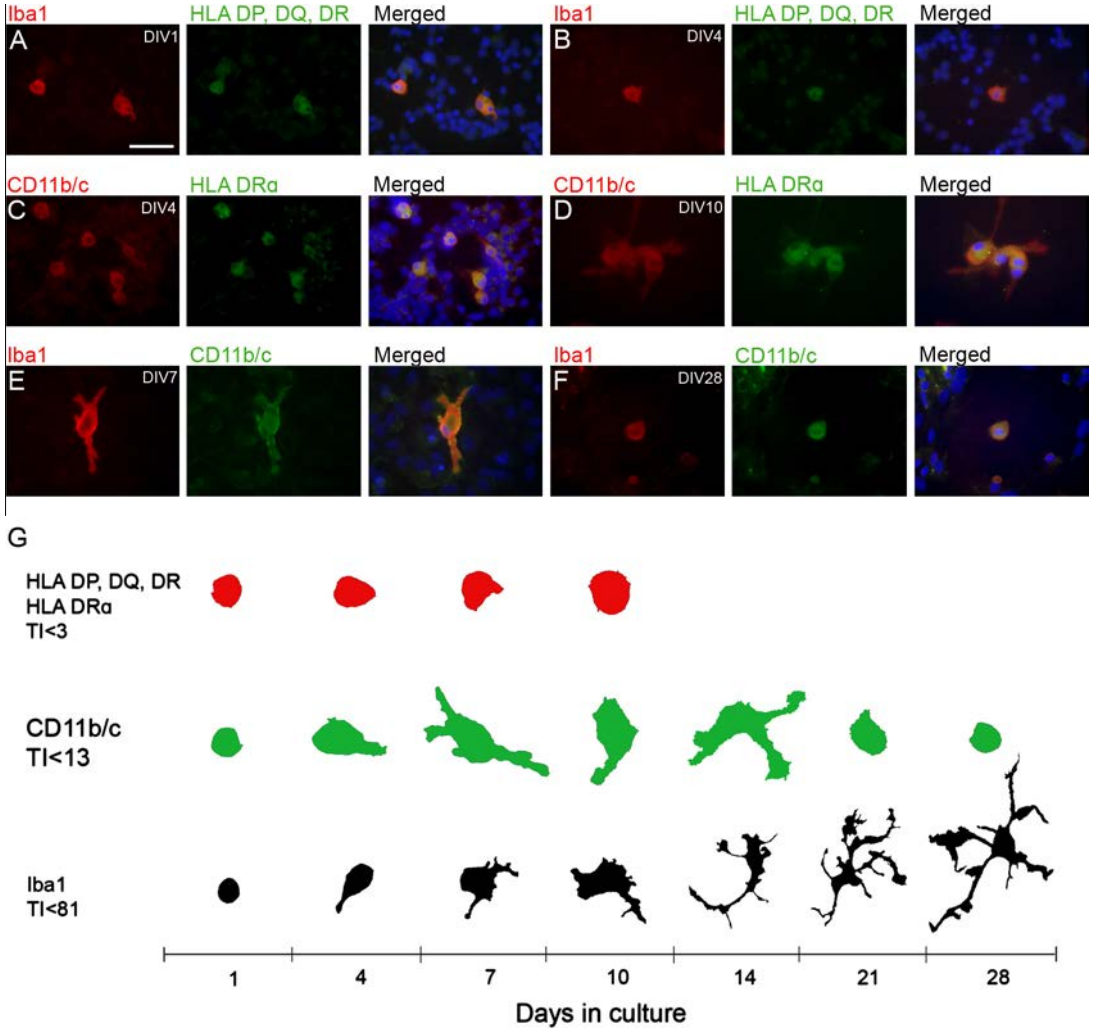

Fig. 9. Colocalizations of specific microglial markers during culturing. Representative fluorescent microphotographs of double-immunopositive microglial cells of the cultures were taken through the red, green and blue channels. Cell nuclei (blue) were stained with Hoechst 33258. The red and green channels, together with the Hoechst-stained nuclei are displayed as their merged pictures. Culturing times are indicated at the upper right corners for each triad. (A, B) Double-immunopositive microglial cells for the coexpression of Iba1 and HLA DP, DQ, DR antigens at DIV1 (A) and DIV4 (B). These antigens are colocalized only in microglial cells of young cultures (up to DIV10), but solely in those that are truly ameboid or have low TI values. (C, D) Double-immunopositive microglial cells for the coexpression of CD11b/c and HLA DRα antigens at DIV4 (C) and DIV10 (D). These antigens are colocalized exclusively in the young cultures and only in microglia with typical ameboid morphology. The CD11b/c-positive microglia are no longer able to express HLA antigens in older cultures. (E, F) Double-immunopositive microglial cells for the coexpression of CD11b/c and Iba1 antigens at DIV7 (E) and DIV28 (F). These antigens are colocalized only in ameboid, proliferating cells with low TI values in both young and old cultures. Iba1-immunopositive microglial cell were morphologically heterogenous as both ameboid and ramified forms were labeled throughout culturing. Scale bar for all fluorescent microscopic pictures: 50 μm. (G) Relationship between TI values and microglia-specific markers. During culturing, only the less differentiated, ameboid microglia (TI < 3) express HLA antigens; these cells will eventually die out or differentiate to more ramified morphologies (TI > 3) that do not express HLA antigens. CD11b/c-positive cells can be observed throughout culturing, but they never become fully ramified (TI < 13). (For interpretation of the references to color in this figure legend, the reader is referred to the web version of this article.)

presence of recruited hematogenous macrophages from the periphery through the blood–brain barrier, were more similar to those in the normal adult (or physiologically aging) brain (e.g. showing no signs of significant neurodegeneration and therefore almost no turnover for the microglial cells with the periphery) than to those in the neuropathologic brain (e.g. in Alzheimer's disease). The large flux of HLA DP, DQ, DR-positive macrophages that entered the E18 brain through the blood–brain barrier soon died or differentiated further in the culture. As a consequence, cultured microglial cells that were doubly positive for Iba1 and HLA DP, DQ, DR antigens were absent from cultures older than DIV10. This is in contrast with earlier reports of an upregulation of HLA class II proteins upon phagocytosis (Becher and Antel, 1996; Beyer et al., 2000; Smith, 2001), a function displayed by ameboid microglial cells throughout the entire culturing, although they were negative for the HLA DP, DQ, DR antigens after DIV10.

The loss of a large number of cells, which peaked on DIV10, concomitantly with the formation of neuronal clumps in the culture, could be coupled causatively to microglial activation and proliferation in two ways: either the massive neuronal death triggered microglia

proliferation or, conversely, the proliferating microglial cells adversely influenced and eventually killed some other cells in the culture. This neuronal loss, mostly prominent around DIV10, was documented by Western analysis and was accompanied by an increase in the phagocytic activity of these cells. Interestingly, microglia proliferation could also be linked to the observed increase in CNPase activity during culturing. Similar phenomenon was observed in neonatal mouse brain cultures (Amur-Umarjee et al., 1990). Such microglia–oligodendrocyte interactions could be due to factors secreted by activated microglia that promote oligodendrocyte proliferation and differentiation (Deierborg et al., 2010).

One of the main roles of microglia is phagocytosis, a process that is critical for the uptake and degradation of infectious agents and senescent cells, and which contributes to the immune response and inflammation (Aderem and Underhill, 1999; Marín-Teva et al., 2004). As reviewed by Neumann et al. (2009), the recent evidence suggests that the phagocytic clearance by the microglia plays a fundamental role in facilitating the reorganization of neuronal circuits and triggering repair mechanisms. For example, there are substantial differences in microglial phagocytosis during the restructuring of neuronal connections (Marín-Teva et al., 2004), in acute CNS injury (Cullheim and Thams, 2007), in multiple sclerosis (Takahashi et al., 2007), in normal development and ageing (Streit, 2006) or in Alzheimer's disease (Meyer-Luehmann et al., 2008), and the insufficient level of clearance seen in certain neurodegenerative diseases might be associated with an inadequate regenerative response such as that in Alzheimer's disease.

We used unstimulated microglial cells to measure phagocytic activity for two reasons: (1) certain immunomodulatory functions could be reduced in stimulated microglia (Magnus et al., 2004), and (2) there could be a differential expression of a number of microglial enzymes and markers upon stimulation (Imamura et al., 1991). Both such effects could lead to the ameboid microglial phenotype being favored, which could interfere with our statistical analysis. The fact that unstimulated ramified microglia do not proliferate (Imamura et al., 1991) ruled out the possibility that the conversion to the ameboid form would be induced, thereby biasing the actual composition of the microglial pool. We found that unstimulated microglial phagocytosis was tightly coupled to the ameboid morphology, as cells with low TI values exhibited much higher phagocytic activity. The ameboid morphology was also related to the proliferation of the microglial cells, as low TI values were always present in the cultures.

As microglial cells participate in both protective and pathogenic mechanisms in the healthy and in the diseased CNS, further correlative morphological, molecular and functional characterizations of cultured rat microglial cell populations similar to that presented here could provide further information concerning the specific roles of the different microglia cells in the physiology and the pathophysiology of the CNS. *In vitro* phenotyping of these cells could also be important in providing detailed information on how different signals may activate the microglial cell populations, on their relation to each other and their origin, on the regulation of their migration, etc. Therapeutic approaches through which to modify the microglial responses could also benefit from *in vitro* studies similar to that presented here.

Acknowledgments—We thank the anonymous referees for the suggestions in general, and for that relating to the use of the Ki67 antibody in particular. At the time of the experiments, M.S. was a Ph.D. student at the University of Szeged. This work was supported by program Project Grants to the University of Szeged from the Ministry of National Resources (TÁMOP-4.2.1.B-09/1/KONV-2010-0005 and TÁMOP-4.2.2.A-11/1/KONV-2012-0052) through the European Union Cohesion Fund. The funders had no role in the study design, the data collection and analysis, the decision to publish, or the preparation of the manuscript. We thank Mrs. Susan Ambrus and Mrs. Olga Daranyi for excellent technical help.

REFERENCES

Abràmoff MD, Magalhães PJ, Ram SJ (2004) Image processing with ImageJ. Biophotonics Int 11:36–42.

Aderem A, Underhill DM (1999) Mechanisms of phagocytosis in macrophages. Annu Rev Immunol 17:593–623.

Amur-Umarjee SG, Dasu RG, Campagnoni AT (1990) Temporal expression of myelin-specific components in neonatal mouse brain cultures: evidence that 2′,3′-cyclic nucleotide 3′-phosphodiesterase appears prior to galactocerebroside. Dev Neurosci 12:251–262.

Auffray C, Sieweke MH, Geissmann F (2009) Blood monocytes: development, heterogeneity, and relationship with dendritic cells. Annu Rev Immunol 27:669–692.

Banerjee A, Roach MC, Trcka P, Ludueña RF (1990) Increased microtubule assembly in bovine brain tubulin lacking the type III isotype of beta-tubulin. J Biol Chem 265:1794–1799.

Becher B, Antel JP (1996) Comparison of phenotypic and functional properties of immediately ex vivo and cultured human adult microglia. Glia 18:1–10.

Bechmann I, Kwidzinski E, Kovac AD, Simbürger E, Horvath T, Gimsa U, Dirnagl U, Priller J, Nitsch R (2001a) Turnover of rat brain perivascular cells. Exp Neurol 168:242–249.

Bechmann I, Priller J, Kovac A, Böntert M, Wehner T, Klett FF, Bohsung J, Stuschke M, Dirnagl U, Nitsch R (2001b) Immune surveillance of mouse brain perivascular spaces by blood-borne macrophages. Eur J Neurosci 14:1651–1658.

Berger JV, Dumont AO, Focant MC, Vergouts M, Sternotte A, Calas AG, Goursaud S, Hermans E (2012) Opposite regulation of metabotropic glutamate receptor 3 and metabotropic glutamate receptor 5 by inflammatory stimuli in cultured microglia and astrocytes. Neuroscience 205:29–38.

Beyer M, Gimsa U, Eyüpoglu IY, Hailer NP, Nitsch R (2000) Phagocytosis of neuronal or glial debris by microglial cells: upregulation of MHC class II expression and multinuclear giant cell formation in vitro. Glia 31:262–266.

Chinnery HR, Ruitenberg MJ, McMenamin PG (2010) Novel characterization of monocyte-derived cell populations in the meninges and choroid plexus and their rates of replenishment in bone marrow chimeric mice. J Neuropathol Exp Neurol 69:896–909.

Cullheim S, Thams S (2007) The microglial networks of the brain and their role in neuronal network plasticity after lesion. Brain Res Rev 55:89–96.

Dalmau I, Finsen B, Tønder N, Zimmer J, González B, Castellano B (1997) Development of microglia in the prenatal rat hippocampus. J Comp Neurol 377:70–84.

Dalmau I, Finsen B, Zimmer J, González B, Castellano B (1998) Development of microglia in the postnatal rat hippocampus. Hippocampus 8:458–474.

Dalmau I, Vela JM, González B, Finsen B, Castellano B (2003) Dynamics of microglia in the developing rat brain. J Comp Neurol 458:144–157.

Davalos D, Grutzendler J, Yang G, Kim JV, Zuo Y, Jung S, Littman DR, Dustin ML, Gan WB (2005) ATP mediates rapid microglial response to local brain injury in vivo. Nat Neurosci 8:752–758.

Deierborg T, Roybon L, Inacio AR, Pesic J, Brundin P (2010) Brain injury activates microglia that induce neural stem cell proliferation ex vivo and promote differentiation of neurosphere-derived cells into neurons and oligodendrocytes. Neuroscience 171:1386–1396.

Durafourt BA, Moore CS, Zammit DA, Johnson TA, Zaguia F, Guiot MC, Bar-Or A, Antel JP (2012) Comparison of polarization properties of human adult microglia and blood-derived macrophages. Glia 60:717–727.

Eglitis MA, Mezey E (1997) Hematopoietic cells differentiate into both microglia and macroglia in the brains of adult mice. Proc Natl Acad Sci U S A 94:4080–4085.

Floden AM, Combs CK (2006) Beta-amyloid stimulates murine postnatal and adult microglia cultures in a unique manner. J Neurosci 26:4644–4648.

Ford AL, Goodsall AL, Hickey WF, Sedgewick JD (1995) Normal adult ramified microglia separated from other central nervous system macrophages by flow cytometric sorting. J Immunol 154:4309–4321.

Frei K, Lins H, Schwerdel C, Fontana A (1994) Antigen presentation in the central nervous system: the inhibitory effect of IL-10 on MHC class II expression and production of cytokines depends on the inducing signals and the types of cell analyzed. J Immunol 152:2720–2728.

Fujita H, Tanaka J, Toku K, Tateishi N, Suzuki Y, Matsuda S, Sakanaka M, Maeda N (1996) Effects of GM-CSF and ordinary supplements on the ramification of microglia in culture: a morphometrical study. Glia 18:269–281.

Gehrmann J, Matsumoto Y, Kreutzberg GW (1995) Microglia: intrinsic immunoeffector cell of the brain. Brain Res Rev 20:269–287.

Gehrmann J (1996) Microglia: a sensor to threats in the nervous system? Res Virol 147:79–88.

Geissmann F, Jung S, Littman DR (2003) Blood monocytes consist of two principal subsets with distinct migratory properties. Immunity 19:71–82.

Geissmann F, Manz MG, Jung S, Sieweke MH, Merad M, Ley K (2010) Development of monocytes, macrophages, and dendritic cells. Science 327:656–661 (Erratum in Science 330:1319).

Ginhoux F, Greter M, Leboeuf M, Nandi S, See P, Gokhan S, Mehler MF, Conway SJ, Ng LG, Stanley ER, Samokhvalov IM, Merad M (2010) Fate mapping analysis reveals that adult microglia derive from primitive macrophages. Science 330:841–845.

Gordon S (2003) Alternative activation of macrophages. Nat Rev Immunol 3:23–35.

Guillemin G, Boussin FD, Croitoru J, Franck-Duchenne M, Le Grand R, Lazarini F, Dormont D (1997) Obtention and characterization of primary astrocyte and microglial cultures from adult monkey brains. J Neurosci Res 49:576–591.

Hailer NP, Jarhult JD, Nitsch R (1996) Resting microglial cells in vitro: analysis of morphology and adhesion molecule expression in organotypic hippocampal slice cultures. Glia 18:319–331.

Hailer NP, Heppner FL, Haas D, Nitsch R (1997) Fluorescent dye prelabelled microglial cells migrate into organotypic hippocampal slice cultures and ramify. Eur J Neurosci 9:863–866.

Hawkes CA, McLaurin J (2009) Selective targeting of perivascular macrophages for clearance of beta-amyloid in cerebral amyloid angiopathy. Proc Natl Acad Sci U S A 106:1261–1266.

Hickey WF, Kimura H (1988) Perivascular microglial cells of the CNS are bone marrow-derived and present antigen in vivo. Science 239:290–292.

Horejsí V, Nmec M, Angelisová P, Kristofová H, Gorga JC, Hilgert I (1986) Characterization of seven new monoclonal antibodies against human DR, DR + DP and DQ1 + DQ3 antigens. Tissue Antigens 28:288–297.

Imai Y, Ibata I, Ito D, Ohsawa K, Kohsaka S (1996) A novel gene iba1 in the major histocompatibility complex class III region encoding an EF hand protein expressed in a monocytic lineage. Biophys Biochem Res Commun 224:855–862.

Imamura K, Suzumura A, Sawada M, Marunouchi T, Takahashi A (1991) Functional and immunohistochemical studies of cultured rat microglia. Rinsho Shinkeigaku 31:127–134.

Ito D, Imai Y, Ohsawa K, Nakajima K, Fukuuchi Y, Kohsaka S (1998) Microglia-specific localisation of a novel calcium binding protein Iba1. Mol Brain Res 57:1–9.

Kim WK, Alvarez X, Fisher J, Bronfin B, Westmoreland S, McLaurin J, Williams K (2006) CD163 identifies perivascular macrophages in normal and viral encephalitic brains and potential precursors to perivascular macrophages in blood. Am J Pathol 168:822–834.

Kortvely E, Varszegi S, Palfi A, Gulya K (2003) Intracellular targeting of calmodulin mRNAs in primary hippocampal cells. J Histochem Cytochem 51:541–544.

Kozlowski C, Weimer RM (2012) An automated method to quantify microglia morphology and application to monitor activation state longitudinally in vivo. PLoS One 7(2):e31814.

Kreutzberg GW (1996) Microglia: a sensor for pathological events in the CNS. Trends Neurosci 19:312–318.

Ladeby R, Wirenfeldt M, Garcia-Ovejero D, Fenger C, Dissing-Olesen L, Dalmau I, Finsen B (2005) Microglial cell population dynamics in the injured adult central nervous system. Brain Res Rev 48:196–206.

Ling EA, Wong WC (1993) The origin and nature of ramified and amoeboid microglia: a historical review and current concepts. Glia 7:9–18.

Ling EA, Kaur LC, Yick TY, Wong WC (1990) Immunocytochemical localization of CR3 complement receptors with OX-42 in amoeboid microglia in postnatal rats. Anat Embryol (Berl) 182:481–486.

Liu B, Du L, Kong LY, Hudson PM, Wilson BC, Chang RC, Abel HH, Hong JS (2000) Reduction by naloxone of lipopolysaccharide-induced neurotoxicity in mouse cortical neuron-glia co-cultures. Neuroscience 97:749–756.

Lowry OH, Rosebrough NJ, Farr AL, Randall RJ (1951) Protein measurement with the Folin phenol reagent. J Biol Chem 193:265–275.

Magnus T, Korn T, Jung S (2004) Chronically stimulated microglial cells do no longer alter their immune functions in response to the phagocytosis of apoptotic cells. J Neuroimmunol 155:64–72.

Marín-Teva JL, Dusart I, Colin C, Gervais A, van Rooijen N, Mallat M (2004) Microglia promote the death of developing Purkinje cells. Neuron 41:535–547.

Meyer-Luehmann M, Spires-Jones TL, Prada C, Garcia-Alloza M, de Calignon A, Rozkalne A, Koenigsknecht-Talboo J, Holtzman DM, Bacskai BJ, Hyman BT (2008) Rapid appearance and local toxicity of amyloid-beta plaques in a mouse model of Alzheimer's disease. Nature 451:720–724.

Milligan CE, Cunningham TJ, Levitt P (1991a) Differential immunochemical markers reveal the normal distribution of brain macrophages and microglia in the developing rat brain. J Comp Neurol 314:125–135.

Milligan CE, Levitt P, Cunningham TJ (1991b) Brain macrophages and microglia respond differently to lesions of the developing and adult visual system. J Comp Neurol 314:136–146.

Mosser DM, Edwards JP (2008) Exploring the full spectrum of macrophage activation. Nat Rev Immunol 8:958–969 (Erratum in Nat Rev Immunol (2010) 10:460).

Neumann H, Kotter MR, Franklin RJ (2009) Debris clearance by microglia: an essential link between degeneration and regeneration. Brain 132:288–295.

Orłowski D, Sołtys Z, Janeczko K (2003) Morphological development of microglia in the postnatal rat brain. A quantitative study. Int J Dev Neurosci 21:445–450.

Otani Y, Yamaguchi Y, Sato Y, Furuichi T, Ikenaka K, Kitani H, Baba H (2011) PLD4 is involved in phagocytosis of microglia: expression and localization changes of PLD4 are correlated with activation state of microglia. PLoS One 6(11):e27544.

Priller J, Flügel A, Wehner T, Boentert M, Haas CA, Prinz M, Fernández-Klett F, Prass K, Bechmann I, de Boer BA, Frotscher M, Kreutzberg GW, Persons DA, Dirnagl U (2001) Targeting gene-modified hematopoietic cells to the central nervous system: use of green fluorescent protein uncovers microglial engraftment. Nat Med 7:1356–1361.

Prinz M, Mildner A (2011) Microglia in the CNS: immigrants from another world. Glia 59:177–187.

Prinz M, Priller J, Sisodia SS, Ransohoff RM (2011) Heterogeneity of CNS myeloid cells and their roles in neurodegeneration. Nat Neurosci 14:1227–1235.

Raivich G, Bohatschek M, Kloss CUA, Werner A, Jones LL, Kreutzberg GW (1999) Neuroglial activation repertoire in the injured brain: graded response, molecular mechanisms and cues to physiological function. Brain Res Rev 30:77–105.

Robinson AP, White TM, Mason DW (1986) Macrophage heterogeneity in the rat as delineated by two monoclonal antibodies MRC OX-41 and MRC OX-42, the latter recognizing complement receptor type 3. Immunology 57:239–247.

Rozovsky I, Finch CE, Morgan TE (1998) Age-related activation of microglia and astrocytes: in vitro studies show persistent phenotypes of aging, increased proliferation, and resistance to down-regulation. Neurobiol Aging 19:97–103.

Scott IS, Heath TM, Morris LS, Rushbrook SM, Bird K, Vowler SL, Arends MJ, Coleman N (2004) A novel immunohistochemical method for estimating cell cycle phase distribution in ovarian serous neoplasms: implications for the histopathological assessment of paraffin-embedded specimens. Br J Cancer 90:1583–1590.

Sezgin M, Sankur B (2004) Survey over image thresholding techniques and quantitative performance evaluation. J Electron Imaging 13:146–165.

Slepko N, Levi G (1996) Progressive activation of adult microglial cells in vitro. Glia 16:241–246.

Smith ME (2001) Phagocytic properties of microglia in vitro: implications for a role in multiple sclerosis and EAE. Microsc Res Tech 54:81–94.

Starborg M, Gell K, Brundell E, Höög C (1996) The murine Ki-67 cell proliferation antigen accumulates in the nucleolar and heterochromatic regions of interphase cells and at the periphery of the mitotic chromosomes in a process essential for cell cycle progression. J Cell Sci 109:143–153.

Stence N, Waite M, Dailey ME (2001) Dynamics of microglial activation: a confocal time-lapse analysis in hippocampal slices. Glia 33:256–266.

Streit WJ, Graeber MB, Kreutzberg GW (1989) Expression of Ia antigens on perivascular and microglial cells after sublethal and lethal neuronal injury. Exp Neurol 105:115–126.

Streit WJ, Walter SA, Pennel NA (1999) Reactive microgliosis. Prog Neurobiol 57:563–581.

Streit WJ (2006) Microglial senescence: does the brain's immune system have an expiration date? Trends Neurosci 29:506–510.

Takahashi K, Prinz M, Stagi M, Chechneva O, Neumann H (2007) TREM2-transduced myeloid precursors mediate nervous tissue debris clearance and facilitate recovery in an animal model of multiple sclerosis. PLoS Med 4:e124.

Tanaka J, Toku K, Matsuda S, Sudo S, Fujita H, Sakanaka M, Maeda N (1998) Induction of resting microglia in culture medium devoid of glycine and serine. Glia 24:198–215.

Town T, Nikolic V, Tan J (2005) The microglial ''activation'' continuum: from innate to adaptive responses. J Neuroinflammation 2:24. http://dx.doi.org/10.1186/1742-2094-2-24.

Ulvestad E, Williams K, Bjerkvig R, Tiekotter K, Antel J, Mørk S (1994a) Human microglial cells have phenotypic and functional characteristics in common with both macrophages and dendritic antigen-presenting cells. J Leukoc Biol 56:732–740.

Ulvestad E, Williams K, Bø L, Trapp B, Antel J, Matre R (1994b) HLA class II molecules (HLA-DR, -DP, -DQ) on cells in the human CNS studied in situ and in vitro. Immunology 82:535–541.

Vallières L, Sawchenko PE (2003) Bone marrow-derived cells that populate the adult mouse brain preserve their hematopoietic identity. J Neurosci 23:5197–5207.

Wang CC, Wu CH, Shieh JY, Wen CY, Ling EA (1996) Immunohistochemical study of amoeboid microglial cells in fetal rat brain. J Anat 189:567–574.

Werry EL, Liu GJ, Lovelace MD, Nagarajah R, Hickie IB, Bennett MR (2011) Lipopolysaccharide-stimulated interleukin-10 release from neonatal spinal cord microglia is potentiated by glutamate. Neuroscience 175:93–103.

Wirenfeldt M, Dissing-Olesen L, Babcock AA, Nielsen M, Meldgaard M, Zimmer J, Azcoitia I, Leslie RG, Dagnaes-Hansen F, Finsen B (2007) Population control of resident and immigrant microglia by mitosis and apoptosis. Am J Pathol 171:617–631.

Xu Y, Qian L, Zong G, Ma K, Zhu X, Zhang H, Li N, Yang Q, Bai H, Ben J, Li X, Xu Y, Chen Q (2012) Class A scavenger receptor promotes cerebral ischemic injury by pivoting microglia/macrophage polarization. Neuroscience 218:35–48.

Zhang L, Chopp M, Zhang RL, Wang L, Zhang J, Wang Y, Toh Y, Santra M, Lu M, Zhang ZG (2010) Erythropoietin amplifies stroke-induced oligodendrogenesis in the rat. PLoS One 5(6):e11016.

(Accepted 13 March 2013)
(Available online 25 March 2013)

ARTICLE II.

Brain Research Bulletin 120 (2016) 41–57

Contents lists available at ScienceDirect

Brain Research Bulletin

journal homepage: www.elsevier.com/locate/brainresbull

Research report

Calmodulin inhibition regulates morphological and functional changes related to the actin cytoskeleton in pure microglial cells

Melinda Szabo, Karolina Dulka, Karoly Gulya*

Department of Cell Biology and Molecular Medicine, University of Szeged, Szeged, Hungary

ARTICLE INFO

Article history:
Received 8 September 2015
Received in revised form 26 October 2015
Accepted 3 November 2015
Available online 10 November 2015

Keywords:
Calmidazolium
Cell viability
Ionized calcium-binding adaptor molecule 1
Lipopolysaccharide
Phagocytosis
Phalloidin
Proliferation
Trifluoperazine

ABSTRACT

The roles of calmodulin (CaM), a multifunctional intracellular calcium receptor protein, as concerns selected morphological and functional characteristics of pure microglial cells derived from mixed primary cultures from embryonal forebrains of rats, were investigated through use of the CaM antagonists calmidazolium (CALMID) and trifluoperazine (TFP). The intracellular localization of the CaM protein relative to phalloidin, a bicyclic heptapeptide that binds only to filamentous actin, and the ionized calcium-binding adaptor molecule 1 (Iba1), a microglia-specific actin-binding protein, was determined by immunocytochemistry, with quantitative analysis by immunoblotting. In unchallenged and untreated (control) microglia, high concentrations of CaM protein were found mainly perinuclearly in ameboid microglia, while the cell cortex had a smaller CaM content that diminished progressively deeper into the branches in the ramified microglia. The amounts and intracellular distributions of both Iba1 and CaM proteins were altered after lipopolysaccharide (LPS) challenge in activated microglia. CALMID and TFP exerted different, sometimes opposing, effects on many morphological, cytoskeletal and functional characteristics of the microglial cells. They affected the CaM and Iba1 protein expressions and their intracellular localizations differently, inhibited cell proliferation, viability and fluid-phase phagocytosis to different degrees both in unchallenged and in LPS-treated (immunologically challenged) cells, and differentially affected the reorganization of the actin cytoskeleton in the microglial cell cortex, influencing lamellipodia, filopodia and podosome formation. In summary, these CaM antagonists altered different aspects of filamentous actin-based cell morphology and related functions with variable efficacy, which could be important in deciphering the roles of CaM in regulating microglial functions in health and disease.

1. Introduction

Microglia originate from bone marrow-derived myeloid precursors as a unique class of the monocyte/macrophage lineage that infiltrates the central nervous system (CNS) during its early development (Ginhoux et al., 2010; Saijo and Glass, 2011). They respond rapidly to inflammatory cues and injury by transforming from a ramified, resting state to an activated, phagocytic ameboid cell type (Kreutzberg, 1996). In their non-activated or resting state, they display a ramified morphology and subdued macrophage-like functional properties. In response to injury, infection, inflammatory or other signals, the microglia become activated and a series of morphological, molecular and functional changes take place that affect proliferation, homing and adhesion to damaged cells, phagocytosis, antigen presentation and cytotoxic and inflammation-mediating signaling (Drew and Chavis, 2000; Prinz and Priller, 2014; Saijo and Glass, 2011; Streit et al., 1999; Town et al., 2005).

Microglial functions such as motility and phagocytosis are closely associated with dynamic changes in the cytoskeleton and related to intracellular calcium (Ca^{2+}) signaling (Greenberg, 1995; Kalla et al., 2003; Mitchison and Cramer, 1996). The ubiquitous Ca^{2+}-binding proteins participate in Ca^{2+}-elicited intracellular events, either as Ca^{2+}-sensing/receptor/trigger or as

Abbreviations: Ca^{2+}, calcium ion; CALMID, calmidazolium, 1-[bis(4-chlorophenyl)methyl]-3-[2-(2,4-dichlorophenyl)-2-(2,4-dichlorobenzyloxy)ethyl]-1H-imidazolium chloride; CaM, calmodulin; CNS, central nervous system; DIV, days in vitro; DMEM, Dulbecco's Modified Eagle's Medium; GAPDH, glyceraldehyde 3-phosphate dehydrogenase (EC 1.2.1.12); Iba1, ionized calcium binding adaptor molecule 1; Ki67, proliferation marker antigen identified by the monoclonal antibody Ki67; LPS, bacterial lipopolysaccharide; mRNA, messenger ribonucleic acid; PBS, phosphate-buffered saline; RT, room temperature; S.E.M., standard error of mean; subDIV, subcloned days in vitro; TBS, tris-buffered saline; TFP, trifluoperazine, 10-[3-(4-methylpiperazin-1-yl) propyl]-2-trifluoromethyl-10H-phenothiazine dihydrochloride; TI, transformation index.

* Corresponding author at: Department of Cell Biology and Molecular Medicine, University of Szeged, 4 Somogyi u., Szeged H-6720, Hungary. Fax: +36 62 544 569.
E-mail address: gulyak@bio.u-szeged.hu (K. Gulya).

http://dx.doi.org/10.1016/j.brainresbull.2015.11.003
0361-9230/

Ca^{2+}-buffering/transport proteins, by binding intracellularly stored Ca^{2+} (Ikura, 1996). They contribute to nearly all aspects of the functioning of the cell, and are important in numerous intracellular signaling processes, from the regulation of cellular homeostasis to learning and memory (Berridge et al., 2000; Clapham, 2007). Calmodulin (CaM), one of the most important intracellular Ca^{2+} receptors, exerts its biological action through its heterogenous population of target proteins, which are involved in a number of cellular regulatory processes (Kennedy, 1989; Palfi et al., 2002).

The nervous tissue is especially abundant in CaM. While its distribution has been characterized in detail for a number of neuronal cell types (Kovacs and Gulya, 2002, 2003; Palfi et al., 1999, 2001, 2005), its localization and functions in glial cells are much less known. Astrocytes express CaM protein in low quantities (Kortvely et al., 2003), but mRNA populations from all three CaM genes could still be localized both perinuclearly and in the astrocytic endfeet (Palfi et al., 2005). The expression of CaM in oligodendroglia is similarly low and has not been characterized extensively, albeit the regulatory effects of this protein on a number of membrane-bound target proteins such as the myelin basic protein (Libich and Harauz, 2008) or the 2′,3′-cyclic nucleotide 3′-phosphodiesterase (Myllykoski et al., 2012) have been established. Of all the glial components, only the microglia seem to have a considerable amount of CaM. They express a relatively large amount of CaM when activated (Casal et al., 2001; Solá et al., 1997), and many aspects of their Ca^{2+} signaling are well documented (Färber and Kettenmann, 2006; Wong and Schlichter, 2014).

CaM immunoreactivity or CaM gene-specific transcripts are often colocalized with those of the target enzymes of CaM within the same cytoplasmic compartments (Erondu and Kennedy, 1985; Sanabria et al., 2008; Seto-Ohshima et al., 1983; Strack et al., 1996). For example, actin is accompanied by CaM in the cell cortex, helping to remodel the actin-based cytoskeleton in accordance with the actual (patho) physiological signals (Mitchison and Cramer, 1996; Psatha et al., 2004). Ionized calcium-binding adaptor molecule 1 (Iba1) is another intracellular Ca^{2+}-binding protein with actin-binding capability that is expressed in macrophages and microglia, and is widely used to detect both resting and activated microglial phenotypes (Imai et al., 1996). CaM and Iba1 proteins share a number of molecular structural variants that are related to either their Ca^{2+} binding or their target protein recognition (Yamada et al., 2006). In contrast with the wide-ranging regulatory roles of CaM, Iba1 plays a much more restricted role in microglial functions, e.g. remodeling the actin cytoskeleton during migration (Siddiqui et al., 2012; Vincent et al., 2012).

The modulatory action of Ca^{2+}-bound CaM on multiple target proteins can be regulated by a number of compounds. Calmidazolium (CALMID; 1-[bis(4-chlorophenyl) methyl]-3-[2-(2,4-dichlorophenyl)-2-(2,4-dichlorobenzyloxy)ethyl]-1H-imidazolium chloride) and trifluoperazine (TFP; 10-[3-(4-methylpiperazin-1-yl)propyl]-2-trifluoromethyl-10H-phenothiazine dihydrochloride) are potent inhibitors of CaM-related cellular activities (Borsa et al., 1986; Sunagawa et al., 2000). It is presumed that, apart from binding to the CaM protein (Matsushima et al., 2000; Vandonselaar et al., 1994; Vertessy et al., 1998), they can also exert their effects on some of the CaM-regulated targets directly (Sunagawa et al., 2000).

In contrast with the extensive studies on the involvement of CaM in a number of neuronal phenomena, only limited information is available on its role in the development and maintenance of the microglial phenotype and its specific functions. Relatively little is known, for example, as concerns the possible involvement of CaM mediation in such important microglial functions as phagocytosis and the cellular functions associated with it, e.g. dynamic cytoskeletal reorganization. Thus, in view of the importance of CaM-mediated cell functions and the paucity of data on specific microglial functions related to and possibly regulated by CaM, we set out to investigate the localization and intracellular distribution of CaM in pure microglial cell populations derived from rat primary mixed forebrain cultures by using immunocytochemical and Western blot techniques. Selected CaM inhibitors such as CALMID and TFP, previously reported to have different modes of action (Matsushima et al., 2000; Sunagawa et al., 2000), were quantitatively tested for their ability to modify the microglial morphology, lamellipodia, filopodia and podosome formation, and specific functions such as cell proliferation and survival, protein expression and phagocytosis in unchallenged (control) and lipopolysaccharide (LPS)-challenged cells. Stimulation with LPS was used to evaluate the ability of microglial cells to respond to activation (Fricker et al., 2012; Song et al., 2014; Tokes et al., 2011).

2. Material and methods

All animal experiments were carried out in strict compliance with the European Council Directive (86/609/EEC) and EC regulations (O.J. of EC No. L 358/1, 18/12/1986) regarding the care and use of laboratory animals for experimental procedures, and followed the relevant Hungarian and local legislation requirements. The experimental protocols were approved by the Institutional Animal Welfare Committee of the University of Szeged (I-74-11/2009/MÁB). The pregnant Sprague-Dawley rats (180–200 g) were kept under standard housing conditions and fed ad libitum.

2.1. Antibodies

The antibodies used in the immunocytochemical and Western blot studies are listed in Table 1. For a thorough characterization of different microglial phenotypes developed in vitro, an antibody against Iba1, an intracellular actin- and Ca^{2+}-binding protein expressed in the CNS specifically in macrophages and microglia (Imai et al., 1996; Ahmed et al., 2007), was used in our immunocytochemical and Western blot analyses. An anti-CaM monoclonal antibody was used to detect both Ca^{2+}-bound and Ca^{2+}-free forms of the antigen (Sacks et al., 1991). The anti-Ki67 antibody was used to detect proliferating cells. Ki67 is a nuclear protein expressed in all active phases of the cell cycle from the late G1 phase through the end of the M phase but is absent in non-proliferating and early G1 phase cells (Scott et al., 2004). The anti-glyceraldehyde 3-phosphate dehydrogenase (GAPDH) antibody was used as an internal control in Western blot experiments (Wu et al., 2012). Dilutions of primary and secondary antibodies, and also incubation times and blocking conditions for each antibody used were carefully tested for both immunocytochemistry and Western blot analysis. To detect the specificities of the secondary antisera, omission control experiments (staining without the primary antibody) were performed. In such cases, no fluorescent or Western blot signals were detected.

2.2. Preparation of primary mixed cortical cell cultures

Mixed primary cortical cell cultures were established from embryonic day 18 (E18) wild-type rat embryos by the use of the methods described previously (Szabo and Gulya, 2013). Briefly, 6–8 fetal rats under deep ether anesthesia were surgically decapitated and the frontal lobe of the cerebral cortex was removed, minced with scissors, and incubated in 9 ml Dulbecco's Modified Eagle's Medium (DMEM; Invitrogen, Carlsbad, CA, USA) containing 1 g/l D-glucose, 110 mg/l Na-pyruvate, 4 mM L-glutamine, 3.7 g/l $NaHCO_3$, 10,000 U/ml penicillin G, 10 mg/ml streptomycin sulfate and 25 μg/ml amphotericin B, and supplemented with 0.25% trypsin (Invitrogen) for 10 min at 37 °C, then centrifuged at 1000 × g

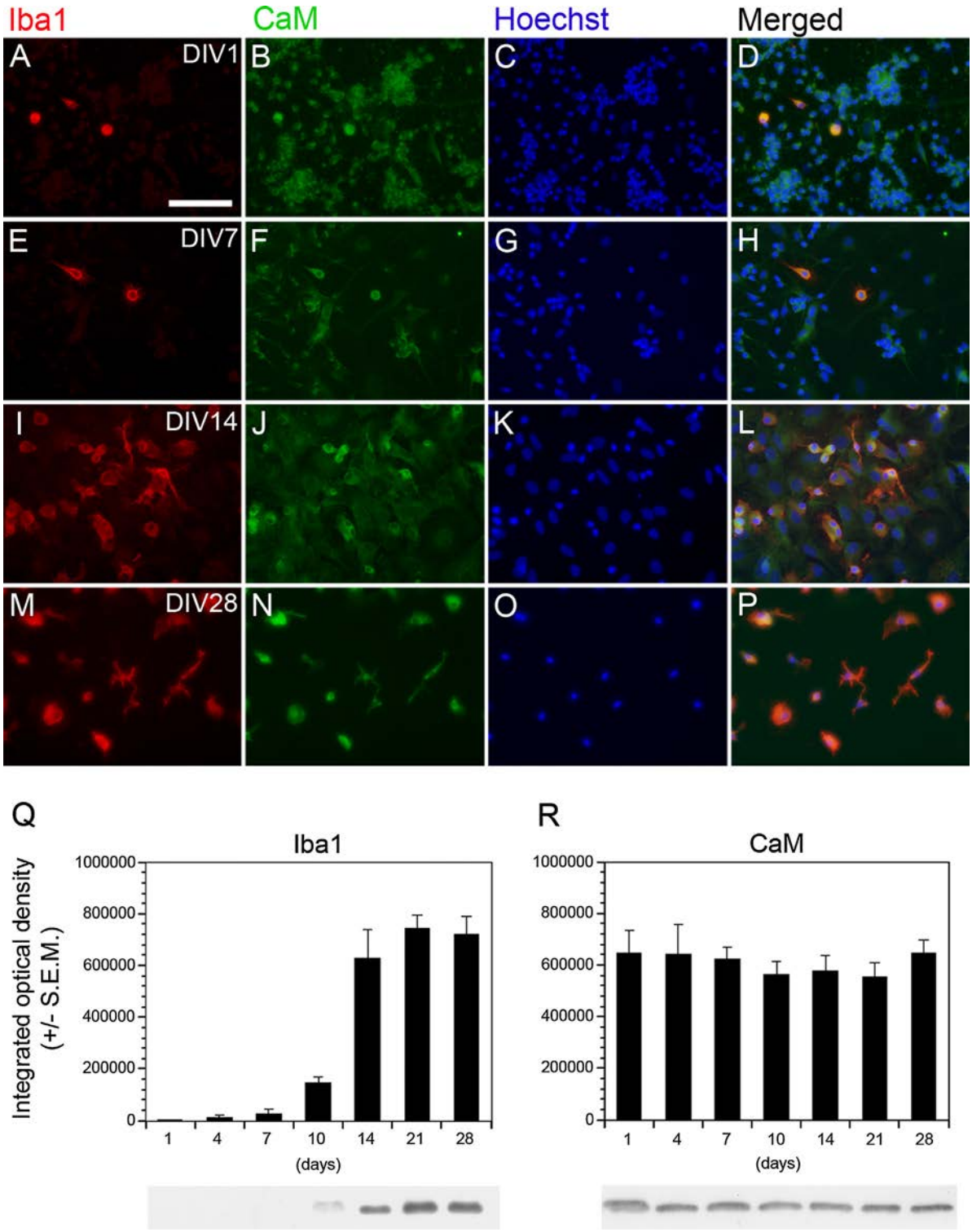

Fig. 1. Development of Iba1 and CaM immunoreactivities in primary mixed cortical cultures (DIV1-DIV28). (For interpretation of the references to colour in this figure legend, the reader is referred to the web version of this article.)

At early culturing times (DIV1 (A–D) and DIV7 (E–H)), all seeded cells displayed CaM immunoreactivity (green), but only a few of them were Iba1-positive microglia (red). The cell nuclei (blue) were labeled with Hoechst 33,258. Since most of the cells present early in the culturing are neurons [48], most of the CaM immunoreactivity seen at DIV1-DIV7 is of neuronal origin. At DIV14 (I–L), a large number of Iba1-positive cells showed CaM positivity, a number of them were ramified. At DIV28 (M–P), the predominant cell type in the culture was the CaM-positive microglia. Note the visibly different Iba1 (M) and CaM contents (N) of the ameboid and ramified microglia at this culturing time. The merged pictures show cells double-positive for Iba1 and CaM (D, H, L, P). The development of Iba1 (Q) and CaM (R) immunoreactivities during culturing (DIV1-DIV28) was quantitatively analyzed on Western blots. Protein samples from primary cultures were separated by gel electrophoresis, transferred to nitrocellulose membranes and probed with either the Iba1 (Q) or CaM (R) antibody. Gray scale digital images of the immunoblots were acquired by scanning the autoradiographic films with a desktop scanner. The images were scanned and processed at identical settings to allow comparisons between the Western blots from different samples. Error bars indicate integrated optical density values (mean ± S.E.M.). Representative Western blot pictures are shown below the graphs. During culturing (DIV1-DIV28), a massive increase in the number of cells with microglial phenotype was observed in the mixed primary cultures, while the CaM content of the cultures remained constant. Most of the gain in Iba1 content occurred between DIV10 and DIV14. Culturing times are indicated at the upper right corners (A, E, I, M). Scale bar in A for all pictures: 50 μm.

Table 1
Antibodies used in immunocytochemistry and Western blot analyses.

Antibodies used in immunocytochemistry					
Primary antibody, abbrev. name	Full name	Final dilution	Company name	Secondary antibody with fluorochrome	Final dilution
Iba1	Rabbit anti-Iba1 monocl. ab.	1/300	Wako, Osaka, Japan	Alexa Fluor 568 goat anti-rabbit, Invitrogen, Carlsbad, CA, USA	1/1,000
Iba1	Rabbit anti-Iba1 monocl. ab.	1/300	Wako, Osaka, Japan	Alexa Fluor 488 goat anti-rabbit, Invitrogen, Carlsbad, CA, USA	1/1,000
CaM	Mouse anti-CaM, monocl. ab.	1/100	Millipore	Alexa Fluor 488 goat anti-mouse, Invitrogen, Carlsbad, CA, USA	1/1,000
CaM	Rabbit anti-CaM, monocl. ab., clone EP799Y	1/100	Abcam, Cambridge, UK	Alexa Fluor 568 goat anti-rabbit, Invitrogen, Carlsbad, CA, USA	1/1,000
Ki67	Rabbit anti-Ki67, monocl. ab., clone SP6	1/100	Thermo Scientific, Fremont, CA, USA	Alexa Fluor 488 goat anti-rabbit, Invitrogen, Carlsbad, CA, USA	1/1,000
Antibodies used in Western studies					
Primary antibody, abbrev. name	Full name	Final dilution	Company name	Secondary antibody	Final dilution
Iba1	Rabbit anti-Iba1 monocl. ab.	1/1,000	Wako, Osaka, Japan	Anti-rabbit IGG, peroxidase conjug., Sigma, St. Louis, MO, USA	1/2,000
CaM	Rabbit anti-CaM, monocl. ab., clone EP799Y	1/2,000	Abcam, Cambridge, UK	Anti-rabbit IGG, peroxidase conjug., Sigma, St. Louis, MO, USA	1/2,000
GAPDH	Mouse anti-GAPDH, monocl. ab., clone GAPDH-71.1	1/20,000	Sigma, St. Louis, MO, USA	Anti-mouse IGG, peroxidase conjug., Sigma, St. Louis, MO, USA	1/3,000

for 10 min at room temperature (RT). The pellet was resuspended and washed twice in 5 ml DMEM containing 10% heat-inactivated fetal bovine serum (FBS; Invitrogen) and centrifuged for 10 min at $1000 \times g$ at RT. The final pellet was resuspended in 2 ml of the same solution as above, after which the cells were seeded in the same medium and cultured at 37 °C in a humidified air atmosphere supplemented with 5% CO_2 in one or other of the following ways: (1) in poly-L-lysine-coated coverslips (18 × 18 mm; 2×10^5 cells/coverslip) for immunocytochemistry; (2) in poly-L-lysine-coated Petri dishes (60 mm × 15 mm; 10^6 cells/dish) for Western blot analyses; or (3) in a poly-L-lysine-coated culture flask (75 cm^2, 12×10^6 cells/flask) for the subsequent generation of pure microglial cell cultures. The mixed primary cultures were maintained up to 28 days (DIV1-DIV28) for immunocytochemistry and Western blot analyses, and for 7 days (DIV7) for the generation of pure microglial cells. For culturing periods longer than 3 days, the DMEM was changed every 3 days.

2.3. Preparation of pure microglial cell cultures

Pure microglial cell cultures were subcloned from mixed primary cultures (DIV7) maintained in a poly-L-lysine-coated culture flask (75 cm^2, 12×10^6 cells/flask) by shaking the cultures at 150 rpm in a platform shaker for 20 min at 37 °C. Microglia from the supernatant were collected by centrifugation at $3000 \times g$ for 10 min at RT and resuspended in 2 ml of DMEM/10% FBS. The cells were seeded at a density of 2×10^5 cells/Petri dish for Western blots and cell viability assays or 10^5 cells/coverslip/Petri dish for immunocytochemistry, proliferation or phagocytosis assays, and cultured in DMEM in a humidified atmosphere supplemented with 5% CO_2 for 4 days at 37 °C. The medium was changed on the first day after seeding (subDIV1). Immunocytochemistry routinely performed on the pure microglial cultures 4 days after seeding (subDIV4) consistently detected a >99% incidence of Iba1-immunopositive microglial cells for the Hoechst 33,258 dye-labeled cell nuclei (Fig. 2).

2.4. Treatment of pure microglial cells with LPS and CaM inhibitors

On the fourth day of subcloning (subDIV4), the DMEM was replaced and the expanded pure microglial cells were treated for 24 h with either LPS (100 ng/ml in final concentration, dissolved in DMEM; Sigma, St. Louis, MO, USA), CALMID (5 nM or 50 nM in final concentration, dissolved in dimethylsulfoxide (DMSO); Sigma) or TFP (10 μM or 20 μM final concentration, dissolved in DMSO; Sigma) alone, or with a combination of LPS and one of these CaM inhibitors, and the effects were compared in a variety of morphological and functional tests. LPS treatment served as an immunochallenge. Unchallenged and untreated (control) cultures were maintained under identical conditions, but without these inhibitors, and received 2 μl DMSO solution instead.

2.5. Immunocytochemistry

For immunocytochemistry, primary cortical cells (DIV1-DIV28) or pure microglial cells (subDIV4) cultured in vitro on poly-L-lysine-

coated coverslips were used. At different time intervals (DIV1, DIV4, DIV7, DIV10, DIV14, DIV21, DIV28), or after different treatments (subDIV4), the cultured cells on the coverslips were fixed in 4% formaldehyde in 0.05 M phosphate-buffered saline (PBS; pH 7.4 at RT) for 5 min and rinsed in 0.05 M PBS for 3 × 5 min. After permeabilization and blocking of the nonspecific sites in 0.05 M PBS solution containing 5% normal goat serum (Sigma), 1% heat-inactivated bovine serum albumin (Sigma) and 0.05% Triton X-100 for 30 min at 37 °C, the cells on the coverslips were incubated with the appropriate primary antibody (Table 1) in the above solution overnight at 4 °C. The cultured cells were washed for 4 × 10 min at RT in 0.05 M PBS, then incubated with the appropriate Alexa Fluor fluorochrome-conjugated secondary antibody (Table 1) in the above solution, but without Triton X-100, in the dark for 3 h at RT. The cells on the coverslip were washed for 4 × 10 min in 0.05 M PBS at RT. At this stage, the cells were occasionally stained with rhodamine-phalloidin (5 μl in 200 μl PBS; Molecular Probes, Eugene, OR, USA) for 30 min at RT, then washed for 2 × 10 min at RT. Finally, the cell nuclei were stained in a 0.05 M PBS solution containing 1 mg/ml polyvinylpyrrollidone and 0.5 μl/ml Hoechst 33,258 dye (Sigma). The coverslips were rinsed in distilled water for 5 min, air-dried and mounted on microscope slides in Vectashield mounting medium (Vector Laboratories, Burlingame, CA, USA). Cells were viewed on a Nikon Microphot-FXA epifluorescent microscope (Nikon Corp., Tokyo, Japan) and photographed with a Spot RT Color CCD camera (SPOT RT/ke, Diagnostic Instruments, Inc., Sterling Heights, MI, USA).

2.6. Western blot analysis

For Western blots, the protocols were optimized for each antibody as regards epitope accessibility, polyacrylamide gel separation, antibody dilution and chemiluminescence signal intensity. Cultured primary cells (DIV1–DIV28) or pure microglial cells (subDIV4) with different treatment regimens were collected through use of a rubber policeman, homogenized in 50 mM Tris–HCl (pH 7.5) containing 150 mM NaCl, 0.1% Nonidet P40, 0.1% cholic acid, 2 μg/ml leupeptin, 1 μg/ml pepstatin, 2 mM phenylmethylsulfonyl fluoride and 2 mM EDTA, and centrifuged at 10,000 × *g* for 10 min at 4 °C. The pellet was discarded and the protein concentration of the supernatant was determined (Lowry et al., 1951). For the Western blot analyses of Iba1, CaM and GAPDH immunoreactivities, 5–10 μg of heat-denatured protein was separated on an SDS polyacrylamide gel. The stacking gel/resolving gel ratio was 4–10% for Iba1 and GAPDH, and 4–16% for CaM immunoreactivities; for CaM Westerns, the stacking gel was complemented with 16% urea and 16% glycerol. Separated proteins were then transferred onto Hybond-ECL nitrocellulose membrane (Amersham Biosciences, Little Chalfont, Buckinghamshire, England). Strips of membranes with the transferred bands for CaM and Iba1 (both around 17 kDa) and GAPDH (37 kDa) were cut and processed separately for CaM, Iba1 or GAPDH immunodetection. The membranes were blocked for 1 h in 5% nonfat dry milk (for Iba1 and GAPDH Westerns) or 5% bovine serum albumin (for CaM Westerns) in Tris-buffered saline (TBS) containing 0.1% Tween 20, and incubated for 1 h with the appropriate primary antibodies (Table 1). After 5 washes in 0.1% TBS–Tween 20, the membranes were incubated for 1 h with the appropriate peroxidase-conjugated secondary antibodies (Table 1), and washed 5 times as before. The enhanced chemiluminescence method (ECL Plus Western blotting detection reagents; Amersham Biosciences) was used to reveal immunoreactive bands according to the manufacturer's protocol. The immunoreactive densities of equally loaded lanes were quantified, and all samples were normalized to internal GAPDH load controls run on the same gels.

2.7. Cell proliferation and cell viability assays

For the assessment of CaM inhibition on cell proliferation and survival, pure microglial cells (subDIV4) were cultured in DMEM with or without the appropriate test compounds in a humidified atmosphere supplemented with 5% CO_2 at 37 °C for 24 h. To analyze the effects of these treatments on cell proliferation, the cultures were processed for Ki67 immunocytochemistry. Proliferation index (PI) was defined as the number of Ki67-positive microglial cell nuclei per 1000 analyzed Iba1-positive cells and usually expressed as % of the total cells analyzed (Brownhill et al., 2014; Yamaguchi et al., 2013). A total of 1454 fields of view with 55,565 Iba1-positive and 783 Ki67-positive/Iba1-positive microglia were analyzed across the groups (mean ± S.E.M.).

To estimate the surviving microglial cells after treatments, the cultures were washed twice with 2 ml of PBS to remove cell debris and treated with 0.25% trypsin solution for 10 min at 37 °C, collected and counted in a Burker cell. The number of viable cells was presented as mean ± S.E.M.

2.8. In vitro phagocytosis assay

The fluid-phase phagocytic capacity of the microglial cells was determined via the uptake of fluorescent microspheres (2 μm in diameter; Sigma) using the general methods described by Szabo and Gulya (2013). Unstimulated (control) and LPS-stimulated pure microglial cell cultures with or without CaM inhibition were tested for 24 h. At the end of the culturing period (subDIV4), 1 μl of a 2.5% aqueous suspension of fluorescent microspheres was added per ml of the culture, which was then further incubated for 60 min at 37 °C. The cells were next washed 5 times with 2 ml of PBS to remove dish- or cell surface-bound residual fluorescent microspheres, and fixed with 4% formalin in PBS. For measurement of the phagocytic activity, Iba1-expressing microglia labeled with phagocytosed microbeads were counted. Negative controls were treated as above with the exception that microglial cultures with beads were incubated for 60 min at 4 °C. At this temperature, the number of beads associated with cell surface averaged less than 1 bead per 100 Iba1-labeled cells. For the study of the effects of CaM inhibitors on the number of phagocytosed beads (mean ± S.E.M.), a total of 873 bead-labeled cells were counted in three separate culturing procedures under a Nikon Microphot-FXA epifluorescent microscope with a 10× or 20× objective.

2.9. Digital image processing and image analysis

Gray scale digital images of the Western blots were acquired by scanning the autoradiographic films with a desktop scanner (Epson Perfection V750 PRO; Seiko Epson Corp., Japan). The images were scanned and processed at identical settings to allow comparisons of the Western blots from different samples. Digital images were acquired with a Nikon Microphot-FXA epifluorescent microscope (Nikon Corp., Tokyo, Japan), using a Spot RT Color CCD camera and Spot RT software (Spot RT/ke Diagnostic Instruments). Microglial cell silhouettes were acquired by transforming the raw digital files of Iba1-immunoreactive cells made under fluorescent microscope light to binary files, using the ImageJ software (version 1.47; developed at the U.S. National Institutes of Health by W. Rasband, and available from the Internet at http://rsb.info.nih.gov/ij). The color cell images were transformed into their binary replicas (silhouettes) through automatic thresholding procedures (Szabo and Gulya, 2013). After thresholding, values for cell perimeter (μm) and cell area (μm^2) were determined from at least 3 separate experiments (at least 2 coverslips in each experiment for each culturing time investigated; about 20 randomly selected cells/coverslip), and the transformation index (TI) reflecting the degree of pro-

cess extension was calculated via an expression [perimeter of cell (μm)]^2/4π[cell area (μm^2)] as previously described (Fujita et al., 1996). For the analysis of TI values, a total of 261 cells were quantitatively measured (mean ± S.E.M.). Digital image production was performed with Adobe Photoshop CS5.1 software (Adobe Systems, Inc., San Jose, CA, USA). Color correction (brightness, contrast) and cropping of the fluorescent images were occasionally performed when individual photomicrographs were assembled to figure panels for publication. No specific feature within an image was enhanced, obscured, introduced, moved or removed.

2.10. Statistical analysis

All statistical comparisons were made with SigmaPlot (v. 12.3, Systat Software Inc., Chicago, IL, USA). Results for the phagocytosis and viability assays and the cell silhouette characteristics (TI values) were analyzed with Kruskal–Wallis one-way analysis of variance, followed by Dunn's method for pairwise multiple comparison procedures for statistically significant differences between the groups. For these studies, values were presented as mean ± S.E.M. from at least three independent experiments and $p < 0.05$ was considered significant. For Western blots, values were presented as mean ± S.E.M. from at least three blots, each representing independent experiments for each time period examined. For the determination of the homogeneity of the subcloned microglial cells, Iba1-positive cells and Hoechst 33,258 dye-positive cell nuclei from at least 50 randomly sampled microscope fields from 2 to 3 coverslips for each subcloned culture were counted and the results are presented as mean ± S.E.M.

3. Results

3.1. CaM is differentially localized in ameboid and ramified microglia both in mixed and pure cultures

The quantity and cell type-specific localization of the CaM protein was first established in mixed primary cultures under unstimulated and untreated (control) conditions. Fluorescent immunocytochemistry (Fig. 1A–P) and Western blot analysis (Fig. 1Q,R) demonstrated that a high concentration of CaM protein was characteristic of the mixed cultures throughout culturing. In young cultures (DIV1–DIV7), when only a few cells double-positive for the Iba1 (Fig. 1A,E) and CaM (Fig. 1B,F) antigens existed (Fig. 1A–H), most of the CaM immunoreactivity was associated with non-microglial, e.g. mainly neuronal, cell forms, as demonstrated earlier (Szabo and Gulya, 2013). From DIV14 (up to DIV28), as more Iba1-positive microglia populated the cultures (Fig. 1I,M), the proportion of CaM immunoreactivity associated with the microglia (Fig. 1J,N) also grew steadily. Both ameboid (Fig. 1A,E) and ramified microglia (a few cells in Fig. 1I,M) expressed CaM immunoreactivity. As the cultures aged, the CaM immunoreactivity localized to microglia became predominant (compare Fig. 1I,M with Fig. 1K,O). Similarly, Western blot studies confirmed the increase in Iba1 immunoreactivity during culturing (Fig. 1Q), during which time the CaM content of the cultures remained unchanged (Fig. 1R). Thus, by DIV14, the microglia had become the main CaM-expressing cell type in the mixed primary forebrain culture.

Subsequent experiments were performed on pure microglial cultures (subDIV4; Fig. 2). In these microglial cells the Iba1 immunoreactivity was most intense in the lamellipodia of the ameboid forms (Fig. 3A,D,G), followed by the perinuclear region (Fig. 3D,G). The strongest CaM immunoreactivity was always observed in the ameboid microglia, where the cell somata, and especially the perinuclear area, were the most intensely labeled (Fig. 3B,E,H). In ameboid microglia, the CaM and Iba1 immunoreactivities were distributed in a complementary manner, as the Iba1 protein tending to localize in the cell cortex and lamellipodia (Fig. 3A–C). The ramified microglia displayed an almost homogenous cytoplasmic Iba1 distribution (Fig. 3J) with a considerably lower CaM content typically localized around the nucleus; the branches had only traces of CaM immunoreactivity (Fig. 3K,L).

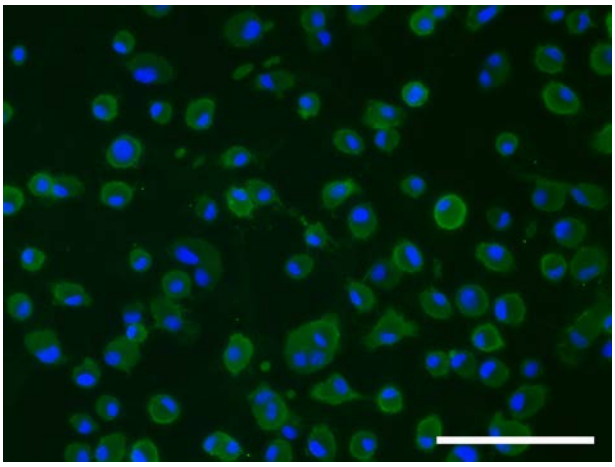

Fig. 2. Localization of Iba1 immunoreactivity in pure microglial cell cultures (subDIV4). (For interpretation of the references to colour in this figure legend, the reader is referred to the web version of this article.)
Representative photomicrograph of Iba1 imunoreactive microglial cells in culture. The purity of this culture is close to 100%, since every Hoechst 33,258-labeled cell nuclei (blue) is surrounded by Iba1 immunopositive cytoplasm (green). Scale bar: 100 μm.

3.2. CALMID and TFP differentially affect microglial proliferation and cell survival

When CaM inhibitors were tested on cell proliferation and cell viability, CALMID and TFP, either alone or in combination with LPS, had different effects (Fig. 4A,B). Proliferation was measured as a function of Ki67-immunopositivity of the microglial cells (PI). Unstimulated (control) microglia (subDIV4) had an average PI value of 2.5% (25.22 ± 8.9 Ki67-positive microglia/1,000 analyzed microglia in the culture; Fig. 4A). LPS challenge inhibited cell proliferation, albeit without reaching significance (PI = 0.41; 16.2% of the control value). According to Ki67 immunocytochemistry, TFP10 significantly decreased microglial cell proliferation both in unchallenged and LPS-challenged microglia with PI values of 0.21% and 0.12%, respectively (Fig. 4A). While CALMID50 treatment alone had no effect on the proliferation of unchallenged microglia, LPS-challenged cells treated with CALMID50 showed some but not significant inhibition.

Cell viability was also investigated in pure microglial cultures (Fig. 4B). In contrast with the ineffectivity of CALMID50 on cell survival in unchallenged and in LPS-challenged microglial populations, TFP10 was highly effective in these cultures. In unchallenged cells, TFP10 significantly decreased cell viability to 62.47% of the control value. Similarly, when the microglial cells were challenged by LPS treatment (100 ng/ml), TFP10 effectively decreased the number of surviving cells to 71.28% of the control (Fig. 4B).

3.3. CaM inhibition affects cell morphology and actin cytoskeleton reorganization

The microglial morphology in the control and experimental groups was analyzed through binary silhouettes (Fig. 5). The quantitative analysis was based on the area, perimeter and TI, the latter being a dimensionless number that is an indicator

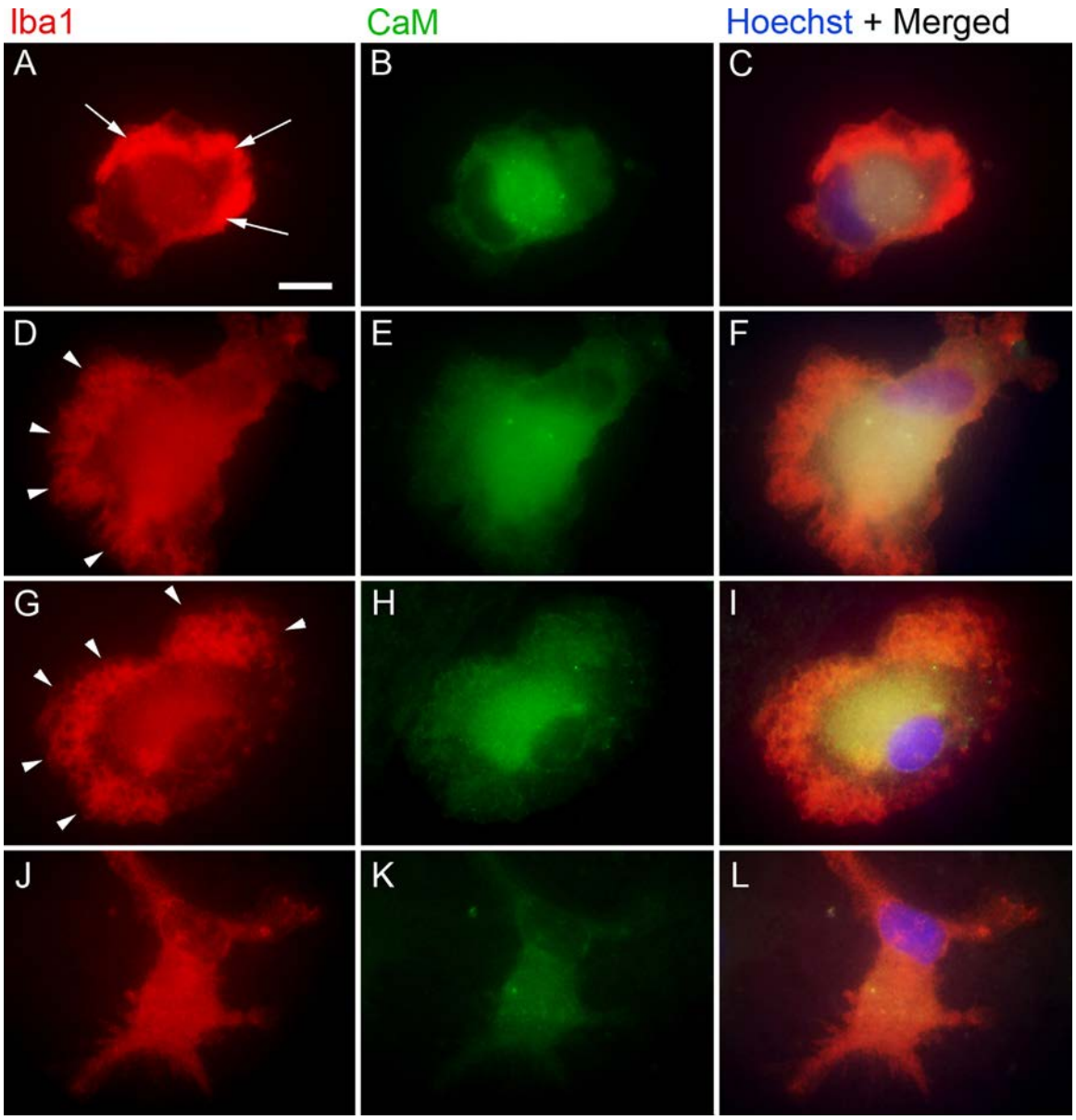

Fig. 3. Distribution of Iba1 and CaM immunoreactivities in pure microglial cells (subDIV4). (For interpretation of the references to colour in this figure legend, the reader is referred to the web version of this article.)
In pure microglial cultures (subDIV4), the majority of the unchallenged cells were ameboid or slightly ramified. While the Iba1 immunoreactivity (red) could be localized into two subcellular compartments, the perinuclear and the cell cortex domains (A, D, G, J), the CaM immunoreactivity (green) was largely confined to the perinuclear region (B, E, H, K), with the cell cortex having a considerably smaller CaM content, which progressively diminished deeper into the branches. Merged pictures (C, F, I, L) show the cell nuclei (blue) and the overlapping Iba1 and CaM immunoreactivities predominantly localized to the perinuclear area. Ameboid microglia have predominantly cortically localized Iba1 immunoreactivity in the leading edges of large lamellipodia (A, arrows), a cytoplasmic domain largely devoid of CaM immunoreactivity (B). Arrowheads (D, G) point to large lamellipodia. Scale bar in A for all pictures: 10 μm.

for the degree of process extension of a cell. Throughout the experiments, microglial cells with TI <3 were considered ameboid. The unchallenged, untreated 4-day-old pure microglia culture (subDIV4) consisted mainly of ameboid cells (Fig. 5, control row; see also controls in Figs. 7, 8, 10) with an average area of $412.91 \pm 27.2\,\mu m^2$, perimeter of $100.73 \pm 5.4\,\mu m$ and a TI of 2.02 ± 0.1 (Fig. 6). When administered alone, CALMID and TFP affected TI and the microglial cell surface area and perimeter differently. For example, both CALMID5 and CALMID50 resulted in increased area, perimeter and TI, whereas TFP alone strongly inhibited these characteristics. When challenged with LPS, the microglia became enlarged and acquired significantly larger perimeter and TI ($A = 777.23 \pm 40.1\,\mu m^2$, $P = 238.97 \pm 8.6\,\mu m$, $TI = 6.14 \pm 0.4$), consistent with these cells becoming activated (Figs. 5, 6 and 7D–F). Interestingly, CALMID5 or CALMID50 alone was not effective but when used in combination with LPS, they significantly increased the cell surface area, perimeter and TI (Figs. 5, 6A,C,E, 7G–I). TFP sigificantly inhibited the expansion of cell surface area and perimeter both in unchallenged and LPS-challenged cells (Fig. 6B,D). As an example, the cell surface area was decreased substantially after TFP or LPS + TFP treatment, to 46.4 or 44.5% of the unchallenged or LPS-challenged control value, respectively. TFP treatment was also very effective in decreasing TI, to 25.53% of the LPS-challenged value (Figs. 5, 6).

CaM inhibition affected the microglial morphology through reorganization of the actin cytoskeleton (Fig. 7). In unchallenged and untreated (control) cultures, the Iba1- and phalloidin-related fluorescence signals largely overlapped in the cell cortex of the

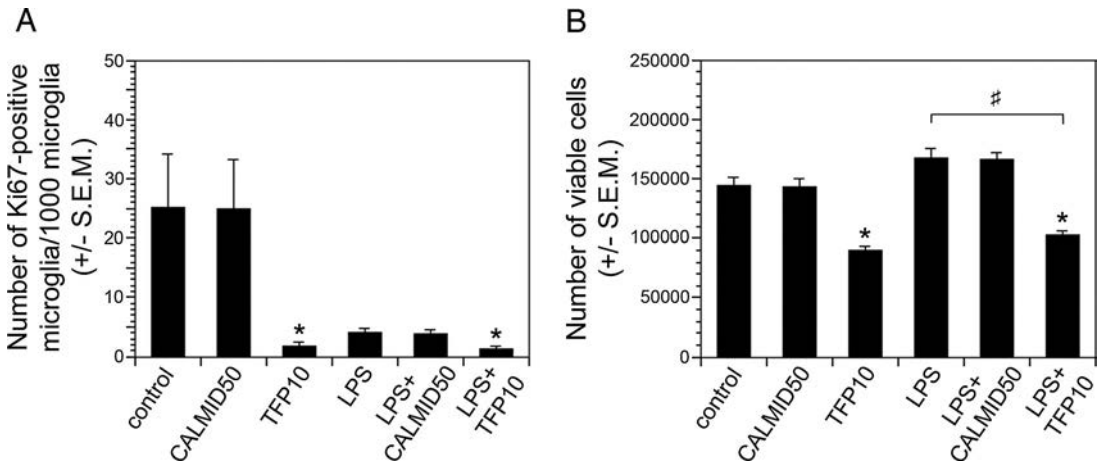

Fig. 4. Effects of CaM inhibitors on microglia proliferation and viability in pure microglial cell cultures.
The number of Ki67-positive microglia (A) and the viable cells (B) were quantitatively analyzed in challenged and untreated (control), LPS-challenged and LPS-challenged and treated cells. CALMID and TFP were tested at 50 nM and 10 μM, respectively, either alone or in combination with 100 ng/ml LPS. TFP, either alone or in combination with LPS, significantly decreased both microglia proliferation (A) and the number of viable cells (B) in the cultures (subDIV4). Interestingly, while the combined treatment of CALMID50 and LPS led to some (but not significant) inhibition on microglia proliferation, it was without any effect on cell viability. For proliferation studies, data (mean ± S.E.M.) were collected from at least 4 independently established cultures, each involving plating on at least 3 Petri dishes. Mean PI values (%) were established as follows: control = 2.52%, CALMID50 = 2.48%, TFP10 = 0.22%, LPS = 0.41%, LPS+CALMID50 = 0.20%, LPS+TFP10 = 0.12%. For viability studies, data (mean ± S.E.M.) were collected from at least 3 separate culturings, each involving plating on at least 6 Petri dishes. Data were analyzed with Kruskal–Wallis one-way ANOVA on ranks, followed by pairwise multiple comparisons (Dunn's method). *Statistically significant from control ($p < 0.05$); #statistically significant from LPS-treated cells ($p < 0.05$). LPS: 100 ng/ml; CALMID50: 50 nM CALMID; TFP10: 10 μM TFP.

mainly ameboid microglia, often in lamellipodia (Fig. 7A–C) as expected, since they both bind to the actin cytoskeleton. When treated with LPS, the microglia that became activated and enlarged displayed a phalloidin distribution much fuzzier than that in the case of Iba1, probably due to the rapid association of fibrous actin, to which phalloidin preferentially binds (Fig. 7D–F). However, spot-like concentrations of phalloidin fluorescence resembling podosomes were often visible in LPS-treated cells (Fig. 7E, arrow). CaM inhibitors affected the Iba1 and phalloidin distributions in different ways. CALMID50 treatment resulted in phalloidin fluorescence that was clearly distributed in two distinct concentric rings in the cytoplasm, one ring in the cell cortex, and the other as a perinuclearly localized cytoplasmic streaming of freshly synthesized fibrous actin (Fig. 7H,K, arrows). Phalloidin-containing filopodia were also obvious in these cells. Similar, albeit less dense, Iba1 distribution was observed after CALMID50 treatments (Fig. 7G). TFP treatment resulted in an overlapping and almost homogenous distribution of both Iba1 immunoreactivity and phalloidin fluorescence (Fig. 7M–O) in the surviving cells. While the Iba1 immunoreactivity remained relatively intact (Fig. 7M), most of the phalloidin fluorescence intensity was lost in TFP-treated microglia (Fig. 7N) indicating that TFP affected actin polymerization.

3.4. *CaM inhibitors differentially alter the intracellular localization of CaM, and affect the Iba1 and CaM protein expressions*

CaM inhibitors altered the intracellular localization of CaM protein (Fig. 8). Both unchallenged and untreated cells (Fig. 8A–C) and LPS-challenged cells (Fig. 8D–F) displayed high CaM content primarily localized in the perinuclear compartment and to a much lesser extent with that in the cell cortex (Fig. 8A,B). Some of the cells with larger TI had CaM immunoreactivity that progressively diminished toward the cell cortex (Fig. 8C). Interestingly, cells treated with CALMID50 alone displayed a more heterogenously translocated CaM immunoreactivity often cortically localized in lamellipodia (Fig. 8J–L, arrowheads). In TFP10-treated cells, the CaM immunoreactivity was very weak and homogenously distributed in the cytoplasm (Fig. 8M–O).

CaM antagonists inhibited Iba1 and CaM protein expressions with different efficacies (Fig. 9). In general, CALMID was less potent than TFP in affecting Iba1 and CAM protein expressions. CALMID, either alone or in combination with LPS, was not able to alter the Iba1 expression significantly (Fig. 9A). TFP was more potent as TFP10 and TFP20 inhibited Iba1 protein expression in a dose-dependent manner both in unchallenged and LPS-challenged cells (Fig. 9C). Similarly to their effects on the Iba1 expression, CALMID and TFP antagonized the CaM protein expression with different efficacy (Fig. 9B,D). When CALMID was used, the CaM immunoreactivity was observed to decrease somewhat dose-dependently in the unchallenged microglia as CALMID50 significantly inhibited the CaM protein expression to 38.6% of the control level (Fig. 9B). Again, TFP20 had a more profound effect on the CaM protein expression (Fig. 9D), as it exhibited a strong inhibition both in the unchallenged and in the LPS-activated microglia (20.8% and 23.4% of the control value, respectively).

3.5. *CaM inhibition impairs phagocytosis in activated microglia*

Cultured microglia readily phagocytosed fluorescently labeled beads (Figs. 10, 11,). On average, unchallenged and untreated microglia had 3.13 ± 0.1 phagocytosed microbeads per cell (Fig. 10A–C and Fig. 11). LPS-challenged microglia displayed a large (about 2.8-fold) increase in phagocytotic activity (8.78 ± 0.3; Figs. 10D–F and 11). CaM inhibitors affected phagocytosis similarly but with different degrees of potency. CALMID dose-dependently inhibited phagocytosis both in unchallenged and LPS-challenged microglia (Fig. 10G–I and Fig. 11A). TFP proved to be a very strong inhibitor of phagocytosis both in unchallenged and LPS-challenged microglia (Fig. 10M–O and Fig. 11B) as it reduced the number of phagocytosed microbeads by almost 90% (to 0.33 ± 0.2; 10.6% of the control value) in unchallenged, and by 76.5% (to 0.75 ± 0.3; 23.5% of the control value) in LPS-challenged cells.

4. Discussion

One of the most ubiquitous Ca^{2+}-sensing proteins is CaM. Its distributions in the developing and the adult rodent brain have

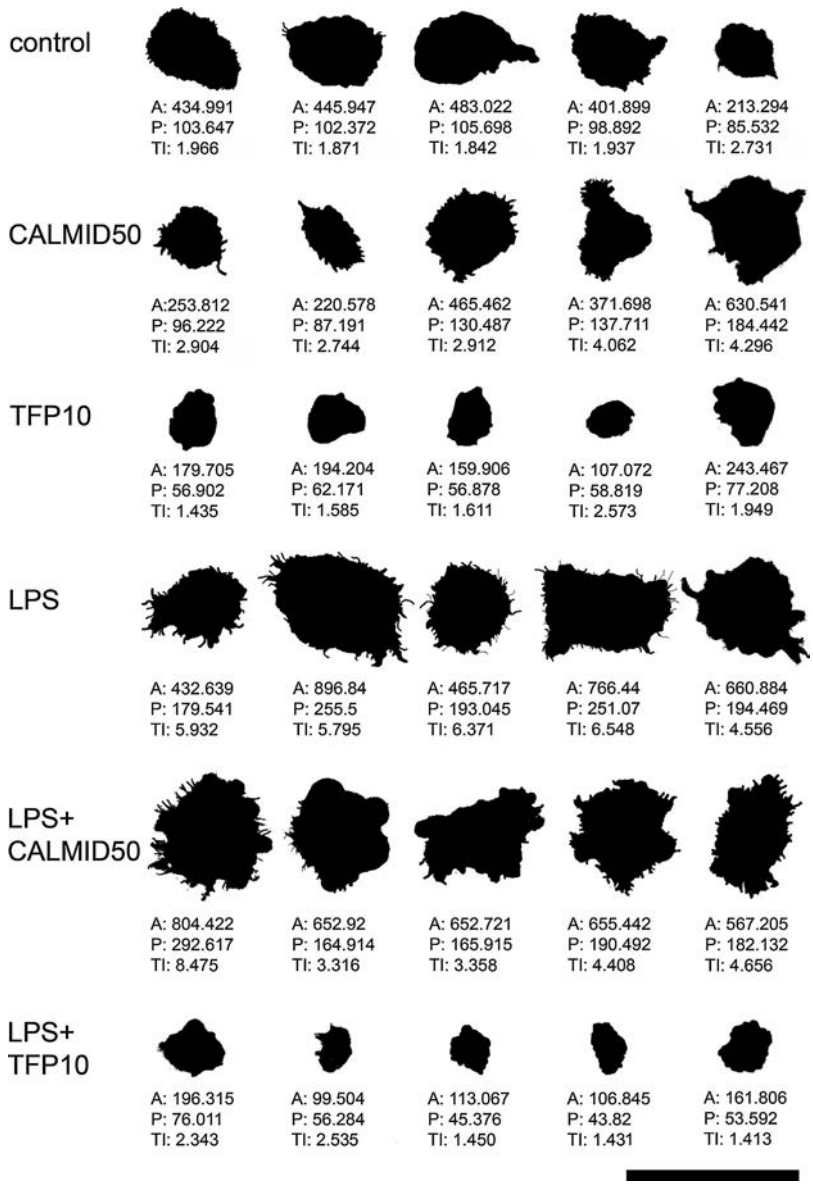

Fig. 5. Representative binary silhouettes from pure microglial cultures after different treatment regimens.
Iba1-positive microglial cells from pure microglial cultures (subDIV4) were photographed, digitized and quantitatively analyzed according to their morphological characteristics. Five representative binary silhouettes are shown at each culturing time. CALMID50, in either control or LPS-challenged microglia, increased the number of filopodia, while the complete absence of filopodia was seen both in TFP10 and in LPS+TFP10-treated microglia. Area (A) in μm^2, perimeter (P) in μm, and TI values (calculated as $[\text{perimeter of cell } (\mu m)]^2/4\pi[\text{cell area } (\mu m^2)]$) are indicated for each digitized cell. LPS: 100 ng/ml; CALMID50: 50 nM CALMID; TFP10: 10 μM TFP. Scale bar for all silhouettes: 50 μm.

been well documented (Caceres et al., 1983; Seto-Ohshima et al., 1983). It is encoded by three different genes in mammals (Palfi et al., 2002; Toutenhoofd and Strehler, 2000). The expression patterns corresponding to the three CaM genes display a broad differential distribution in the developing (Kortvely et al., 2002) and the adult rat CNS under both physiological (Kovacs and Gulya, 2002, 2003; Palfi et al., 1999; Solá et al., 1996) and pathophysiological conditions (Palfi et al., 2001; Palfi and Gulya, 1999; Vizi et al., 2000). Quantitative analysis of the expression patterns of these genes indicated a differential dendritic targeting of the CaM mRNAs (Kortvely et al., 2003; Palfi et al., 1999, 2005); differential intracellular targeting of selected CaM mRNA populations could serve for the local translation of the necessary CaM proteins that regulate the numerous target proteins in that particular cytoplasmic compartment (Kortvely and Gulya, 2004).

CaM expression could be regulated by a number of different physiological and pathophysiological cues. Although its gene expression is generally very stable (Kortvely and Gulya, 2004; Palfi et al., 2002), we have identified many factors that could differentially affect the expressions of the individual CaM genes in neurons with distinct phenotypes from different brain regions (Orojan et al., 2006; Palfi et al., 1999, 2002; Bakota et al., 2005), e.g. inflammation (Orojan et al., 2008), ischemia (Palfi et al., 2001), dehydration (Palfi and Gulya, 1999), and chronic ethanol treatment and withdrawal (Vizi et al., 2000). Apart from the neurons, the microglia display a considerable amount of CaM. This CaM expression, however, is strongly dependent on the phenotype. After a kainic acid challenge, CaM immunoreactivity was earlier demonstrated in reactive microglia of the hippocampus (Solá et al., 1997), where the thickened and shortened microglial processes accumulated CaM protein.

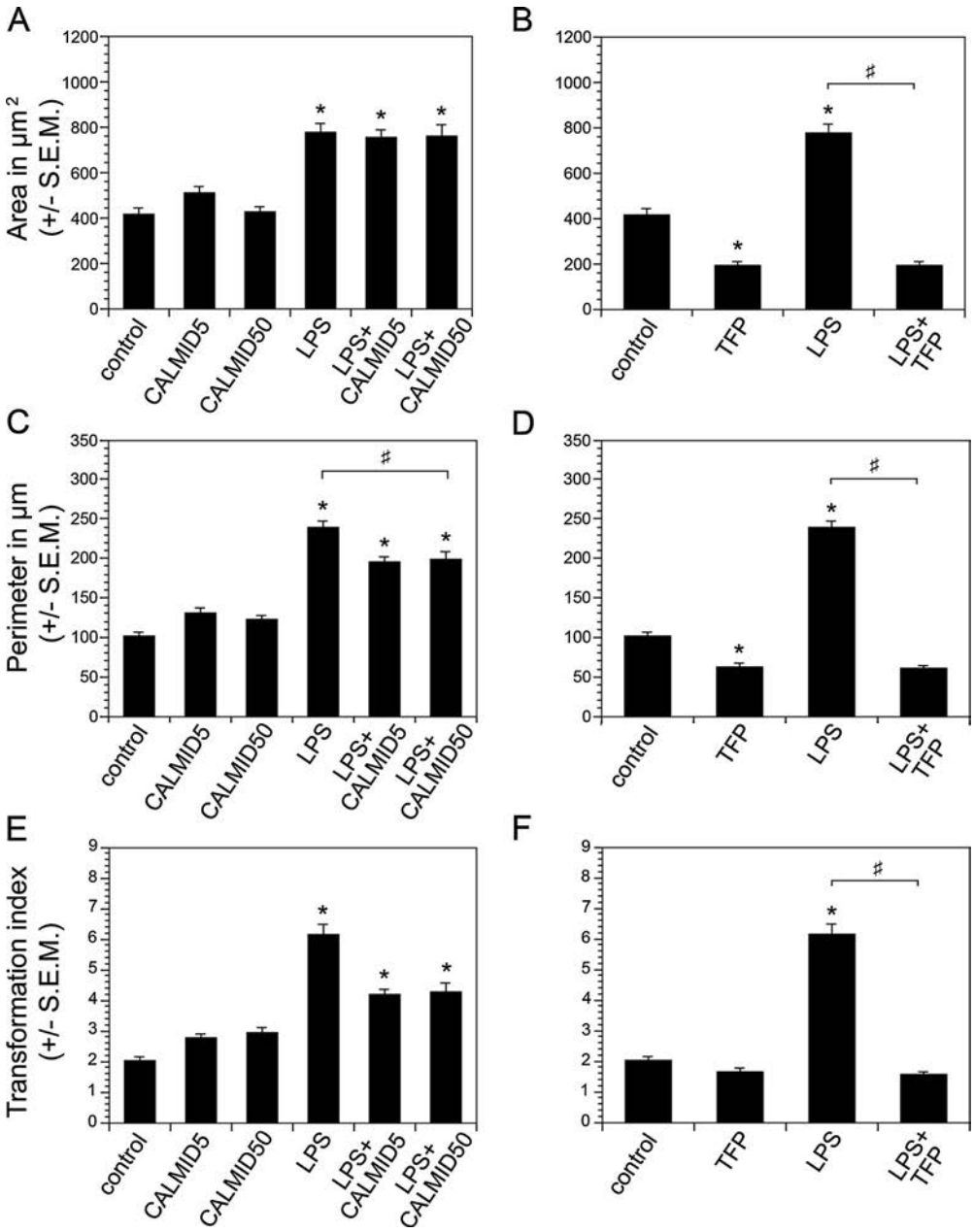

Fig. 6. Effects of CaM inhibitors on selected morphological parameters of pure microglial cells.
Surface area (A, B) in μm^2, perimeter (C, D) in μm, and TI values (E, F) of the microglia for CALMID (A, C, E) and TFP (B, D, F) were analyzed in pure unchallenged and LPS-challenged microglial cell cultures. All statistical comparisons were made by using SigmaPlot (v. 12.3, Systat Software Inc., Chicago, IL, USA) and analyzed with Kruskal–Wallis one-way analysis of variance, followed by Dunn's method for pairwise multiple comparison procedures for statistically significant differences between the groups. Values (mean ± S.E.M.) were computed from at least three independent culturing experiments. *Statistically significant from control ($p < 0.05$); #statistically significant from LPS-treated cells. LPS: 100 ng/ml; CALMID5: 5 nM CALMID; CALMID50: 50 nM CALMID; TFP10: 10 µM TFP.

In our studies, CaM was localized both in developing microglial cells of primary cortical cultures established from E18 wild-type rat embryos maintained for up to 28 days (DIV1-28) and in pure microglial cells subcultured from DIV7 cultures for 4 days (sub-DIV4). Moreover, the presence of CaM protein was demonstrated not only in reactive microglia (treated with LPS alone or in combination with one of the CaM inhibitors), but also, at a lower protein level, in unchallenged proliferating ameboid or even ramified, microglial cells. We observed morphologically and functionally different microglial populations within the range from weak to strong levels of CaM expression during culturing, as evidenced by their quantitative assessment by fluorescent immunocytochemical and Western blotting methods. In mixed primary cortical cultures, ameboid microglia, the predominant form in the early stages but always present (in much smaller numbers) during culturing (Szabo and Gulya, 2013), expressed strong CaM immunoreactivity throughout the cytoplasm, while ramified microglia, the typical form in the later stages of microglial development, showed a weaker and more evenly distributed CaM immunoreactivity. A similar intracellular distribution of CaM protein expression was observed in pure microglial cultures. In unchallenged and LPS-challenged cultures, most of the microglia was ameboid and had strong CaM immunoreactivity throughout the cytoplasm. Treatments with CaM inhibitors, both in unchallenged and LPS challenged cells, resulted in a weaker and more homogenously localized CaM immunoreactivity.

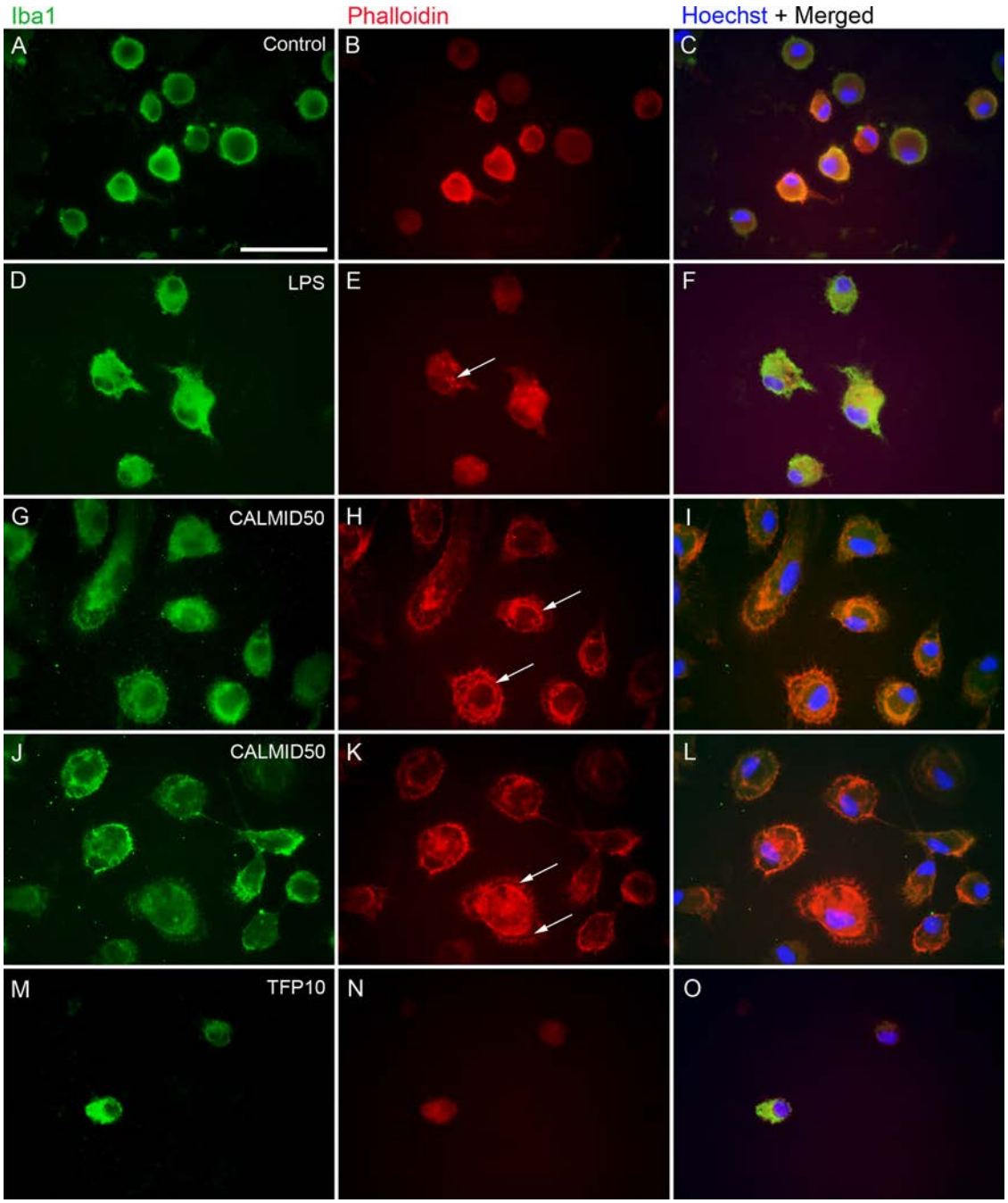

Fig. 7. Immunocytochemical localization of actin-binding proteins in pure microglial cells. (For interpretation of the references to colour in this figure legend, the reader is referred to the web version of this article.)
Iba1 immunoreactivity (A, D, G, J, M; shown here in green) and phalloidin fluorescence (B, E, H, K, N; shown in red) were colocalized in unchallenged and untreated (control) cells and in microglia treated with LPS or CaM inhibitors in pure microglial cultures (subDIV4). Merged pictures (C, F, I, L, O) show the Hoechst 33,258-labeled cell nuclei (blue) and the colocalization of Iba1 immunoreactivity and phalloidin fluorescence. Filamentous actin often forms continuous ring-like lamellipodia in unchallenged microglia (B). In LPS-challenged microglial cells, lamellipodia were less dominant, but the toxin stimulated podocyte formation, as indicated by several puncta delineated by phalloidin fluorescence (arrow, E). When CALMID50 was used, strong lamellipodia formation was observed, often accompanied by a perinuclear cytoplasmic streaming of filamentous actin (arrows, H, K), giving a double-ringed appearance of these cells. TFP treatment abolished the formation of filamentous actin bundles as detected by phalloidin fluorescence microscopy (N). LPS: 100 ng/ml; CALMID50: 50 nM CALMID; TFP10: 10 μM TFP. Scale bar in panel A for all pictures: 50 μm.

We found that the intracellular localization of CaM immunoreactivity described above was closely related, and typically complementary, to the filamentous actin cytoskeleton, comprised mainly of branched F-actin (Rotty et al., 2013). F-actin was visualized in our studies by the distributions of an actin-binding protein, Iba1, and phalloidin, a bicyclic heptapeptide that recognizes F-actin only, e.g. the form that possesses cellular functionality. Iba1 is an intracellular Ca^{2+}-binding protein that plays an important role in regulation of the intracellular actin dynamics through the direct binding of actin, enhances membrane ruffling and participates in phagocytosis and cell motility (Ohsawa et al., 2000, 2004), functions that require large amounts of cortical F-actin. Our immunocytochemical observations showed that ramified cells (characterized by larger TI values) that displayed minimal or no ruffling at all had only modest quantities of CaM proteins in the cell cortex as compared with ameboid or reactive microglia. Coincidentally, the amount of

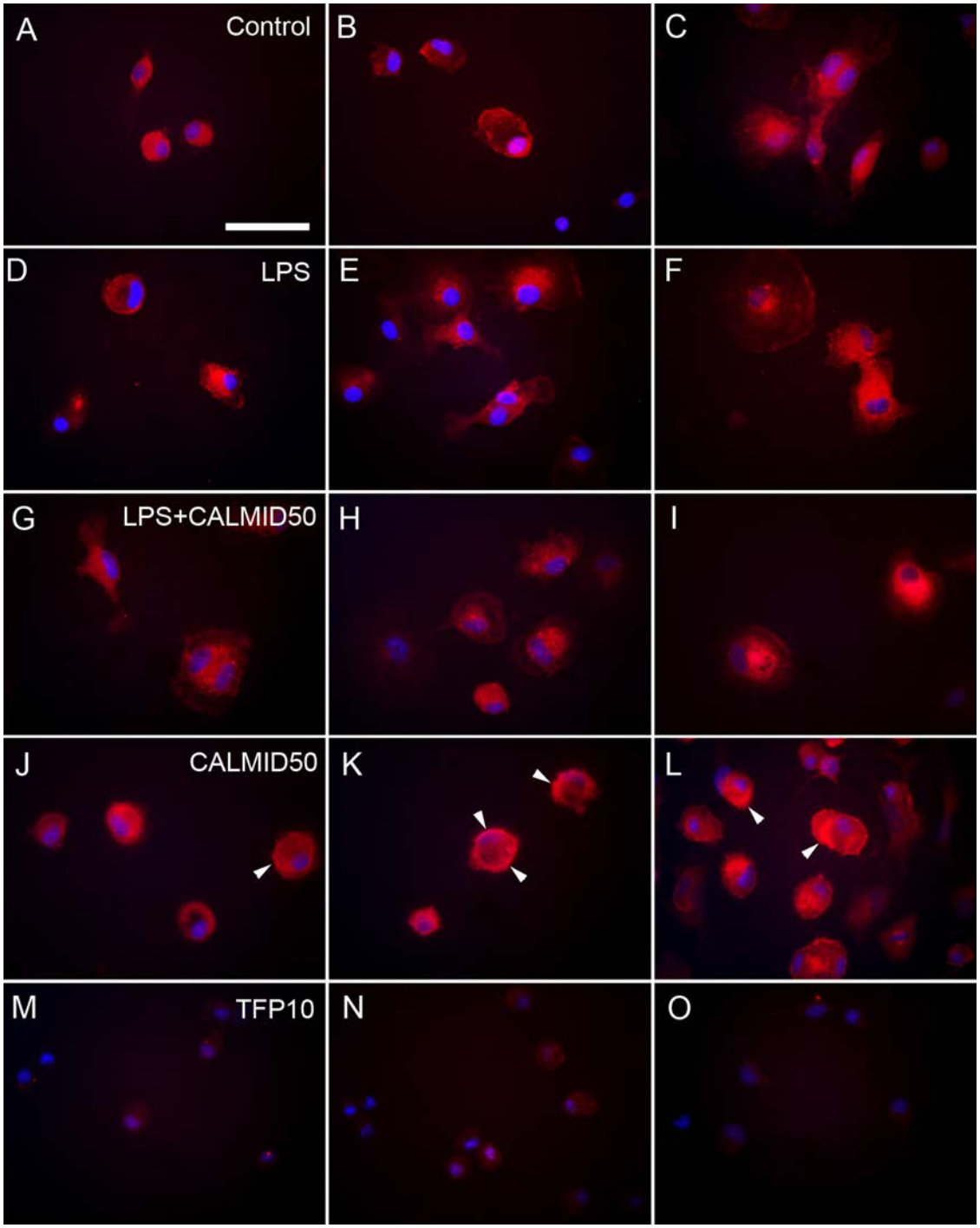

Fig. 8. Effects of CaM inhibitors on the intracellular localization of CaM immunoreactivity in pure microglial cells. (For interpretation of the references to colour in this figure legend, the reader is referred to the web version of this article.)
Representative immunocytochemical pictures showing the intracellular distribution of CaM immunopositivity (red) in pure microglia cells (subDIV4). The merged pictures show the cell nuclei (blue) that were stained with Hoechst 33,258. The unchallenged and untreated (control) microglia (A–C) and LPS-challenged cells (D–F) showed mainly perinuclearly localized CaM immunoreactivity. LPS-challenged and treated cells (G–I), and more typically CALMID50-treated microglia (J–L) displayed CaM distribution often more targeted to the cell cortex and developing lamellipodia (arrowheads). TFP treatment resulted in a significant cell death (see Fig. 4) and a homogenous cytoplasmic distribution of CaM immunoreactivity in the surviving microglia (M–O). LPS: 100 ng/ml; CALMID50: 50 nM CALMID; TFP10: 10 μM TFP. Scale bar in panel A for all pictures: 50 μm.

cortical F-actin was likewise less in ramified microglia, and the reorganization of the actin cytoskeleton determined the intracellular distribution of CaM. Concomitantly increased levels of Iba1 and CaM protein expression, however, were evident both in unchallenged ameboid and in LPS- or LPS and CaM inhibitor-challenged, e.g. activated/reactive microglia. Our observations relating to the intracellularly redistributed CaM vs. F-actin are consistent with the findings in mast cells in previous studies. For example, Sullivan et al. (2000) demonstrated that CaM promoted the disassembly of cortical F-actin, while Psatha et al. (2004) found that the disassembly of the actin cytoskeleton eliminated CaM localization.

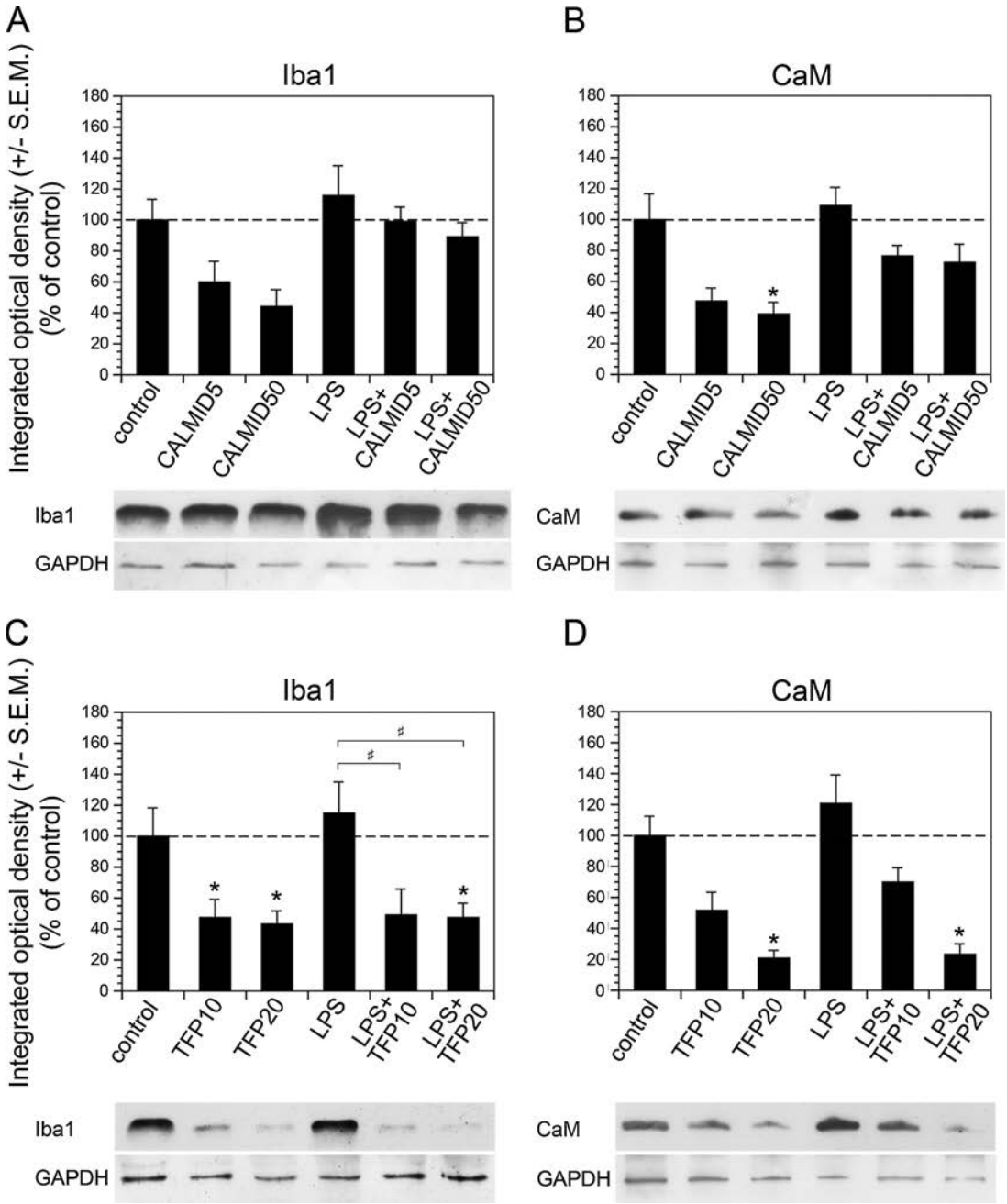

Fig. 9. Effects of CaM inhibitors on Iba1 and CaM protein expression in pure microglial cells, as detected by Western blot analysis.
Quantitative Western blot analysis of Iba1 (A, C) and CaM (B, D) immunoreactivities in pure microglial cell cultures (subDIV4). Representative Western blot pictures of the respective immunoreactivities are shown below the graphs together with the GAPDH immunoreactive bands that served as inner standards in the same gel. Protein samples were collected from 3 separate culturings, each involving plating on at least 6 Petri dishes, electrophoresed and quantitatively analyzed as described in the Section 2. The integrated optical density data (mean ± S.E.M.), normalized to GAPDH immunoreactivities, were analyzed with Kruskal–Wallis one-way ANOVA on ranks, followed by pairwise multiple comparisons (Dunn's method). *Statistically significant from control ($p < 0.05$); #statistically significant from LPS-treated cells. Iba1: ionized calcium-binding adaptor molecule 1; CaM: calmodulin; LPS: 100 ng/ml; CALMID5 and CALMID50: 5 and 50 nM CALMID; TFP10 and TFP20: 10 and 20 μM TFP; GAPDH: glyceraldehyde 3-phosphate dehydrogenase.

LPS activation renders microglia ameboid, induces several pro- and anti-inflammatory signaling molecules (Lim et al., 2015; Zhu et al., 2014) and neurotoxic substances through binding to the CD14/MD-2/Toll-like receptor 4-complex (Fricker et al., 2012; Tokes et al., 2011), and gives rise, among others, to cell spreading by interfering with the organization of the actin cytoskeleton through the alteration of integrin clustering (Abram and Lowell, 2009). Microglia activation was shown to involve the signaling pathways nuclear factor κB and p38 mitogen-activated protein kinase (Bachstetter et al., 2011; Cao et al., 2014; Kaushal et al., 2007). It must be noted, however, that the activation of microglial cells by LPS is not proliferative (Suzumura et al., 1991).

In our studies, LPS challenge did not display a significant effect on microglial cell survival or CaM and Iba1 protein expression, but resulted in significant cell spreading, documented in increases in cell surface, perimeter and TI, and in a repositioning of intracellular actin filaments toward podosome and filopodia formation. In spite of this lack of interaction between the LPS challenge and CaM protein expression, some of the effects of LPS are mediated through CaM-related phenomena in macrophages (Sweet and

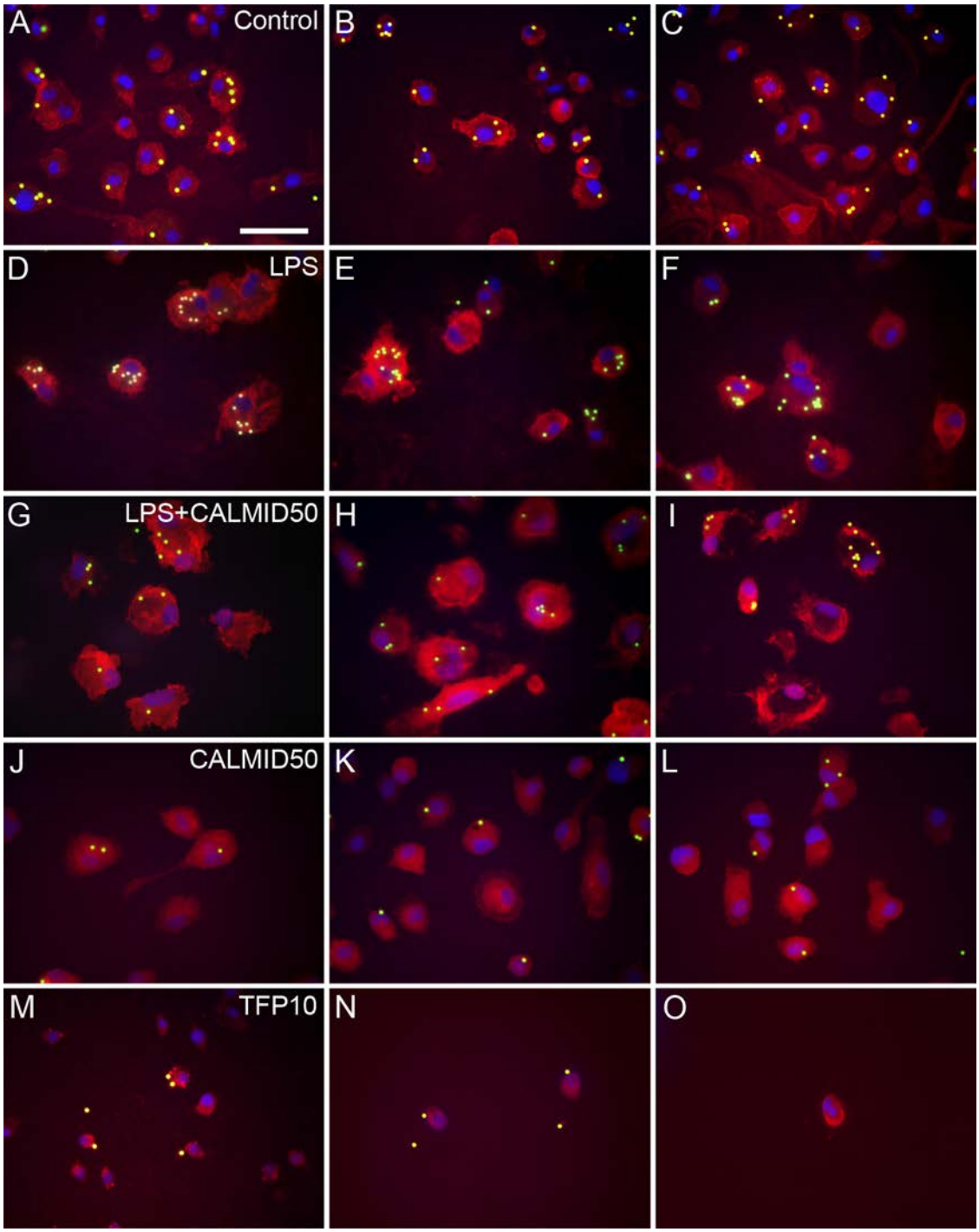

Fig. 10. Effects of CaM inhibitors on the phagocytic activity of microglial cells in pure microglial cultures. (For interpretation of the references to colour in this figure legend, the reader is referred to the web version of this article.)
Distribution of phagocytosed microbeads in pure microglial cultures. Representative pictures showing Iba1-immunopositive microglia demonstrate that the unstimulated and untreated (control) (A–C), LPS-challenged (D–F), LPS + CALMID50-treated (G–I), CALMID50-treated (J–L) and TFP10-treated (M–O) microglia displayed different degrees of phagocytosis, as evidenced by the number of phagocytosed microbeads. Fluorescent dye-coated latex microbeads ($d = 2\ \mu m$) (green) were added to the media and phagocytosed by microglial cells. After exposure to the fluorospheres, the culture was rinsed, the cells were formalin-fixed, labeled first with anti-Iba1 antibody (red), and then with Alexa Fluor fluorochrome-conjugated secondary antibody, and the cell nuclei (blue) were stained with Hoechst 33,258. LPS: 100 ng/ml; CALMID50: 50 nM CALMID; TFP10: 10 μM TFP. Scale bar in panel A for all pictures: 50 μm.

Hume, 1996). An LPS challenge, for example, elevated the intracellular Ca^{2+} concentration in brain macrophages via the activation of phosphatidylinositol (3,4,5)-trisphosphate-sensitive stores that, in turn, activated the actin cytoskeleton (Bader et al., 1994). Such an inflammatory response was recently identified as one developed through the activation of CaM-dependent kinase kinase 2 via Toll-like receptors (Racioppi et al., 2012). Thus, the effects of LPS could be attributed, at least in part, to CaM-related phenomena regulating the actin cytoskeleton without directly affecting the CaM protein expression. In another study, CaM was involved in spontaneous microglial ramification and the activation of proliferation from quiescence as it inhibited the spontaneous ramification and decreased

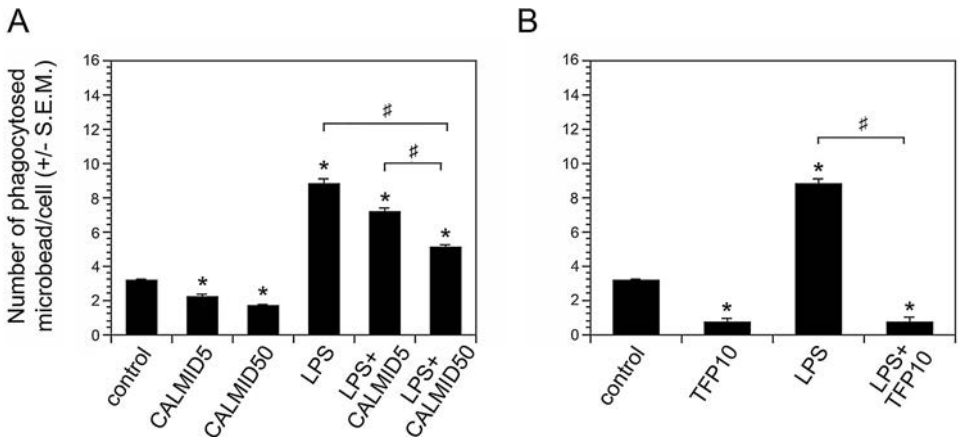

Fig. 11. Effects of CaM inhibitors on the phagocytic activity of microglial cells in pure microglial cultures.
Quantitative analysis of the number of phagocytosed microbeads after treatment with CALMID (A) or TFP (B) in unchallenged and in LPS-challenged microglial cells. For the study of the effects of CaM inhibitors on the number of phagocytosed beads (mean ± S.E.M.), a total of 873 bead-labeled cells were counted in three separate culturing procedures. Data were analyzed with Kruskal–Wallis one-way ANOVA on ranks, followed by pairwise multiple comparisons (Dunn's method). *Statistically significant from control ($p < 0.05$); #statistically significant from LPS-treated cells. LPS: 100 ng/ml; CALMID5: 5 nM CALMID; CALMID50: 50 nM CALMID; TFP10: 10 μM TFP.

the proliferation of these cells (Casal et al., 2001). The loss of ramification was reported to be induced by the elevation of intracellular Ca^{2+} via direct or indirect routes (Kalla et al., 2003) that eventually resulted in CaM activation and/or accumulation in the cell cortex.

A number of studies demonstrated that cell cycle and proliferation could be regulated by CaM inhibitors (Berchtold and Villalobo, 2014; Borsa et al., 1986; Sunagawa et al., 2000). Borsa et al. (1986) compared the effects of CALMID and TFP in cycling and non-cycling cells and demonstrated that they were both preferentially cytotoxic for cycling cells. Cell proliferation studies on the osteosarcoma cell line (Tseng et al., 2004), pancreatic beta-cell line cells (Hügl and Merger, 2007) and human lung cancer stem-like cells (Yeh et al., 2012) demonstrated that CaM inhibitors effectively inhibited cell division. TFP inhibited cancer stem cell tumor formation and growth through Wnt/beta-catenin signaling (Yeh et al., 2012) and cell migration (Finlayson and Freeman, 2009; Linxweiler et al., 2013), and was shown to induce apoptosis in human lung adenocarcinoma cell lines (Chen et al., 2009). In our proliferation studies, unstimulated microglia (subDIV4) exhibited a low PI value (2.5%) indicating the presence of only a few mitotically active cells. This value would not be considered a prognostic feature in a number of human cancer types (Brownhill et al., 2014; Yamaguchi et al., 2013). Proliferation was strongly inhibited by LPS and TFP as they reduced the number of Ki67-positive microglia very effectively. CALMID, however, had no effect on cell proliferation in unchallenged cultures, albeit it did have some inhibitory effect in LPS-treated cells. Cell viability was also similarly differentially affected as TFP was more effective than CALMID in inhibiting the survival of pure microglial cells.

Both CALMID and TFP were previously shown to inhibit CaM activity primarily by binding directly to the protein (Matsushima et al., 2000; Sunagawa et al., 2000). However, CALMID and TFP probably exert many of their actions not only via their binding to CaM, but also by interfering directly with a number of upstream (Qin et al., 2009) or downstream targets of CaM signaling (James et al., 2009; Sunagawa et al., 2000). For example, the Rho family GTPases, e.g. Cdc42, Rac and Rho, are known to be intracellular switches that regulate remodeling of the actin cytoskeleton (Hall, 1998). They participate in membrane ruffling, lamellipodia and podosome formation and phagocytosis (Dovas et al., 2009; Kanazawa et al., 2002; Seasholtz et al., 2004). As recent studies led to the consculsion that CaM can regulate the activation of both Rac1 and Cdc42 in megakaryocytes and platelets (Elsaraj and Bhullar, 2008; Xu and Bhullar, 2011; Xu et al., 2012), a direct involvement of CaM in cytoskeleton remodeling was established. By acting on a number of proteins simultaneously, these CaM antagonists could therefore have more complex effects, which differ from each other and may involve several signaling pathways, thereby further impairing a number of cellular functions. Taken together, these features could explain the differences seen in the efficacies of these CaM inhibitors as concerns various aspects of microglial morphology and function.

The ability of CaM to activate many target proteins depends on its highly flexible conformation, enabling it to interact with a wide variety of proteins (Yamniuk and Vogel, 2004). We hypothesize that this conformational flexibility is limited to different degrees when CaM inhibitors are applied; consequently, many of the CaM-regulated effects will be differentially affected by CaM inhibition. Thus, given the number of CaM-interacting target proteins and their participation in the various intracellular signaling pathways involved in, for example, the remodeling of the actin cytoskeleton during lamellipodia, filopodia or podosome formation (Evans et al., 2003; Murphy and Courtneidge, 2011; Sunagawa et al., 2000; Vincent et al., 2012), cell migration or phagocytosis (Sierra et al., 2013), it is difficult at present to give an accurate explanation as to how different CaM antagonists might interfere with the outcome of the signaling processes. It seems clear, however, that CaM inhibition interferes strongly with both morphological and functional aspects of the microglial cells. Future experiments may shed light on whether the effects of CaM inhibition seen in selected morphological and functional properties of microglia are uniquely characteristic of these cells or may perhaps be typical of other cell types too, and may promote an understanding of the cell type-specific roles of CaM.

5. Conclusion

CaM is a key factor in the regulation of a number of morphological aspects of the microglia through the modulation of the actin cytoskeleton that affects the formation and maintenance of lamellipodia, filopodia and podosomes of these cells. Acting on many target proteins, among which actin is of paramount importance, it regulates several cellular functions such as phagocytosis, cell proliferation and survival. CALMID and TFP, two prototypical CaM antagonists acting through different molecular mechanisms on the CaM protein, have differential effects on these morphological and fuctional aspects, including Iba1 and CaM protein expression, when tested both in unchallenged and LPS-challenged pure microglial cells. In general, TFP was more potent in provoking these struc-

tural alterations and functional changes. Dechipering the roles of CaM in microglial functions, perhaps through use of different CaM-specific inhibitors, could be important in understanding the roles and modes of action of microglia in health and disease.

Author Contributions

Conceived and designed the experiments: K.G., M.S. Performed the experiments: M.S., K.D. Analyzed the data: MS, K.D. Contributed reagents/materials/analysis tools: K.G. Wrote the paper: K.G., M.S. Edited the paper: K.G..

Conflict of interest

The authors have declared that no competing interests exist.

Acknowledgements

We thank Mrs. Susan Ambrus for excellent technical help and Ms. Diana Kata for helpful discussions. This work was supported by program project grants to the University of Szeged from the Hungarian Ministry of National Resources (TÁMOP-4.2.1.B-09/1/KONV-2010-0005 and TÁMOP-4.2.2.A-11/1/KONV-2012-0052) through the European Union Cohesion Fund to KG. The funders had no role in the study design, the data collection and analysis, the decision to publish, or the preparation of the manuscript.

References

Abram, C.L., Lowell, C.A., 2009. The ins and outs of leukocyte integrin signaling. Annu. Rev. Immunol. 27, 339–362.
Ahmed, Z., Shaw, G., Sharma, V.P., Yang, C., McGowan, E., Dickson, D.W., 2007. Actin-binding proteins coronin-1a and IBA-1 are effective microglial markers for immunohistochemistry. J. Histochem. Cytochem. 55, 687–700.
Bachstetter, A.D., Xing, B., de Almeida, L., Dimayuga, E.R., Watterson, D.M., Van Eldik, L.J., 2011. Microglial p38α MAPK is a key regulator of proinflammatory cytokine up-regulation induced by toll-like receptor (TLR) ligands or beta-amyloid (Aβ). J. Neuroinflammation 8, 79.
Bader, M.F., Taupenot, L., Ulrich, G., Aunis, D., Ciesielski-Traska, J., 1994. Bacterial endotoxin induces [Ca^{2+}]i transients and changes the organization of actin in microglia. Glia 11, 336–344.
Bakota, L., Orojan, I., Gulya, K., 2005. Intranuclear differences in calmodulin gene expression in the trigeminal nuclei of the rat. Acta Biol. Szeged 49, 9–14.
Berchtold, M.W., Villalobo, A., 2014. The many faces of calmodulin in cell proliferation, programmed cell death, autophagy, and cancer. Biochim. Biophys. Acta 1843, 398–435.
Berridge, M.J., Lipp, P., Bootman, M.D., 2000. The versatility and universality of calcium signalling. Nat. Rev. Mol. Cell. Biol. 1, 11–21.
Borsa, J., Einspenner, M., Sargent, M.D., Hickie, R.A., 1986. Selective cytotoxicity of calmidazolium and trifluoperazine for cycling versus noncycling C3H10T1/2 cells in vitro. Cancer Res. 46, 133–136.
Brownhill, S., Cohen, D., Burchill, S., 2014. Proliferation index: a continuous model to predict prognosis in patients with tumours of the Ewing's sarcoma family. PLoS One 9, e104106.
Caceres, A., Bender, P., Snavely, L., Rebhun, L.I., Steward, O., 1983. Distribution and subcellular localization of calmodulin in adult and developing brain tissue. Neuroscience 10, 449–461.
Cao, H., Zang, K.K., Han, M., Zhao, Z.Q., Wu, G.C., Zhang, Y.Q., 2014. Inhibition of p38 mitogen-activated protein kinase activation in the rostral anterior cingulate cortex attenuates pain-related negative emotion in rats. Brain Res. Bull. 107, 79–88.
Casal, C., Tusell, J.M., Serratosa, J., 2001. Role of calmodulin in the differentiation/activation of microglial cells. Brain Res. 902, 101–107.
Chen, Q.Y., Wu, L.J., Wu, Y.Q., Lu, G.H., Jiang, Z.Y., Zhan, J.W., Jie, Y., Zhou, J.Y., 2009. Molecular mechanism of trifluoperazine induces apoptosis in human A549 lung adenocarcinoma cell lines. Mol. Med. Rep. 2, 811–817.
Clapham, D.E., 2007. Calcium signaling. Cell 131, 1047–1058.
Dovas, A., Gevrey, J.C., Grossi, A., Park, H., Abou-Kheir, W., Cox, D., 2009. Regulation of podosome dynamics by WASp phosphorylation: implication in matrix degradation and chemotaxis in macrophages. J. Cell Sci. 122, 3873–3882.
Drew, P.D., Chavis, J.A., 2000. Inhibition of microglial cell activation by cortisol. Brain Res. Bull. 52, 391–396.
Elsaraj, S.M., Bhullar, R.P., 2008. Regulation of platelet Rac1 and Cdc42 activation through interaction with calmodulin. Biochim. Biophys. Acta 1783, 770–778.
Erondu, N.E., Kennedy, M.B., 1985. Regional distribution of type II Ca^{2+}/calmodulin-dependent protein kinase in rat brain. J. Neurosci. 5, 3270–3277.
Evans, J.G., Correia, I., Krasavina, O., Watson, N., Matsudaira, P., 2003. Macrophage podosomes assemble at the leading lamella by growth and fragmentation. J. Cell Biol. 161, 697–705.
Färber, K., Kettenmann, H., 2006. Functional role of calcium signals for microglial function. Glia 54, 656–665.
Finlayson, A.E., Freeman, K.W., 2009. A cell motility screen reveals role for MARCKS-related protein in adherens junction formation and tumorigenesis. PLoS One 4, e7833.
Fricker, M., Oliva-Martín, M.J., Brown, G.C., 2012. Primary phagocytosis of viable neurons by microglia activated with LPS or Aβ is dependent on calreticulin/LRP phagocytic signalling. J. Neuroinflammation 9, 196.
Fujita, H., Tanaka, J., Toku, K., Tateishi, N., Suzuki, Y., Matsuda, S., Sakanaka, M., Maeda, N., 1996. Effects of GM-CSF and ordinary supplements on the ramification of microglia in culture: a morphometrical study. Glia 18, 269–281.
Ginhoux, F., Greter, M., Leboeuf, M., Nandi, S., See, P., Gokhan, S., Mehler, M.F., Conway, S.J., Ng, L.G., Stanley, E.R., Samokhvalov, I.M., Merad, M., 2010. Fate mapping analysis reveals that adult microglia derive from primitive macrophages. Science 330, 841–845.
Greenberg, S., 1995. Signal transduction of phagocytosis. Trends Cell Biol. 5, 93–99.
Hall, A., 1998. Rho GTPases and the actin cytoskeleton. Science 279, 509–514.
Hügl, S.R., Merger, M., 2007. Prolactin stimulates proliferation of the glucose-dependent beta-cell line INS-1 via different IRS-proteins. J. Pancreas 8, 739–752.
Ikura, M., 1996. Calcium binding and conformational response in EF-hand proteins. Trends Biochem. 21, 14–17.
Imai, Y., Ibata, I., Ito, D., Ohsawa, K., Kohsaka, S., 1996. A novel gene iba1 in the major histocompatibility complex class III region encoding an EF hand protein expressed in a monocytic lineage. Biophys. Biochem. Res. Commun. 224, 855–862.
James, L.R., Griffiths, C.H., Garthwaite, J., Bellamy, T.C., 2009. Inhibition of nitric oxide-activated guanylyl cyclase by calmodulin antagonists. Br. J. Pharmacol. 158, 1454–1464.
Kalla, R., Bohatschek, M., Kloss, C.U., Krol, J., Von Maltzan, X., Raivich, G., 2003. Loss of microglial ramification in microglia-astrocyte cocultures: involvement of adenylate cyclase, calcium, phosphatase, and Gi-protein systems. Glia 41, 50–63.
Kanazawa, H., Ohsawa, K., Sasaki, Y., Kohsaka, S., Imai, Y., 2002. Macrophage/microglia-specific protein Iba1 enhances membrane ruffling and Rac activation via phospholipase C-gamma -dependent pathway. J. Biol. Chem. 277, 20026–20032.
Kaushal, V., Koeberle, P.D., Wang, Y., Schlichter, L.C., 2007. The Ca^{2+}-activated K^{+} channel KCNN4/KCa3.1 contributes to microglia activation and nitric oxide-dependent neurodegeneration. J. Neurosci. 27, 234–244.
Kennedy, M.B., 1989. Regulation of neuronal function by calcium. Trends Neurosci. 12, 417–420.
Kortvely, E., Gulya, K., 2004. Calmodulin, and various ways to regulate its activity. Life Sci. 74, 1065–1070.
Kortvely, E., Palfi, A., Bakota, L., Gulya, K., 2002. Ontogeny of calmodulin gene expression in rat brain. Neuroscience 114, 301–316.
Kortvely, E., Varszegi, S., Palfi, A., Gulya, K., 2003. Intracellular targeting of calmodulin mRNAs in primary hippocampal cells. J. Histochem. Cytochem. 51, 541–544.
Kovacs, B., Gulya, K., 2002. Differential expression of multiple calmodulin genes in cells of the white matter of the rat spinal cord. Mol. Brain Res. 102, 28–34.
Kovacs, B., Gulya, K., 2003. Calmodulin gene expression in the neural retina of the adult rat. Life Sci. 73, 3213–3224.
Kreutzberg, G.W., 1996. Microglia: a sensor for pathological events in the CNS. Trends Neurosci. 19, 312–318.
Libich, D.S., Harauz, G., 2008. Backbone dynamics of the 18.5 kDa isoform of myelin basic protein reveals transient alpha-helices and a calmodulin-binding site. Biophys. J. 94, 4847–4866.
Lim, H.W., Park, J.I., More, S.V., Park, J.Y., Kim, B.W., Jeon, S.B., Yun, Y.S., Park, E.J., Yoon, S.H., Choi, D.K., 2015. Anti-neuroinflammatory effects of DPTP, a novel synthetic clovamide derivative in in vitro and in vivo model of neuroinflammation. Brain Res. Bull. 112, 25–34.
Linxweiler, M., Schorr, S., Schäuble, N., Jung, M., Linxweiler, J., Langer, F., Schäfers, H.J., Cavalié, A., Zimmermann, R., Greiner, M., 2013. Targeting cell migration and the endoplasmic reticulum stress response with calmodulin antagonists: a clinically tested small molecule phenocopy of SEC62 gene silencing in human tumor cells. BMC Cancer 13, 574.
Lowry, O.H., Rosebrough, N.J., Farr, A.L., Randall, R.J., 1951. Protein measurement with the Folin phenol reagent. J. Biol. Chem. 193, 265–275.
Matsushima, N., Hayashi, N., Jinbo, Y., Izumi, Y., 2000. Ca^{2+}-bound calmodulin forms a compact globular structure on binding four trifluoperazine molecules in solution. Biochem. J. 347, 211–215.
Mitchison, T.J., Cramer, L.P., 1996. Actin-based cell motility and cell locomotion. Cell 84, 371–379.
Murphy, D.A., Courtneidge, S.A., 2011. The 'ins' and 'outs' of podosomes and invadopodia: characteristics, formation and function. Nat. Rev. Mol. Cell Biol. 12, 413–426.
Myllykoski, M., Itoh, K., Kangas, S.M., Heape, A.M., Kang, S.U., Lubec, G., Kursula, I., Kursula, P., 2012. The N-terminal domain of the myelin enzyme 2′,3′-cyclic nucleotide 3′-phosphodiesterase: direct molecular interaction with the calcium sensor calmodulin. J. Neurochem. 123, 515–524.

Ohsawa, K., Imai, Y., Kanazawa, H., Sasaki, Y., Kohsaka, S., 2000. Involvement of Iba1 in membrane ruffling and phagocytosis of macrophages/microglia. J. Cell Sci. 113, 3073–3084.
Ohsawa, K., Imai, Y., Sasaki, Y., Kohsaka, S., 2004. Microglia/macrophage-specific protein Iba1 binds to fimbrin and enhances its actin-bundling activity. J. Neurochem. 88, 844–856.
Orojan, I., Bakota, L., Gulya, K., 2006. Differential calmodulin gene expression in the nuclei of the rat midbrain-brain stem region. Acta Histochem. 108, 455–462.
Orojan, I., Bakota, L., Gulya, K., 2008. Trans-synaptic regulation of calmodulin gene expression after experimentally induced orofacial inflammation and subsequent corticosteroid treatment in the principal sensory and motor trigeminal nuclei of the rat. Neurochem. Int. 52, 265–271.
Palfi, A., Gulya, K., 1999. Water deprivation upregulates the three calmodulin genes in exclusively the supraoptic nucleus of the rat brain. Mol. Brain Res. 74, 111–116.
Palfi, A., Kortvely, E., Fekete, E., Gulya, K., 2005. Multiple calmodulin mRNAs are selectively transported to functionally different neuronal and glial compartments in the rat hippocampus. An electron microscopic in situ hybridization study. Life Sci. 77, 1405–1415.
Palfi, A., Kortvely, E., Fekete, E., Kovacs, B., Varszegi, S., Gulya, K., 2002. Differential calmodulin gene expression in the rodent brain. Life Sci. 70, 2829–2855.
Palfi, A., Simonka, J.A., Pataricza, M., Tekulics, P., Lepran, I., Papp, G., Gulya, K., 2001. Postischemic calmodulin gene expression in the rat hippocampus. Life Sci. 68, 2373–2381.
Palfi, A., Vizi, S., Gulya, K., 1999. Differential distribution and intracellular targeting of mRNAs corresponding to the three calmodulin genes in rat brain: a quantitative in situ hybridization study. J. Histochem. Cytochem. 47, 583–600.
Prinz, M., Priller, J., 2014. Microglia and brain macrophages in the molecular age: from origin to neuropsychiatric disease. Nat. Rev. Neurosci. 15, 300–312.
Psatha, M., Koffer, A., Erent, M., Moss, S.E., Bolsover, S., 2004. Calmodulin spatial dynamics in RBL-2H3 mast cells. Cell Calcium 36, 51–59.
Qin, J., Zima, A.V., Porta, M., Blatter, L.A., Fill, M., 2009. Trifluoperazine: a ryanodine receptor agonist. Pflugers Arch. 458, 643–651.
Racioppi, L., Noeldner, P.K., Lin, F., Arvai, S., Means, A.R., 2012. Calcium/calmodulin-dependent protein kinase kinase 2 regulates macrophage-mediated inflammatory responses. J. Biol. Chem. 287, 11579–11591.
Rotty, J.D., Wu, C., Bear, J.E., 2013. New insights into the regulation and cellular functions of the ARP2/3 complex. Nat. Rev. Mol. Cell Biol. 14, 7–12.
Sacks, D.B., Porter, S.E., Ladenson, J.H., McDonald, J.M., 1991. Monoclonal antibody to calmodulin: development, characterization, and comparison with polyclonal anti-calmodulin antibodies. Anal. Biochem. 194, 369–377.
Saijo, K., Glass, C.K., 2011. Microglial cell origin and phenotypes in health and disease. Nat. Rev. Immunol. 11, 775–787.
Sanabria, H., Digman, M.A., Gratton, E., Waxham, M.N., 2008. Spatial diffusivity and availability of intracellular calmodulin. Biophys. J. 95, 6002–6015.
Scott, I.S., Heath, T.M., Morris, L.S., Rushbrook, S.M., Bird, K., Vowler, S.L., Arends, M.J., Coleman, N., 2004. A novel immunohistochemical method for estimating cell cycle phase distribution in ovarian serous neoplasms: implications for the histopathological assessment of paraffin-embedded specimens. Br. J. Cancer 90, 1583–1590.
Seasholtz, T.M., Radeff-Huang, J., Sagi, S.A., Matteo, R., Weems, J.M., Cohen, A.S., Feramisco, J.R., Brown, J.H., 2004. Rho-mediated cytoskeletal rearrangement in response to LPA is functionally antagonized by Rac1 and PIP2. J. Neurochem. 91, 501–512.
Seto-Ohshima, A., Kitajima, S., Sano, M., Kato, K., Mizutani, A., 1983. Immunohistochemical localization of calmodulin in mouse brain. Histochemistry 79, 251–257.
Siddiqui, T.A., Lively, S., Vincent, C., Schlichter, L.C., 2012. Regulation of podosome formation, microglial migration and invasion by $Ca^{(2+)}$-signaling molecules expressed in podosomes. J. Neuroinflammation 9, 250.
Sierra, A., Abiega, O., Shahraz, A., Neumann, H., 2013. Janus-faced microglia: beneficial and detrimental consequences of microglial phagocytosis. Front. Cell. Neurosci. 7 (6).
Solá, C., Tusell, J.M., Serratosa, J., 1996. Comparative study of the pattern of expression of calmodulin messenger RNAs in the mouse brain. Neuroscience 75, 245–256.
Solá, C., Tusell, J.M., Serratosa, J., 1997. Calmodulin is expressed by reactive microglia in the hippocampus of kainic acid-treated mice. Neuroscience 81, 699–705.
Song, X.Y., Hu, J.F., Sun, M.N., Li, Z.P., Zhu, Z.X., Song, L.K., Yuan, Y.H., Liu, G., Chen, N., 2014. IMM-H004, a novel coumarin derivative compound, attenuates the production of inflammatory mediatory mediators in lipopolysaccharide-activated BV2 microglia. Brain Res. Bull. 106, 30–38.
Strack, S., Wadzinski, B.E., Ebner, F.F., 1996. Localization of the calcium/calmodulin-dependent protein phosphatase, calcineurin, in the hindbrain and spinal cord of the rat. J. Comp. Neurol. 375, 66–76.
Streit, W.J., Walter, S.A., Pennel, N.A., 1999. Reactive microgliosis. Progr. Neurobiol. 57, 563–581.
Sullivan, R., Burnham, M., Török, K., Koffer, A., 2000. Calmodulin regulates the disassembly of cortical F-actin in mast cells but is not required for secretion. Cell Calcium 28, 33–46.
Sunagawa, M., Kosugi, T., Nakamura, M., Sperelakis, N., 2000. Pharmacological actions of calmidazolium, a calmodulin antagonist, in cardiovascular system. Cardiovasc. Drug Rev. 18, 211–221.
Suzumura, A., Marunouchi, T., Yamamoto, H., 1991. Morphological transformation of microglia in vitro. Brain Res. 545, 301–306.
Sweet, M.J., Hume, D.A., 1996. Endotoxin signal transduction in macrophages. J. Leukoc. Biol. 60, 8–26.
Szabo, M., Gulya, K., 2013. Development of the microglial phenotype in culture. Neuroscience 241, 280–295.
Tokes, T., Eros, G., Bebes, A., Hartmann, P., Várszegi, S., Varga, G., Kaszaki, J., Gulya, K., Ghyczy, M., Boros, M., 2011. Protective effects of a phosphatidylcholine-enriched diet in lipopolysaccharide-induced experimental neuroinflammation in the rat. Shock 36, 458–465.
Toutenhoofd, S.L., Strehler, E.E., 2000. The calmodulin multigene family as a unique case of genetic redundancy: multiple levels of regulation to provide spatial and temporal control of calmodulin pools? Cell Calcium 28, 83–96.
Town, T., Nikolic, V., Tan, J., 2005. The microglial activation continuum: from innate to adaptive responses. J. Neuroinflammation 2, 24.
Tseng, L.L., Huang, C.J., Hsu, S.S., Chen, J.S., Cheng, H.H., Chang, H.T., Jiann, B.P., Jan, C.R., 2004. Effect of calmidazolium on $Ca^{(2+)}$ movement and proliferation in human osteosarcoma cells. Clin. Exp. Pharmacol. Physiol. 31, 732–737.
Vandonselaar, M., Hickie, R.A., Quail, J.W., Delbaere, L.T., 1994. Trifluoperazine-induced conformational change in $Ca^{(2+)}$-calmodulin. Nat. Struct. Biol. 1, 795–801.
Vertessy, B.G., Harmat, V., Bocskei, Z., Naray-Szabo, G., Orosz, F., Ovadi, J., 1998. Simultaneous binding of drugs with different chemical structures to Ca^{2+}-calmodulin: crystallographic and spectroscopic studies. Biochemistry 37, 15300–15310.
Vincent, C., Siddiqui, T.A., Schlichter, L.C., 2012. Podosomes in migrating microglia: components and matrix degradation. J. Neuroinflammation 9, 190.
Vizi, S., Palfi, A., Gulya, K., 2000. Multiple calmodulin genes exhibit systematically differential responses to chronic ethanol treatment and withdrawal in several regions of the rat brain. Mol. Brain Res. 83, 63–71.
Wong, R., Schlichter, L.C., 2014. PKA reduces the rat and human KCa3. 1 current, CaM binding, and Ca^{2+} signaling, which requires Ser332/334 in the CaM-binding C terminus. J. Neurosci. 34, 13371–13383.
Wu, Y., Wu, M., He, G., Zhang, X., Li, W., Gao, Y., Li, Z., Wang, Z., Zhang, C., 2012. Glyceraldehyde-3-phosphate dehydrogenase: a universal internal control for Western blots in prokaryotic and eukaryotic cells. Anal. Biochem. 423, 15–22.
Xu, B., Bhullar, R.P., 2011. Regulation of Rac1 and Cdc42 activation in thrombin- and collagen-stimulated CHRF-288-11 cells. Mol. Cell. Biochem. 353, 73–79.
Xu, B., Chelikani, P., Bhullar, R.P., 2012. Characterization and functional analysis of the calmodulin-binding domain of Rac1 GTPase. PLoS One 7, e42975.
Yamada, M., Ohsawa, K., Imai, Y., Kohsaka, S., Kamitori, S., 2006. X-ray structures of the microglia/macrophage-specific protein Iba1 from human and mouse demonstrate novel molecular conformation change induced by calcium binding. J. Mol. Biol. 364, 449–457.
Yamaguchi, T., Fujimori, T., Tomita, S., Ichikawa, K., Mitomi, H., Ohno, K., Shida, Y., Kato, H., 2013. Clinical validation of the gastrointestinal NET grading system: Ki67 index criteria of the WHO 2010 classification is appropriate to predict metastasis or recurrence. Diagn. Pathol. 8, 65.
Yamniuk, A.P., Vogel, H.J., 2004. Calmodulin's flexibility allows for promiscuity in its interactions with target protein and peptides. Mol. Biotechnol. 27, 33–57.
Yeh, C.T., Wu, A.T., Chang, P.M., Chen, K.Y., Yang, C.N., Yang, S.C., Ho, C.C., Chen, C.C., Kuo, Y.L., Lee, P.Y., Liu, Y.W., Yen, C.C., Hsiao, M., Lu, P.J., Lai, J.M., Wang, L.S., Wu, C.H., Chiou, J.F., Yang, P.C., Huang, C.Y., 2012. Trifluoperazine an antipsychotic agent, inhibits cancer stem cell growth and overcomes drug resistance of lung cancer. Am. J. Respir. Crit. Care Med. 186, 1108–1180.
Zhu, M.D., Zhao, L.X., Wang, X.T., Gao, Y.J., Zhang, Z.J., 2014. Ligustilide inhibits microglia-mediated proinflammatory cytokines production and inflammatory pain. Brain Res. Bull. 109, 54–60.